



Strål
säkerhets
myndigheten

Swedish Radiation Safety Authority

Research

Residual stress distributions in nickel-based dissimilar metal pipe welds

2024:14

Author: Etienne Bonnaud, Daniel Mångård, och Jens Gunnars,
Kiwa Technical Consulting AB, Solna

Date: October 2024

Report number: 2024:14

ISSN: 2000-0456

Available at www.ssm.se



Strål
säkerhets
myndigheten

Swedish Radiation Safety Authority

Author: Etienne Bonnaud, Daniel Mångård, och Jens Gunnars,
Kiwa Technical Consulting AB, Solna

2024:14

Residual stress distributions
in nickel-based dissimilar metal
pipe welds

Date: October 2024

Report number: 2024:14

ISSN: 2000-0456

Available at www.stralsakerhetsmyndigheten.se

This report was commissioned by the Swedish Radiation Safety Authority (SSM). The conclusions and viewpoints presented in the report are those of the author(s) and do not necessarily coincide with those of SSM.

SSM perspektiv

Bakgrund

Det är vanligt att nickelbasmaterial används som tillsatsmaterial vid svetsning av så kallade blandskarvar, det vill säga svetsning av olika metaller exempelvis austenitiskt rostfritt stål, ferritiskt stål eller nickelbaserade legeringar. Svetsfogen i sådana blandskarvar tillverkas vanligtvis genom att först svetsa ett nickelbasmaterial på den ferritiska komponenten för att bilda en övergångssektion kallad buttring. Därefter värmebehandlas och maskinbearbetas svetsfogen för att minska svetssegenspänningar i det ferritiska stålet respektive bereda svetsfogen. Slutligen svetsas komponenten av austenitiskt rostfritt stål eller nickelbaserad legering till buttringen.

Vid tillverkning av blandskarvar uppstår vanligtvis höga restspänningar. Restspänningar som i sin tur har stor inverkan på initiering och tillväxt av sprickliknande defekter som kan uppstå i mekaniska anordningar. Vid brottmekanisk utvärdering används vanligtvis ett konservativt tillvägagångssätt genom att anta övre gränsdata för restspänningsfördelningen i kombination med övre gränsdata för spricktillväxt för spänningskorrosion. Konservatismerna resulterar ibland i mycket höga postulerade spricktillväxthastigheter och motsvarande korta inspektionsintervall. Erfarenheterna av skador i drift stämmer dock inte överens med detta, och det finns därför ett behov av att skapa mer realistiska restspänningsprofiler.

Resultat

Restspänningar har modellerats och beräknats för ett antal vanligt förekommande stumsvetsar i nickelbasmaterial. Svetsarna skiljer sig åt bland annat vad gäller material, utförande på buttring, godstjocklek, radie, antal svetssträngar, sträckenergi och svetsprocess. De erhållna resultaten har jämförts med väldokumenterade experiment och visar god överensstämmelse mot uppmätningar. Baserat på resultaten har så kallade "best-estimate" restspänningsprofiler utvecklats längs svetsens centrumlinje och längs värmepåverkad zon samt buttring. Känslighetsanalyser har utförts av tillförd sträckenergi, vilka visar på att ändringar i tillförd sträckenergi har störst påverkan på restspänningens storlek för så kallade medeltjocka rör.

Relevans

Det genomförda projektet har förbättrat förståelsen kring restspänningars storlek och fördelning för ett antal vanligt förekommande stumsvetsar i nickelbasmaterial i svenska kärnkraftsreaktorer. Resultaten från projektet är viktiga för att kunna ta fram ändamålsenliga skadetålighetsanalyser för inspektionsprogram eller för att bedöma säkerhetsmarginaler vid eventuella defekter.

Behov av fortsatt forskning

Det genomförda projektet har tagit fram restspänningsprofiler grundade på axisymmetri. En sådan approximation innebär att lokala effekter från exempelvis start- och stoppositioner för svetssträngen inte beaktas. Lokala effekter kan vara av särskilt intresse vid skadetålighetsanalys av montagesvetsar med ansamlingar av start- och stoppositioner. I två pågående projekt (SSM2018-1621 och SSM2021-3706) undersöks effekter av start- och stoppositioner i montageskarvar.

Project information

Kontaktperson SSM: Fredrik Forsberg

Referens: SSM2012-1079

SSM perspective

This report concerns a study which has been conducted for the Swedish Radiation Safety Authority, SSM. The conclusions and viewpoints presented in the report are those of the author/authors and do not necessarily coincide with those of the SSM.

Abstract

It is common for nickel-base materials to be used as filler metals in the welding of dissimilar metal welds. Dissimilar metal welds are usually made by first welding a nickel base material onto a ferritic component to form a transition section called buttring. The weld is then heat treated to reduce weld stresses in the ferritic steel and machined prepared. Finally, a component of austenitic stainless steel or nickel-based alloy is welded to the buttring.

High residual stresses are usually generated in the production of dissimilar welds. Residual stresses have a major impact on the initiation and growth of crack-like defects that can occur in mechanical components. Conservative approaches are used when performing fracture mechanics evaluation. Typically, by assuming upper limit data for the residual stress distribution in combination with upper limit data for crack growth for stress corrosion cracking. The conservatism sometimes result in very high postulated crack growth rates and correspondingly short inspection intervals. However, in-service experiences are different, and there is therefore a need to create more realistic residual stress profiles.

Background

Residual stresses have been modelled and calculated for a number of commonly used butt welds in nickel-based materials. The welds differ in terms of material, buttring design, material thickness, radius, number of weld beads, strain energy and welding process. The results obtained have been compared with well-documented experiments and show good agreement with measurements. Based on the results, best-estimate residual stress profiles have been developed along the weld centre-line and along the heat affected zone and buttring. Sensitivity analyses have been performed on the applied strain energy, which show that changes in applied strain energy have the largest impact on the magnitude of the residual stress for so-called medium thickness pipes.

Results

The project has improved the understanding of the magnitude and distribution of residual stresses for a number of commonly used butt welds in nickel-based materials in Swedish nuclear power reactors. The results from the project are important for developing appropriate damage tolerance analyses for inspection programmes or for assessing safety margins for defects.

Conclusions

The project has developed residual stress profiles based on axi-symmetry. Such an approximation means that local effects from, for example, start and stop positions of the weld bead are not considered. Local effects can be of particular interest when analysing the damage resistance of welds with accumulations of start and stop positions. Two ongoing projects (SSM2018-1621 and SSM2021-3706) are investigating the effects of start and stop positions in welds.

Project information

Contact person SSM: Fredrik Forsberg
Reference: SSM2012-1079

Summary

Residual stress profiles for nickel-based dissimilar metal welds used for joining stainless steel pipes to ferritic steel nozzles and pipes have been analysed by numerical welding simulation. The welds included, have been selected based on an inventory of welds in Swedish nuclear power plants. The nickel-based welds were grouped into different weld types based on the design of materials constituting the joint, including the buttering configuration. Each weld type contains several weld cases encompassing different thickness, pipe radius, number of weld passes, arc energy and welding process.

Recommended weld residual stress profiles have been developed for the selected weld cases along paths in the weld centreline, HAZ regions and in the buttering when present. Typical data has been used for influencing parameters with the aim to establish best-estimate through-thickness stress distributions.

Welds deviating from the conditions assumed in this report are recommended to be handled with individual simulations.

Contents

1. Background	3
2. Scope	5
3. Dissimilar metal welds in Swedish nuclear power plants	6
4. Modelling	10
4.1 Manufacturing of DMWs and analysis steps	10
4.1.1 Welding of the buttering and PWHT	11
4.1.2 Welding of dissimilar metal weld	11
4.1.3 PWHT of final weld	13
4.1.4 Machining of DMW to final dimensions	13
4.1.5 Pressure testing	13
4.2 Welding simulation	14
4.2.1 Transient thermal analysis	14
4.2.2 Stress analysis	16
4.2.3 Material properties	18
4.2.4 Phase transformations in carbon steel	18
4.3 Comparison with experimental measurements	18
5. Effect of different simulation steps	20
5.1 Sensitivity study of reduction in heat input	20
5.2 Effect from pressure testing	22
5.3 Effect from detailed simulation of buttering	24
5.4 Effect from extensive machining of welds	24
6. Results for recommended residual stress profiles	26
6.1 Weld type I	27
6.2 Weld type II	32
6.3 Weld type III	37
6.4 Weld type IV	39
6.5 Weld type V	44
6.6 Weld type VI	46
7. Conclusions	48
8. Suggested further work	50
9. Acknowledgments	51
10. References	52
Appendix A – Material properties	55
Appendix B – Detailed results	60
Weld case I.1	60
Weld case I.2	66
Weld case I.3	72
Weld case I.4	78
Weld case II.1	84
Weld case II.2	89
Weld case II.3	94
Weld case II.4	99
Weld case III.1	104
Weld case IV.1	109
Weld case IV.2	115
Weld case IV.3	121
Weld case IV.4	127
Weld case V.1	133
Weld case VI.1	139
Appendix C – Effect from pressure testing	146
Appendix D – Sensitivity study of reduction in heat input	151
Appendix E – Effect from extensive machining of welds	156

1. Background

It is a common practice to use nickel-based filler material to weld dissimilar metals involving austenitic stainless steel, ferritic steel (carbon or low alloy ferritic steel) and nickel-based alloys. For dissimilar metals, the weld joint is typically made by first welding a nickel-based filler material on to the ferritic steel component, to form a transition section called buttering. The buttering is then subjected to post weld heat treatment (PWHT) at a temperature designed to relax the welding residual stress in the ferritic steel. Afterwards, the machining is carried out for weld joint preparation. Lastly, the austenitic stainless steel component or nickel-based alloy component is welded to the buttering by using nickel-based filler metal.

The manufacturing of dissimilar metal welds (DMW) will in general generate high weld residual stresses. There are many factors that can influence these residual stresses such as heat input, filler metal properties etc. Heat treatment to achieve stress relief in the stainless steel or nickel base weld is not applied, due to hazard of sensitization with respect to stress corrosion cracking (SCC) if these materials are subjected to high temperatures. In nuclear power plants, nickel-based material Alloy 600 and its compatible weld filler metals Alloy 82 and Alloy 182 are usually used to make the welded joint with ferritic nozzles and austenitic piping. More recently Alloy 690 and compatible weld filler metals Alloy 52 and Alloy 152 (with higher resistance to initiation of SCC) have also been used as replacement materials.

Weld residual stresses have a large influence on initiation and growth of crack like defects that could possibly occur in a component under operation. Under certain conditions, nickel-based weld material is subjected to hazard of SCC. Generally compressive residual stresses at a surface exposed to a corrosive environment are beneficial with respect to SCC, while tensile residual stresses are disadvantageous. For some situations, an initiated SCC crack can grow into a compressive region and arrest. Residual stresses also influence the crack growth due to fatigue. Furthermore, residual stresses influence the failure mechanism fracture, and must be considered when evaluating the safety margin to fracture for upset loads and other loads that could occur. Thus, to accomplish relevant integrity assessments and inspection planning [1], information regarding the residual stress distributions through the thickness of pipes and components is needed.

When evaluating the defect tolerance, a conservative approach is to assume upper bound data for the residual stress distribution combined with upper bound crack growth data for SCC. This conservatism results in very high postulated crack growth rates and corresponding short inspection intervals. However, operational experience of damages is not consistent with this, and for that reason, efforts have been made to establish more realistic residual stress profiles by use of numerical methods. Accurate prediction of weld residual stress fields is essential for evaluation of cracking and arrive at realistic inspection intervals that ensure safe operation.

The residual stresses induced by welding are dependent on manufacturing variables such as component geometry, weld joint geometry, filler metal properties, welding process, heat input, bead sequence, heat transfer characteristics, mechanical constraints, manufacturing sequence, machining of welds, and design of any PWHT. Operational variables important for the residual stresses include pressure testing, operation temperature, and may be influenced by operational load transients that occur. For accurate prediction of residual stresses at welds, these factors need to be considered in the numerical modelling.

Welding is a complicated process and requires detailed modelling. This involves deposition of molten filler material, localized heating with steep thermal gradients, and strain cycling from successive weld passes influencing previously deposited weld material as well as base material. The weld and base materials undergo complex thermo-mechanical cycles involving elastic, plastic and creep deformation. This results in residual stresses and strains as well as altered material properties. The weld may interact with other welds and undergo subsequent processing which also influences the residual stress field.

The distribution of residual stresses from welding can be predicted numerically using finite element (FE) analysis. The first detailed modelling of weld residual stresses for components in Swedish nuclear power plants was performed in 1996-1999,[2],[3],[4]. Development has continuously been carried out to improve the prediction of weld residual stresses by experimental methods and numerical modelling. Examples of this are given by NESC-III TG6 [5], NET TG1 [6],[7],[8], Swedish projects [9],[10] and an international validation project [11]. These projects have resulted in increased understanding and improvements of the numerical procedures, material constitutive modelling and heat source modelling methods. Comparison between numerical predictions and experimental measurements indicate that weld residual stress profiles need to be revised for nickel-based dissimilar metal welds.

The current work has the aim to develop best-estimate residual stress distributions for dissimilar metal welds in nozzle and primary piping configurations common in Swedish nuclear power plants. Detailed numerical welding simulation is applied with typical data. The results represent best-estimate predictions of through-thickness residual stress distributions for these welds.

2. Scope

Weld residual stress distributions are developed for dissimilar metal welds common in Swedish nuclear power plants. Weld residual stresses are analysed by numerical FE-modelling based on the most credible validated knowledge, in particular regarding heat source modelling and materials modelling for nickel-based material.

The work has been carried out through following steps:

- Review to identify dissimilar metal welded pipes in Swedish nuclear power plants (NPPs). Grouping of welded joints and documentation of weld geometry and welding specifications.
- Numerical FE-modelling of welding residual stresses. Six weld configurations with different pipe thicknesses are analysed. Sensitivity studies are performed with respect to weld geometry and heat input.
- Assessment of FE-results and development of recommended polynomials for welding residual stress profiles for each weld configuration.
- The results have been revised to include detailed simulation of the buttering process and the corresponding PWHT. The results have also been revised for some of the nozzles to account for the effect of extensive machining.

3. Dissimilar metal welds in Swedish nuclear power plants

In this section, the material and geometric configurations for different nickel-based butt welded joints (relevant to Swedish NPPs) are outlined. The nickel-based welds are formed either between a ferritic and nickel-based pipe or stainless steel and nickel-based pipe.

Dissimilar metal welds at nozzles, safe-ends, piping and penetrations made of Ni-base material Alloy 600 and its compatible weld alloys Alloy 182 and Alloy 82 have been considered. The Alloy 182 nickel-based filler material is for shielded metal arc welding (SMAW). The root passes are performed with filler material Alloy 82 and gas tungsten arc welding (GTAW), also known as tungsten inert gas (TIG) welding. (Sometimes Alloy 182 and Alloy 82 are also denoted Inconel 182 and Inconel 82.)

Dissimilar metal weld geometries relevant to the Swedish nuclear power plants were identified and grouped in [2] to [4]. This compilation was the starting point for the current project. The survey within this project resulted in the conclusion that the list from the previous investigations is complete, and the survey provided detailed information for the welds.

Note that the welds unique to Forsmark were not included in the current survey update, since they were not participating in the project. Forsmark has replaced Alloy 182 weld material (including Alloy 82 root pass) by a few millimetres inlay welding with weld material Alloy 82 at the interior surface. This is analogous to repair welding and is expected to result in increased tensile stress at the interior surface, see [12].

The different pipe welds were grouped into six main configurations based on the design of materials constituting the joint, including the buttering configuration. The six main weld configuration types are shown in Figure 1. Note that in a few cases welds were performed without buttering to the ferritic steel, type III and V. For each weld configuration type there exists several welds with different thickness, pipe radius, number of weld passes, arc energy and welding process. Welds having similar geometries were grouped together in order to reduce the number of simulations. A total of 15 different main weld cases were modelled and the cases are summarized in Table 1.

Table 2 summarizes components in Swedish power plants where each weld type have been identified. Note that this table is based on the inventory available in [2] to [4] and input during the project, there may be additional components not listed herein.

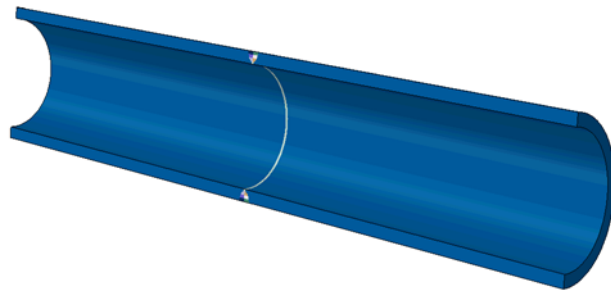
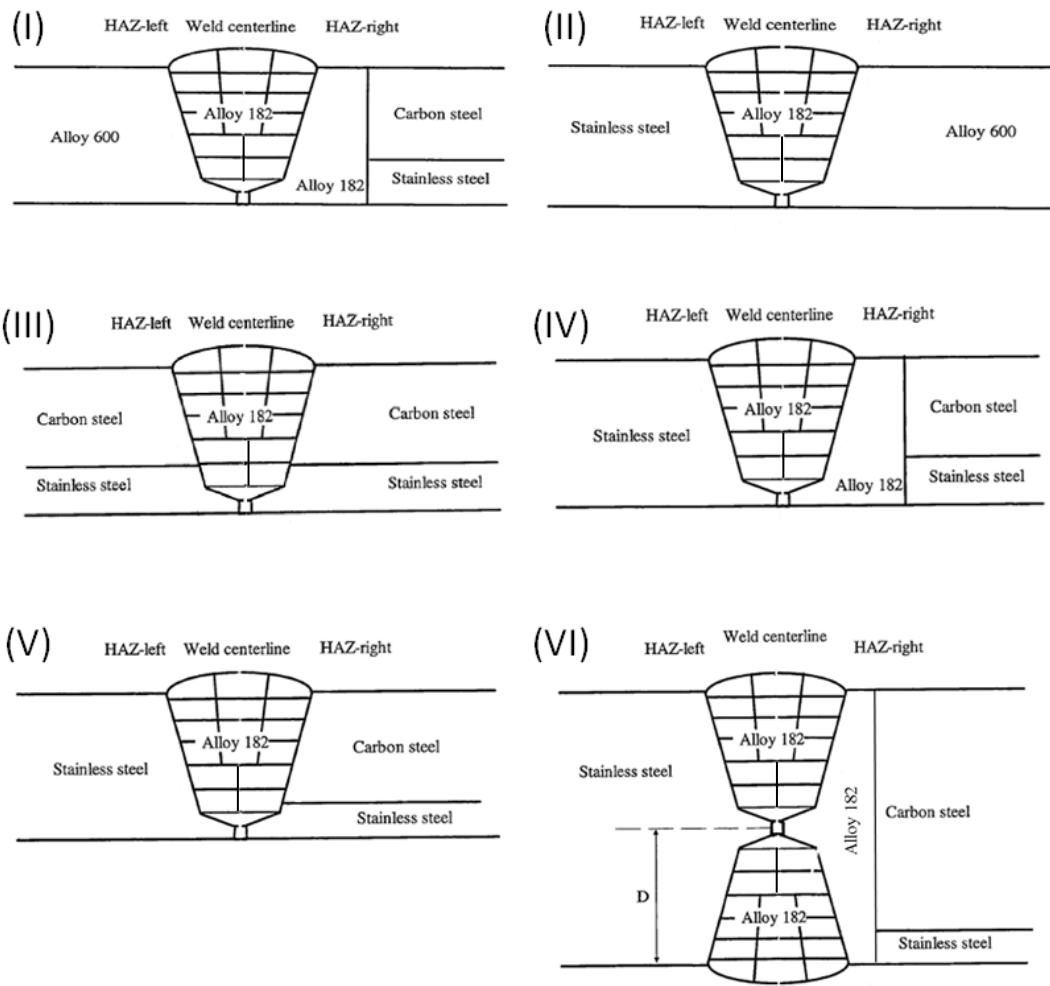


Figure 1 Main weld configuration types, labelled I to VI.

Table 1 Summary of weld types and cases, after grouping of similar cases.

Weld type	Case number	Pipe thickness [mm]	Inner radius /Thickness	Welding process	Arc energy [MJ/m]
I	I.1	34.5	3.70	SMAW	0.81 - 1.62
	I.2	25.5	5.47	SMAW	0.78 - 1.56
	I.3	40.5	2.37	SMAW	0.94 - 1.88
	I.4	12.7	7.63	SMAW	0.56 - 1.12
II	II.1	16.5	7.79	SMAW	0.63 - 1.26
	II.2	4.5	5.71	GTAW	0.31 - 0.83
	II.3	6.3	7.94	GTAW	0.31 - 0.83
	II.4	12.5	7.77	SMAW	0.56 - 1.12
III	III.1	35.0	8.57	SMAW	~ 1.3
IV	IV.1	40.0	7.50	SMAW	~ 1.5
	IV.2	15.5	3.89	SMAW	~ 1.0
	IV.3	42.0	3.60	SMAW	0.6 - 1.2
	IV.4	21.5	3.07	SMAW	~ 1.0
V	V.1	67.0	4.48	SMAW	~ 1.3
VI	VI.1	79.5	4.38	SMAW	~ 1.5

Table 2 Components in Swedish nuclear power plants were each weld case have been identified.

Weld case	Component description	Power plant
I.1	Feed water nozzle, connection between nozzle and safe end	O3/F1/F2/F3
I.2	Emergency cooling nozzle, connection between nozzle and safe end	O3/F3
I.3	Emergency spray cooling nozzle, connection between nozzle and safe end	O3/F3
I.4	Shutdown nozzle, connection between nozzle and safe end	O3/F3
II.1	Feed water nozzle, connection between safe end and pipe	F1/F2
	Feed water nozzle, connection between safe end and pipe	O3/F3
	Emergency cooling nozzle, connection between safe end and pipe	O3/F3
	Emergency spray cooling nozzle, connection between safe end and pipe	O3/F3
II.2	Boron injection nozzle, connection to pipe	F1/F2
	Evacuation nozzle, connection to pipe	F1/F2
	Evacuation nozzle, connection to pipe	O3/F3
II.3	Head cooling spray inlet nozzle, connection to pipe	F1/F2
	Auxiliary feed water nozzle, connection to pipe	O3/F3
	Head cooling spray inlet nozzle, connection to pipe	O3/F3
II.4	Shutdown nozzle, connection between safe end and pipe	O3/F3
III.1	Weld between outlet nozzle and pipe bend in the main circulation system (313)	O1
	Weld between pipe and pump/valve in system 313	O2/B1/B2
IV.1	System 313, straight pipe weld	O2/B1/B2
IV.2	Connection pressurizer – spray nozzle	R2/R3/R4
IV.3	Connection pressurizer – surge nozzle	R2/R3/R4
IV.4	Connection pressurizer – safety and relief nozzle	R3/R4
V.1	Weld between pump case and pipe	O2/B1/B2
VI.1	System 211, connection to RPV-nozzles	R3/R4
O1/O2/O3 are OKG BWR units R2/R3/R4 are Ringhals PWR units F1/F2/F3 are Forsmark BWR units B1/B2 are Barsebäck BWR units		

4. Modelling

4.1 Manufacturing of DMWs and analysis steps

The manufacturing of dissimilar metal welds (DMW) typically involves the following steps that are summarized below. Each step influences the build-up and relaxation of weld residual stresses.

1. Buttering process i.e. welding of a nickel-based filler on to the ferritic steel component to form a buttering layer. In most of the cases, the buttering process is usually carried out before welding the dissimilar metals.
2. Post-weld heat treatment (PWHT) of the buttering layer, performed at a temperature of 620 °C. PWHT will reduce the welding residual stresses in the ferritic steel and to some degree in the nickel-based buttering.
3. Machining of the buttering layer for weld joint preparation.
4. Welding of the dissimilar metal weld joint, see Figure 1 and Table 1.
5. In some cases, a post-weld heat treatment at 450 °C may have been applied to the final welded joint.
6. Machining of the dissimilar metal weld joint to final dimensions.
7. The final welded joint is subjected to pressure testing.

Following approximations and assumptions are used to numerically model the above mentioned manufacturing steps.

- Buttering process (step 1) is modelled and investigated in detail, as limited relaxation of the residual stresses in the nickel-based material occurs during the PWHT of the buttering (step 2).
- Machining of the buttering layer for joint preparation (step 3) is assumed to have an insignificant effect on the redistribution of the residual stresses and therefore it is not modelled in the analysis.
- The post-weld heat treatment at 450 °C (step 5) will result in negligible residual stress relaxation and is therefore not modelled.
- Machining of the welded joint to final dimensions (step 6) is normally assumed to have small influence on the redistribution of through thickness welding residual stresses. However, in some cases, extensive machining was used to reach the final dimensions which consequently can redistribute the welding residual stresses.
- The effect of pressure testing (step 7) is modelled to assess the final state of the welding residual stresses.

The details regarding modelling and analysis of the manufacturing steps considered in this investigation are described in the following section.

4.1.1 Welding of the buttering and PWHT

Buttering process i.e. welding of a buttering layer to ferritic steel is modelled as bead-by-bead deposition, see Section 4.2 for the description of the methodology.

The welding procedure specification for the buttering process was not available, however several sources indicate that 1 MJ/m arc energy is reasonable for the buttering process. As-welded buttering is then subjected to PWHT at 620 °C. Same welding procedure specification for buttering was applied for all weld cases that involve buttering i.e. all weld cases of type I, IV and VI.

At first, the project scope did not include a detailed simulation of the buttering process. It was initially assumed that PWHT of the buttering at 620°C would completely relax the weld residual stresses within the buttering. However, due to the high heat resistance of nickel-based materials, only a limited relaxation of residual stresses is achieved during PWHT at 620°C. Since residual stresses within the buttering are only partially relaxed, a detailed simulation of the buttering process and PWHT was included.

4.1.2 Welding of dissimilar metal weld

The welding process is simulated as bead-by-bead deposition according to the methodology described in Section 4.2.

According to the available welding procedure specifications (WPS), the welding process is SMAW (MMA), except for the root passes, which are performed using GTAW (TIG). This same WPS is also assumed for the welds that lacks documentation.

The WPS provides the information regarding the current and voltage. However, information regarding the actual welding speed is usually not included. This makes the estimation of heat input, which is directly proportional to the applied welding speed, more challenging. Based on the specified welding parameters the welding speed is estimated and hence a reasonable heat input for each specific weld.

The welding parameters specified in the available WPS are used to calibrate the heat source model for the 2D axisymmetric FE-simulation. An example of WPS is given in Figure 2.

BABCOCK Rohrbau		Anlage: Oskarshamn 3 Plant: DB Kom.-Nr. 51-5534 Job No.		DB - W - 1.52	
Schweiß-Detail-Blatt für Werkstatt- und/oder Baustelle Welding detail sheet for shop and/or site				Nahtform: Weld Preparation:	
Grundwerkstoff: Inconel 600 Base material					
geschweißt gegen: 1.4541 1.4306 1.4301 welded to:					
Geltungsbereich: min. max. Validity range: Wandstärke: $s \geq 12 \text{ mm} \dots \leq 18$ Wall thickness: Durchmesser: $\phi \geq 168,3 \text{ mm}$		Schweißposition: welding position: w, s, ü, q			
Draht WIG: E Ni Cr 3; ASTM-AWS Wire GTAW: Inconel 62					
Elektrode: E Ni Cr Fe 3; ASTM-AWS Electrode: Inconel 182					
Draht UP: Wire SAW: ./					
Pulver UP: Flux SAW: ./					
Schutzgas: Argon 99,99 % Shield gas:		Gasmenge: 8-12 l/min. Flowrate:			
Spülgas: Argon 99,99 % Purge:		Gasmenge: 5-50 l/min. Flowrate:			
Vorwärmtemp.: Preheat temp.: ./					
Zwischenlagentemp.: < 100 °C Interpass temp.:				Kantenversatz: Mismatch: $\pm 0,8 \text{ mm}$	
Wärmebehandlung nach dem Schweißen: Postweld heat treatment: ./					
Schweißverfahren Welding Process		GTAW	SHAW	SHAW	
Lage Nr. Part No.		Kurz- 2-lagig	Füll- lage	Deck- lage	
Elektroden Ø Electrode Ø		1,6-2,4	2,4-3,25	2,4-3,25	
Schweißstrom Current (A)		1.L. 60-100 2.L. 70-110	2,4Ø = 40-65 3,25Ø = 65-95	2,4Ø = 40-65 3,25Ø = 65-95	
Polarität Elec. Polarity		= (-)	= (+)	= (+)	
Spannung Voltage (V)		5-15	15-30	15-30	
Ausziehlänge Length of bead		./	Ø 2,4: >30 mm Ø 3,25: >65 mm	Ø 2,4: >30 mm Ø 3,25: >65 mm	
Pendelbreite Width of oscill		./	max. 3 x Ø	max. 3 x Ø	
Schweißgeschw. Travel Speed		1.L.: >2,2 cm/min. 2.L.: >2,4 cm/min.	./	./	
Verfahrensprüfung Nr. Procedure qualification No.				Genehmigungsstempel Kunde/TÜV Approval Stamp Customer/TÜV	
siehe Übersichtsliste über VP				rev. 1 approved BILCOB	
Arbeitsprüfung Nr. Requalification test No.					
Schweißer-Qualifikation: Welder qualification:		GTAW R IV A g SHAW R IV A g			
Spezifikation: Specification:				DB-W-1.0	
Zusätzl. Vorschriften: Additional Instructions:				DB-W-3,0; 6,0; 7,0	
Rev. Nr. Rvw. No.		Datum: Date:		Erstellt: Prepared:	
1		16.05.01		Geprüft: Checked:	
Ausg.		Qualitätsstelle Quality		Seite: 2 von: 2	

Für diese Technische Unterlage behalten wir uns alle Rechte vor.

Figure 2 An example of WPS valid for weld case II.1 and II.4.

4.1.3 PWHT of final weld

According to the available documentation, the PWHT of the final weld was performed only for weld type III. The PWHT was performed for 1 hour at a temperature of 450 °C. However, this temperature and duration will result in a very limited stress relaxation due to the creep properties of the carbon steel, stainless steel and nickel-based materials. PWHT of the final welds at this temperature is therefore not considered in the simulations.

4.1.4 Machining of DMW to final dimensions

The effect of machining after final welding was simulated for the weld cases I.1 and I.4. Machining was simulated by removal of elements.

4.1.5 Pressure testing

Pressure testing is included in the simulations as it can result in relaxation of residual stresses. The magnitude of relaxation of residual stresses due to the pressure testing depends on a number of parameters, including test pressure, radius-to-thickness ratio of the pipe and the presence of any mechanical constraints (such as the proximity to a thick walled nozzle). It is assumed that no large disturbances, e.g. a rigid valve, exists within the influence length $2.5\sqrt{Rt}$.

The butt-welds are subjected to pressure testing when put into operation, with a test pressure in relation to the design pressure of the system.

Design pressure 171.3 bar(e) is the basis for hydrostatic test of PWR-cases (Ringhals). Design pressure 85 bar(e) is the basis for hydrostatic test of BWR-cases (Forsmark and OKG). A list of the simulated weld cases and the corresponding power plant unit types is given in Table 2.

The hydrostatic pressure testing was simulated using 1.3 times the design pressure at 20°C.

4.2 Welding simulation

The modelling method used in this report which is detailed below was first presented in [9] and subsequently improved and validated in [10] and [11]. The welding simulation method is based on a sequential transient thermal and mechanical analysis. A series of finite element models were developed for each dissimilar metal weld type to accommodate all cases in **Table 1**.

4.2.1 Transient thermal analysis

The weld residual stress modelling procedure starts with a transient thermal analysis of the welding heat flow. Addition of new molten weld material is modelled using an element-activation technique. The transient thermal response serves as input for a subsequent incremental thermo-plastic analysis. The thermal material properties are temperature-dependent. A heat transfer boundary condition is applied at all free surfaces of the component. The free boundary is continuously updated as new weld passes are added. The boundary condition published in [13] is based on a heat transfer coefficient α_h approximating both convection and radiation

$$\begin{aligned} \alpha_h &= 0.0668 \cdot T & \frac{\text{W}}{\text{m}^2\text{°C}} & 20 \text{ °C} \leq T \leq 500 \text{ °C} \\ \alpha_h &= 0.231 \cdot T - 82.1 & \frac{\text{W}}{\text{m}^2\text{°C}} & 500 \text{ °C} < T \end{aligned} \quad (\text{Eq. 1})$$

The heat source model needs to be calibrated for the specific welding process and may be performed using theoretical models and/or experimental data. From etched cross sections of a weld for the specific welding process and filler material, metallurgical information can help to identify the temperatures that have been attained in the weld and heat affected zone. Cross sections also give information regarding the shape of the bead fusion zone and heat affected zone resulting from the welding process and heat input. Information for the heat source modelling can also be provided from thermal response measurements at different distances from the weld passes, and by thermal imaging methods for assessing the length of the weld pool.

The efficiency of the welding process η governs how much of the arc energy that is transferred into the weld pool. The average heat input H can be calculated from welding process parameters as:

$$H = \eta \frac{UI}{v} \quad (\text{Eq. 2})$$

where U the voltage, I is the current and v the welding speed.

When an 2D axisymmetric approximation is used, the assumed conditions in the model imply a simultaneous deposition of the weld pass along the entire circumference. The heat conduction in the welding travel direction is by

definition ignored and the heat input to the structure is exaggerated. This implies that calibration of the heat source in the 2D axi-symmetrical model must account for this effect.

A typical heat source model for arc welding processes such as SMAW/MMA and GTAW/TIG is illustrated by Figure 3. The figure shows the temperature within the newly added weld metal. The temperature rapidly rises to the melting temperature T_{melt} and the filler material holds that temperature under the period τ_2^i , before it cools down and solidifies, as the weld pool moves away. For these welding processes the dominating part of the molten material is new added filler material, and the majority of the heat input is consumed within the newly added weld metal. The time τ_1^i is short compared to τ_2^i . The material continues to cool down and reaches the temperature T_{intpass} at the instant τ_3^i when the next adjacent weld pass is added. The temperature T_{intpass} is the inter-pass temperature, and is often in the range 20-150°C. The time τ_3^i is long compared to τ_2^i .

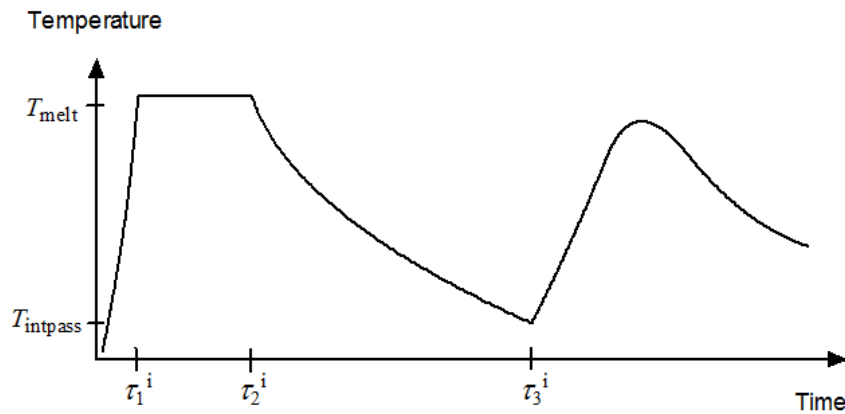


Figure 3 A typical heat source model for arc welding processes.

The steps in the transient thermal analysis of a weld are described below. A 2D axi-symmetrical model is considered, and a description of a procedure for the heat source calibration is included. Any specified pre-heating is modelled by a corresponding initial temperature step for the pipe. The thermal modelling of a new weld pass involves the following steps:

- 1) A new weld pass to be deposited receives a temperature slightly higher than the melting temperature T_{melt} . The addition of molten weld material is modelled using the element-activation technique for a predefined set of elements.
- 2) A transient heat conduction analysis is then performed to simulate the subsequent heat transfer process after the new weld bead is introduced. The weld bead has the temperature T_{melt} under the time period τ_2^i , before it cools down and solidifies as the weld pool passes by. For calibration of the heat source, the time τ_2^i is determined based on the following considerations:

- The time τ_2^i is determined based on the use of an analytical 3D moving heat source solution [14] , [15] , [16] , [17] , [18] , [19] . The influence of the pipe thickness is accounted for by using a solution developed from several mirrored travelling heat sources.
- The heat affected zone (HAZ) size is determined by the 3D analytical solution for a given pipe thickness, the thermal diffusivity of the material, and the linear heat input and the travelling speed for the actual weld pass.
- The HAZ size can be described by the width of regions undergoing phase transformation outside the fusion line.

The effectiveness of this calibration method has been evaluated and verified by detailed finite element calculations performed by Battelle, as documented in [20] as well as during the NRC International Weld Residual Stress Round Robin [11] .

- 3) The inter-pass time τ_3^i is adjusted to receive the prescribed overall inter-pass temperature T_{intpass} before the next weld pass is activated.
- 4) The procedure is repeated until all weld beads are added, and then the entire model is let to cool down to room temperature.

4.2.2 Stress analysis

The thermal response predicted using the procedure described above is the basis for calculating the stresses and strains by a mechanical analysis. The mechanical analysis is performed bead-by-bead. Small strain theory is normally used.

Temperature-dependent elastic-plastic material properties have been used. Incremental plasticity is used with the von Mises yield criterion and associated flow rule. The material hardening law is assumed to be isotropic hardening for the ferritic steel and nickel-based materials, and mixed isotropic-kinematic hardening for stainless steel.

Comparisons with measured weld residual stress fields indicate that through thickness stress profiles for nickel-based materials are generally better captured by using an isotropic hardening model, see [10] , [11] and [21] . Isotropic hardening leads to conservative results in the sense that stress magnitudes are somewhat overestimated. If detailed cyclic stress-strain material properties are available, then a mixed isotropic-kinematic hardening model could be used (an expanding and translating yield surface). Whether the effect of the isotropic hardening part dominates over the kinematic part may depend on the stress state for different welds, see e.g. [22] and [23] .

The multi-pass weld is modelled by activating the elements belonging to the current pass at a time consistent with the transient thermal analysis procedure. Weld and base material adjacent to a subsequent weld bead will reach high temperatures or even re-melt. The annealing capability in ABAQUS is utilized for simulation of strain relaxation in hot and re-molten metal.

Few experimental results are reported about the exact extent of which weld strains are annealed, or the extent of strain relaxation in re-heated or re-molten material. Local stress-strain curves in as-welded material are presented in [24] and [25] where the measured local yield stress in as-welded filler material and in HAZ corresponds to 5 - 10% strain hardening of the base/virgin material. This could indicate some degree of strain relaxation, since simulations often generate higher residual strains than those actually measured.

Annealing and strain relaxation arises at high temperatures, due to microstructural processes such as recrystallization and rapid creep. Conventional annealing is performed using long hold times (hours) and starts with temperatures at 1/3 of the melting temperature. However, for the rapid temperature transient during welding the amount of annealing in different regions, and the dominating process, is not fully understood. It is expected that annealing effects are only seen in regions of much higher temperatures than 1/3 of the melting temperature, because of the short effective hold time.

By utilizing the anneal temperature capability in ABAQUS it is possible to prescribe a temperature above which accumulated plastic strains and hardening are reset to zero. The anneal temperature can simulate rapid strain relaxation at high temperatures, or in re-molten material. Data for the rate of recrystallization or creep at high temperatures is however scarce. An anneal temperature of approximately 1000 °C has been used, which is supported by the findings in [26].

4.2.3 Material properties

The temperature dependent thermal, physical and mechanical properties for nickel based alloy 82, austenitic stainless steel 316 and ferritic steel 508 Class 3 are described in Appendix A.

4.2.4 Phase transformations in carbon steel

Phase transformations in carbon steel has not been modelled in this project since the weld residual stresses in the nickel-based material are expected to be only moderately influenced by the phase transformations.

Carbon steel experiences phase transformations when exposed to sufficiently large temperature changes. These phase transformations cause volumetric contraction and expansion at the microstructural level. Residual stresses may be locally influenced by the formation of different microstructural phases. Transformation to a martensitic microstructure introduces a volumetric change which is greater than that from the other relevant phases. A prerequisite for the martensitic phase transformation is a sufficiently rapid cooling from high temperatures. Martensitic phase transformation may appear only as a narrow band within the heat affected zone of weld beads. This will influence the residual stresses locally within the heat affected zone in carbon steel. However, the effect on the residual stress profiles across the weld is moderate since the weld residual stresses around the weld are mainly caused by nonhomogeneous plastic deformation.

4.3 Comparison with experimental measurements

Experimental weld residual measurements for nickel-based welds are scarce in the published literature. Results were published in [11] for the NRC round robin based on a nozzle with an internal weld repair and subsequent welding of a short safe-end. There was a very good agreement between the numerical predictions and experimental measurements for that case. Another case, more similar to the weld types in the current project, can be found in [27] .

Results from a validation program for dissimilar butt welds have been published by EPRI [27] . Harvested plant nozzles were prepared, welded and examined. During phase 3, the residual stresses were measured by deep-hole-drilling (DHD) and the contour method (Contour) on a cancelled plant pressurizer safety/relief nozzle. These nickel-based welds have a thickness of 35 mm and pipe inner radius of 65 mm. The geometry and materials are identical to weld type IV in the current project. Weld residual stress profiles were numerically predicted by four different modelling approaches and compared to the experimentally measured profiles [27] .

The ratio of 1.85 between inner radius and thickness for the nozzle weld from [27] is very low. Weld case IV.4 in the current project has a ratio of 3.07 was chosen for comparison since it is closest to the nozzle weld ratio

among the weld cases in this project. Weld case VI.4 has a thickness of 21.5 mm and pipe inner radius 66 mm.

Figure 4 shows the comparison where blue lines are predictions for weld case VI.4 (prior to pressure testing), green lines are experimental measurements and red lines are numerical predictions for the nozzle weld from [27]. The blue curves have been scaled from 21.5 mm to 35 mm in order to allow comparison with EPRI results.

The comparison shows a good agreement between the current predictions (blue lines) and the measurements by deep-hole-drilling (green lines, DHD), considering the difference in the ratio between inner radius and thickness.

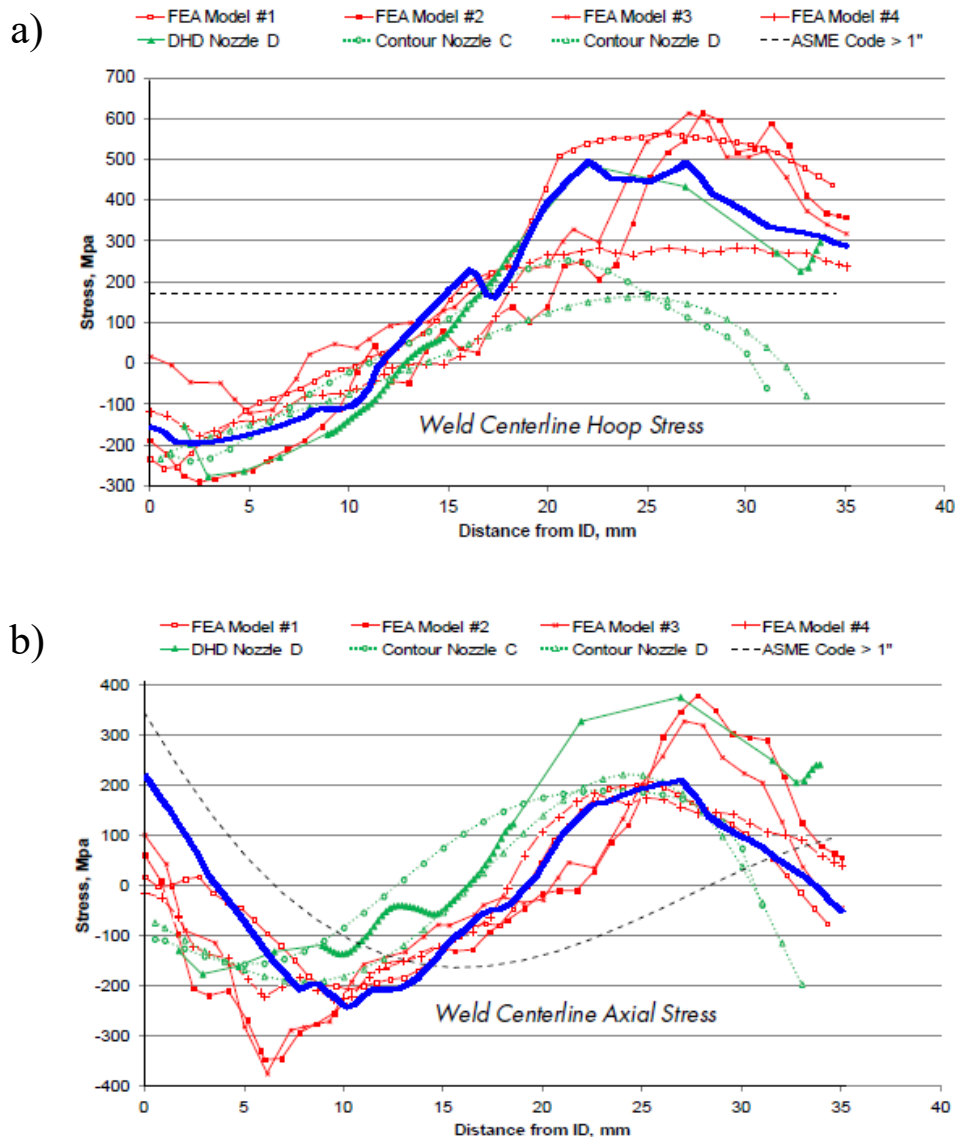


Figure 4 Comparison of experimentally measured and numerically predicted weld residual stresses for weld case VI.4 (prior to pressure testing) and the nozzle weld from [27].

5. Effect of different simulation steps

5.1 Sensitivity study of reduction in heat input

Heat input during manual welding may vary as a result from e.g. variations in arc length and welding speed. The current and process efficiency are both predetermined by the welding procedure. A thick pipe is expected to allow heat to spread much quicker into the work piece as opposed to a thin pipe. This means that thick walled pipes show limited sensitivity to a variation in heat input whereas a thin pipe would possibly show a high degree of sensitivity. A variation in heat input may influence the weld residual stresses regarding both the stress levels and the stress profile through the thickness.

A sensitivity study was performed on the weld types I and II to investigate the effect from uncertainties in heat input. The sensitivity analysis was performed by keeping the welding power fixed and alternating between three welding speeds. Information from the Swedish utilities suggest a welding speed of 60 mm/min for GTAW and 80 mm/min for SMAW. The three welding speeds considered in the sensitivity study are 80 mm/min (as suggested by the utilities), 120 mm/min and 160 mm/min.

Since the welding power was kept fixed and heat input is proportional to the welding speed, an increase in welding speed from 80 mm/min to 160 mm/min decreases the heat input. This was not compensated by increasing the number of weld beads and is in that sense less realistic, although it contributes with valuable information regarding uncertainties in heat input.

Axial residual stresses for selected thin, medium thick and thick pipes are presented in Figure 5. Observations for all pipes included in the sensitivity analysis are summarized in Table 3. The results show that the most noteworthy change in residual stress level and profile can be expected for medium thick pipes, for this sensitivity study. The cases in this study with thin and thick-walled pipes show low effects on stress level and profile.

Appendix D shows detailed results for weld type IV.3, and illustrates that for thick pipes the profile is stable for the studied reduction in heat input.

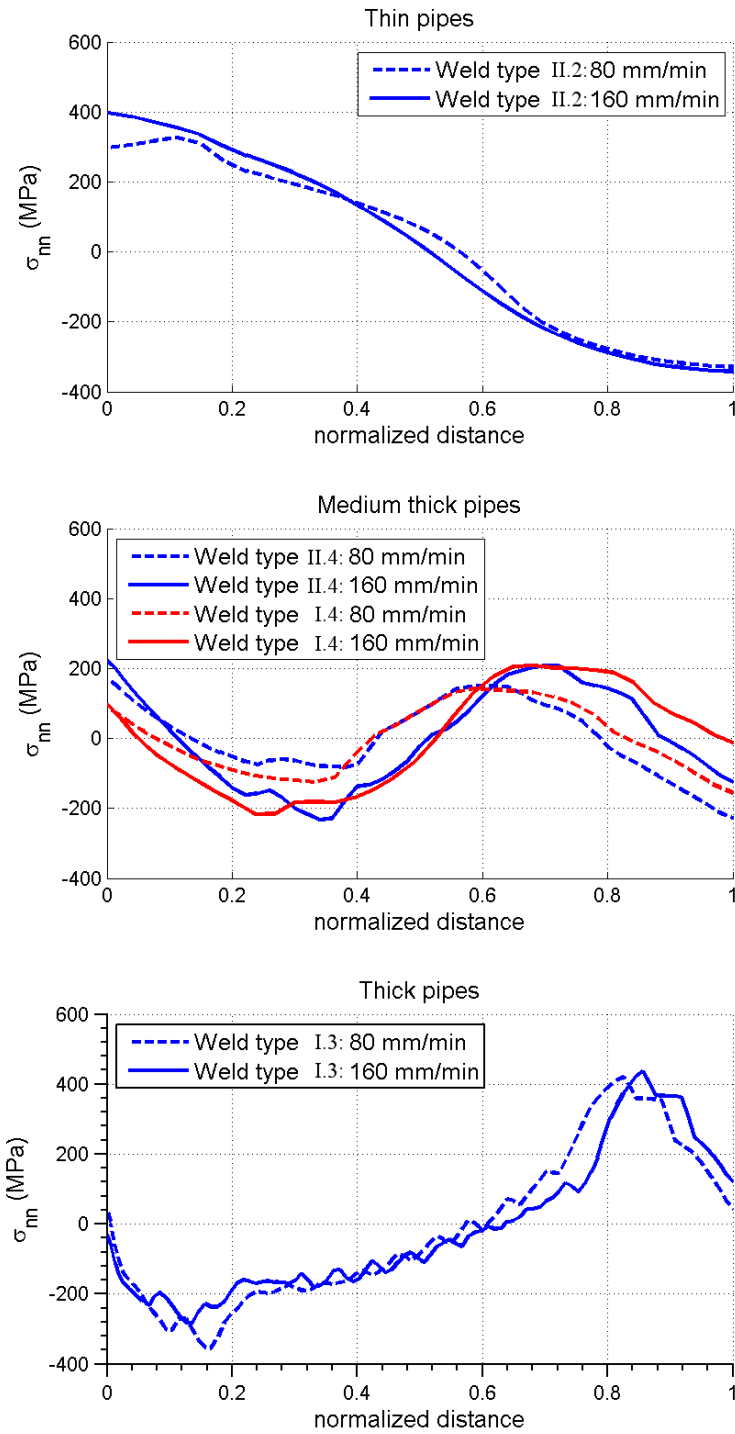


Figure 5 Axial weld residual stress profiles along the weld centre line at operation temperature for a) thin-walled pipes, b) medium thick pipes and c) thick-walled pipes. Results for typical heat input and reduced heat input.

Table 3 Effect on stress levels and stress profile due to reduced heat input.

Weld case	Thickness [mm]	σ_{33}		σ_{nn}	
		Level	Profile	Level	Profile
II.2	4.5	High	Low	Low	Low
II.3	6.3	High	Low	Low	Low
II.4	12.5	High	High	High	High
I.4	12.7	High	High	High	High
II.1	16.0	High	Low	Low	Low
I.2	25.5	Low	Low	Low	Low
I.1	34.5	Low	Low	Low	Low
I.3	40.5	Low	Low	Low	Low
IV.3	42.0	Low	Low	Low	Low

5.2 Effect from pressure testing

Pressure testing is applied to all weld cases in this report and is included in all results in Section 6. In this section, the effect is illustrated for a few weld cases.

In Figure 6, the effect of pressure testing on the weld residual stress field is illustrated for a nozzle-to-safe end weld (weld case I.3) and a safe end-to-piping weld (weld case II.3). Both these weld cases belong to BWR units and are therefore exposed to the same test pressure. However, the ratio between radius and thickness differ substantially between these two cases which implies different stress levels due to the pressure. The effect from pressure testing on a weld with a lower radius to thickness ratio is small. The effect can be significant for welds with a higher radius to thickness ratio.

Appendix B shows detailed results for weld case IV.2. This weld case belongs to PWR units and is therefore exposed to a higher test pressure compared to the weld cases in Figure 6. The effect from pressure testing is small to moderate for this weld case.

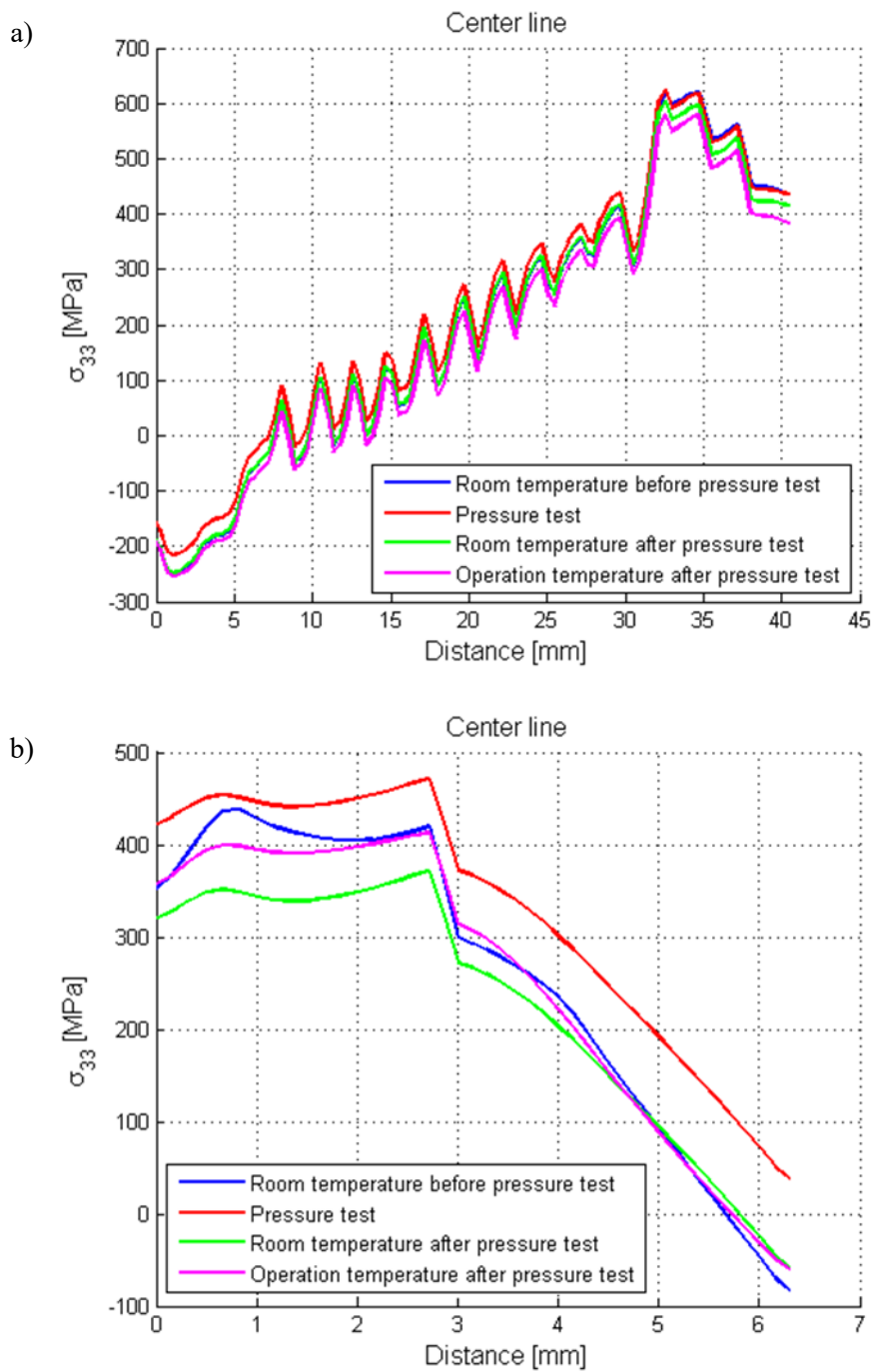


Figure 6 Effect from pressure testing for weld case (a) I.3 and (b) II.3. Both cases belong to BWR units but have different ratio between pipe radius and thickness.

5.3 Effect from detailed simulation of buttering

All weld cases with buttering (weld type I, IV and VI) were simulated including a detailed modelling of the buttering welding process and the corresponding PWHT.

The first version of this report did not include a detailed modelling of the buttering welding process since it was not included in the initial project scope. A comparison between results with and without simulation of the buttering welding process shows a limited influence for paths distant to the buttering region (HAZ Left and Center Line). The comparison for stress levels at the pipe inner diameter close to the buttering (HAZ Right) shows an influence less than ± 100 MPa.

5.4 Effect from extensive machining of welds

After the first revision of this report, it has been found that extensive machining was used to reach final dimensions in some cases, and this can substantially redistribute the stresses and needs to be modelled. The initially supplied documentation was based on the weld geometry in the final state after machining, and therefore information was lacking regarding the extensive machining. The influence from machining at the inner diameter has been studied for weld case I.1 and I.4, see Figure 7 and Figure 8.

In Appendix E, a comparison between results with and without simulation of the machining is presented.

The profiles for axial and hoop stress for weld case I.1 are moderately influenced by the machining. The stresses remain in compression at the inner diameter during normal operation, but the influence is larger for hoop stress for which the depth of the compressive zone is reduced.

The profiles for axial stress for weld case I.4 are highly influenced by the machining, particularly at the inner diameter where the stress state changes from tensile to compressive. The profiles for hoop stress are also highly redistributed, and the tensile stresses increase at the inner diameter.

The influence from machining is larger for weld case I.4, which is explained by the greater thickness reduction (41% for weld case I.4 compared to 21 % for weld case I.1).

Contrary to regular weld capping removal, the investigations shows that machining at the inner diameter of 20 % or more may influence the residual stress state. The analysed weld cases show that the influence is not necessarily beneficial for the residual stress state after machining.

The influence depends on the state prior to machining, component geometry and extent of machining relative to the weld thickness. It is difficult to present a general conclusion and each specific situation should in general be analysed.

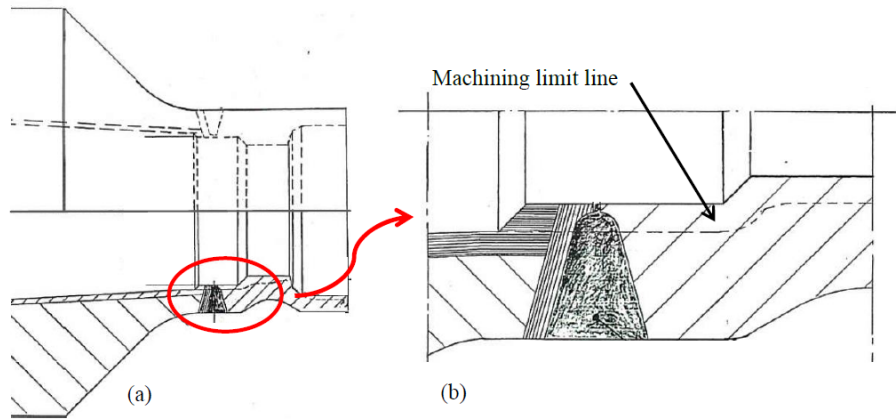


Figure 7 Weld case I.1: (a) Global and (b) detailed view of the feed water nozzle to safe-end weld. The machining results in a thickness reduction of 21 %. The final thickness is 34.5 mm.

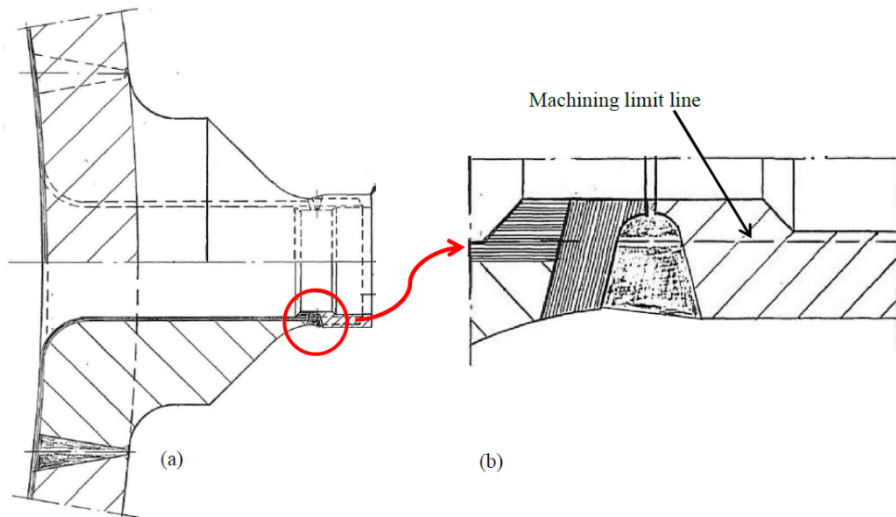


Figure 8 Weld case I.4: (a) Global and (b) detailed view of the shutdown nozzle to safe-end weld. The machining results in a thickness reduction of 41 %. The final thickness is 12.5 mm.

6. Results for recommended residual stress profiles

Results for the weld types and weld cases summarized in Table 1 are presented in this section. Polynomials for the residual stress profiles along paths in the weld centreline, heat affected zones to the left and right of the weld (and in the buttering when available) are presented for each weld case. Detailed stress results for each weld are available in Appendix B.

The residual stresses at room temperature (RT) and operation temperature 286 °C (OT) have been extracted along each path. 5th order polynomials are generated from the through thickness profiles for hoop stress and normal stress. Recommended residual stress profiles are given by the polynomials and the corresponding tabulated coefficients.

As a basis, the results are predicted from analyses with typical heat input data. The sensitivity analyses with reduction in heat input in Section 5.1 show that thin and thick-walled pipes are less sensitive to this change in heat input. However, the most noteworthy change in residual stress level and profile was obtained for medium thick pipes.

This is taken into account for the recommended residual stress profiles for medium thick pipes by choosing results with increased tensile normal stress in the region close to the inner diameter. The motivation behind these choices is that the potential damage mechanism in nickel-based welds is SCC, which can initiate at the inner diameter since it requires a corrosive environment and tensile stress.

The profiles for normal stress are of linear type for thin-walled pipes and of sinusoidal type for thick-walled pipes. The transition from linear type to sinusoidal type occurs gradually for the intermediate pipe thicknesses.

6.1 Weld type I

The geometry and material configuration for weld type I is shown in Figure 9. Arrows in red colour represent the paths evaluated at the positions HAZ Left, Center Line, HAZ Right and in the buttering. The dimensions and welding parameters are tabulated in Table 4.

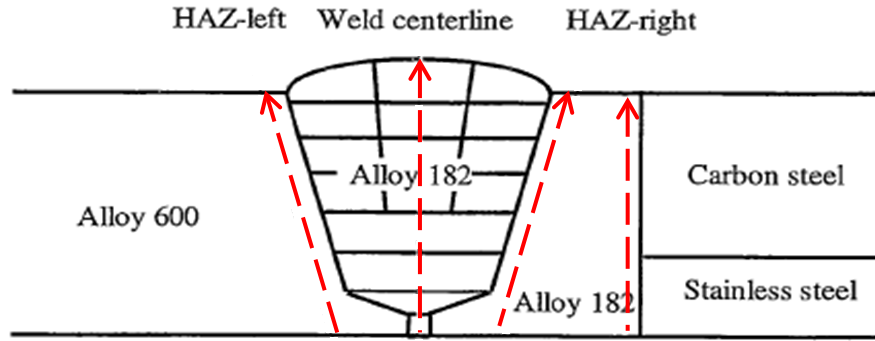


Figure 9 The geometry of weld type I.

Table 4 Dimensions and welding parameters of weld type I.

Weld case	Inner radius [mm]	Thickness [mm]	Passes	Arc energy [MJ/m]	Welding process
I.1	127.5	34.5	35	0.81-1.62	MMA
I.2	139.5	25.5	24	0.78-1.56	MMA
I.3	96.0	40.5	47	0.94-1.88	MMA
I.4	96.9	12.7	11	0.56-1.12	MMA

The weld residual stresses across the thickness for weld case I.1 is described by a 5th degree polynomial. The corresponding coefficients for hoop stress and normal stress are given in Table 5 and Table 6, respectively.

$$\sigma = c_0 + c_1\left(\frac{u}{t}\right) + c_2\left(\frac{u}{t}\right)^2 + c_3\left(\frac{u}{t}\right)^3 + c_4\left(\frac{u}{t}\right)^4 + c_5\left(\frac{u}{t}\right)^5 \quad [\text{MPa}]$$

Table 5 Coefficients for hoop stress along paths for weld case I.1.

Position	Temperature	c ₀	c ₁	c ₂	c ₃	c ₄	c ₅
HAZ Left	Room Temperature	-26.202	-208.31	5546.9	-16678	21477	-9704.9
	Operation Temperature	-31.241	-216.1	5499.9	-16653	21598	-9814.8
Center Line	Room Temperature	-19.278	195.66	3387.8	-10968	14587	-6780.7
	Operation Temperature	-21.722	110.1	3657.2	-11480	15053	-6924.7
HAZ Right	Room Temperature	-1.9706	-306.46	5455.6	-14527	17279	-7573.6
	Operation Temperature	-13.533	-250.15	5236.7	-14231	17096	-7511.4
Buttering	Room Temperature	-441.55	-78.036	3420.4	-7367	6032.7	-1398.3
	Operation Temperature	-430.59	653.68	-1669.8	5039.3	-6648.7	3258.1

Table 6 Coefficients for normal stress along paths for weld case I.1.

Position	Temperature	c ₀	c ₁	c ₂	c ₃	c ₄	c ₅
HAZ Left	Room Temperature	-129.99	-744.73	5566.3	-15762	21541	-10393
	Operation Temperature	-133.15	-655.69	5238.4	-15161	20920	-10137
Center Line	Room Temperature	-87.669	-1497.6	8559.1	-19864	22101	-8881.6
	Operation Temperature	-95.658	-1412	8349	-19609	21946	-8865
HAZ Right	Room Temperature	-231.84	236.11	1756.9	-7948	12779	-6354
	Operation Temperature	-239.66	286.09	1875.4	-8607	13561	-6643.2
Buttering	Room Temperature	-117.39	-2329.3	13697	-30784	31856	-11876
	Operation Temperature	-199.06	-482.47	3440	-7510	8558.3	-3353.9

The weld residual stresses across the thickness for weld case I.2 is described by a 5th degree polynomial. The corresponding coefficients for hoop stress and normal stress are given in Table 7 and Table 8, respectively.

$$\sigma = c_0 + c_1\left(\frac{u}{t}\right) + c_2\left(\frac{u}{t}\right)^2 + c_3\left(\frac{u}{t}\right)^3 + c_4\left(\frac{u}{t}\right)^4 + c_5\left(\frac{u}{t}\right)^5 \quad [\text{MPa}]$$

Table 7 Coefficients for hoop stress along paths for weld case I.2.

Position	Temperature	c ₀	c ₁	c ₂	c ₃	c ₄	c ₅
HAZ Left	Room Temperature	20.089	-44.964	-1294.9	12886	-20811	9653.7
	Operation Temperature	13.099	-219.92	-454.73	11039	-18953	8969.8
Center Line	Room Temperature	102.92	-1392.3	9171.2	-15866	12873	-4613.7
	Operation Temperature	88.763	-1439.7	9059.3	-15207	12119	-4370.3
HAZ Right	Room Temperature	96.014	-1364.6	5090.7	824.66	-10585	6330.8
	Operation Temperature	84.876	-1497.5	5652.9	-274.98	-9571.6	5983.4
Buttering	Room Temperature	-363.17	-1452.6	9998.1	-23267	23586	-8499.7
	Operation Temperature	-382.15	-967.33	7447.8	-17603	18052	-6521

Table 8 Coefficients for normal stress along paths for weld case I.2.

Position	Temperature	c ₀	c ₁	c ₂	c ₃	c ₄	c ₅
HAZ Left	Room Temperature	31.138	-3074.8	11363	-12971	4267	604.26
	Operation Temperature	12.089	-2867.3	10591	-11525	2945.3	1060.4
Center Line	Room Temperature	39.811	-3252.4	11392	-15166	12804	-5901.8
	Operation Temperature	18.513	-3075.4	10896	-14352	11964	-5526.7
HAZ Right	Room Temperature	68.944	-3838.2	14342	-17270	6815.7	96.97
	Operation Temperature	48.771	-3632.4	13618	-16015	5760.3	434.33
Buttering	Room Temperature	47.281	-5249.6	27556	-59584	60524	-22959
	Operation Temperature	-75.428	-3182.3	17563	-38499	40121	-15576

The weld residual stresses across the thickness for weld case I.3 is described by a 5th degree polynomial. The corresponding coefficients for hoop stress and normal stress are given in Table 9 and Table 10, respectively.

$$\sigma = c_0 + c_1\left(\frac{u}{t}\right) + c_2\left(\frac{u}{t}\right)^2 + c_3\left(\frac{u}{t}\right)^3 + c_4\left(\frac{u}{t}\right)^4 + c_5\left(\frac{u}{t}\right)^5 \quad [\text{MPa}]$$

Table 9 Coefficients for hoop stress along paths for weld case I.3.

Position	Temperature	c ₀	c ₁	c ₂	c ₃	c ₄	c ₅
HAZ Left	Room Temperature	-229.09	1024.7	922.72	-8048.2	14615	-7987.2
	Operation Temperature	-231.88	872.44	1743.7	-9896.6	16400	-8598.5
Center Line	Room Temperature	-267.86	1002.8	4731.1	-22629	33946	-16437
	Operation Temperature	-273.06	892.82	5274.5	-23909	35342	-17009
HAZ Right	Room Temperature	-209.45	571.81	3945.5	-14468	20470	-10024
	Operation Temperature	-215.58	438.04	4753.6	-16456	22564	-10809
Buttering	Room Temperature	-314.8	-1314.7	10766	-25123	24815	-8846.7
	Operation Temperature	-338.85	-1067.6	9790.9	-23349	23429	-8463

Table 10 Coefficients for normal stress along paths for weld case I.3.

Position	Temperature	c ₀	c ₁	c ₂	c ₃	c ₄	c ₅
HAZ Left	Room Temperature	-157.01	-1915.5	13102	-31245	33859	-13389
	Operation Temperature	-174.08	-1687	12193	-29636	32632	-13090
Center Line	Room Temperature	-169.32	-3343.7	27949	-80559	98452	-42253
	Operation Temperature	-189.22	-3063.4	26425	-76697	94112	-40512
HAZ Right	Room Temperature	-172.02	-2017.5	14129	-33829	36605	-14461
	Operation Temperature	-187.18	-1830.5	13347	-32414	35547	-14218
Buttering	Room Temperature	-149.17	-3619	21989	-49436	51108	-19543
	Operation Temperature	-228.17	-2313.4	15861	-36892	39298	-15370

The weld residual stresses across the thickness for weld case I.4 is described by a 5th degree polynomial. The corresponding coefficients for hoop stress and normal stress are given in Table 11 and Table 12, respectively.

$$\sigma = c_0 + c_1\left(\frac{u}{t}\right) + c_2\left(\frac{u}{t}\right)^2 + c_3\left(\frac{u}{t}\right)^3 + c_4\left(\frac{u}{t}\right)^4 + c_5\left(\frac{u}{t}\right)^5 \quad [\text{MPa}]$$

Table 11 Coefficients for hoop stress along paths for weld case I.4.

Position	Temperature	c ₀	c ₁	c ₂	c ₃	c ₄	c ₅
HAZ Left	Room Temperature	-30.655	703.1	-260.86	-12.365	-387.98	221.55
	Operation Temperature	-16.322	621.13	-173.63	-108.07	-273.71	170.72
Center Line	Room Temperature	-1.8244	1750.8	-6988.4	18474	-21753	8841.4
	Operation Temperature	17.43	1673.4	-6911.3	18391	-21663	8800
HAZ Right	Room Temperature	51.779	-54.648	3273.7	-3237.2	-1904.7	2186.7
	Operation Temperature	68.859	1.6741	2805.6	-1928.5	-3429.1	2796.4
Buttering	Room Temperature	-458.06	-252.4	5905.1	-18981	25331	-11348
	Operation Temperature	-405.98	235.87	3673.7	-14707	21470	-10026

Table 12 Coefficients for normal stress along paths for weld case I.4.

Position	Temperature	c ₀	c ₁	c ₂	c ₃	c ₄	c ₅
HAZ Left	Room Temperature	-32.026	-860.27	3688.8	-6218.3	5582.5	-2024
	Operation Temperature	-15.773	-811.2	3364.4	-5611.5	4970.7	-1790.7
Center Line	Room Temperature	-88.214	372.32	-3459.6	12401	-15397	6187.1
	Operation Temperature	-71.365	422.69	-3891.1	13396	-16493	6623.9
HAZ Right	Room Temperature	-256.42	1045	-3198.8	10924	-15370	6811.5
	Operation Temperature	-236.75	887.02	-2594.9	10034	-14978	6822.5
Buttering	Room Temperature	-69.438	-1687.1	11207	-30262	36458	-15376
	Operation Temperature	-132.9	-122.83	1637.4	-6772	11683	-6051.9

6.2 Weld type II

The geometry and material configuration for weld type II is shown in Figure 10. Arrows in red colour represent the paths evaluated at the positions HAZ Left, Center Line and HAZ Right. The dimensions and welding parameters are tabulated in Table 13.

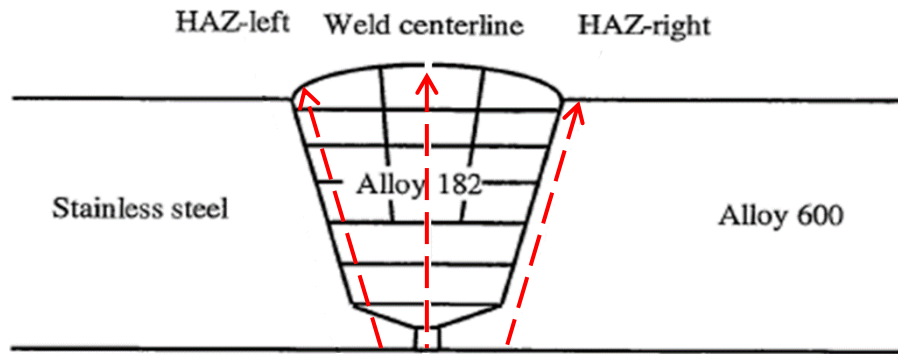


Figure 10 The geometry of weld type II.

Table 13 Dimensions and welding parameters of weld type II.

Type	Inner radius [mm]	Thickness [mm]	Passes	Arc energy [MJ/m]	Welding process
II.1	128.5	16.5	20	0.63-1.26	SMAW
II.2	25.7	4.5	4	0.31-0.83	GTAW
II.3	50.0	6.3	4	0.31-0.83	GTAW
II.4	97.1	12.5	16	0.56-1.12	SMAW

The weld residual stresses across the thickness for weld case II.1 is described by a 5th degree polynomial. The corresponding coefficients for hoop stress and normal stress are given in Table 14 and Table 15, respectively.

$$\sigma = c_0 + c_1\left(\frac{u}{t}\right) + c_2\left(\frac{u}{t}\right)^2 + c_3\left(\frac{u}{t}\right)^3 + c_4\left(\frac{u}{t}\right)^4 + c_5\left(\frac{u}{t}\right)^5 \quad [\text{MPa}]$$

Table 14 Coefficients for hoop stress along paths for weld case II.1.

Position	Temperature	c ₀	c ₁	c ₂	c ₃	c ₄	c ₅
HAZ Left	Room Temperature	288.97	-2004.8	4576.2	5946.3	-19412	10966
	Operation Temperature	115.61	-555.36	3925.1	-1676.6	-5858.6	4398.5
Center Line	Room Temperature	167.26	-1146.0	3392.6	6036	-17294	9099.0
	Operation Temperature	192.94	-763.01	1497.8	9749	-20365	9895.2
HAZ Right	Room Temperature	179.52	-1124.8	2105.2	10923	-23873	12083
	Operation Temperature	225.90	-1199.7	1961.9	11706	-24901	12494

Table 15 Coefficients for normal stress along paths for weld case II.1.

Position	Temperature	c ₀	c ₁	c ₂	c ₃	c ₄	c ₅
HAZ Left	Room Temperature	194.84	-911.85	-10158	45823	-59990	25138
	Operation Temperature	116.48	-422.89	-8318.4	34899	-44424	18157
Center Line	Room Temperature	324.33	-3025.6	-2791.9	36259	-54156	23315
	Operation Temperature	199.91	-1360.7	-8796.5	46521	-62940	26224
HAZ Right	Room Temperature	199.32	-3049.9	2547.2	20190	-37683	17764
	Operation Temperature	192.80	-2765.7	2076.1	19794	-36785	17415

The weld residual stresses across the thickness for weld case II.2 is described by a 5th degree polynomial. The corresponding coefficients for hoop stress and normal stress are given in Table 16 and Table 17, respectively.

$$\sigma = c_0 + c_1\left(\frac{u}{t}\right) + c_2\left(\frac{u}{t}\right)^2 + c_3\left(\frac{u}{t}\right)^3 + c_4\left(\frac{u}{t}\right)^4 + c_5\left(\frac{u}{t}\right)^5 \quad [\text{MPa}]$$

Table 16 Coefficients for hoop stress along paths for weld case II.2.

Position	Temperature	c ₀	c ₁	c ₂	c ₃	c ₄	c ₅
HAZ Left	Room Temperature	351.18	71.07	-2482.5	6482.1	-7488.7	3089.5
	Operation Temperature	262.07	-167.57	-4379.0	20334	-28854	12915
Center Line	Room Temperature	272.24	1204.0	-8118.1	20311	-23011	9239.1
	Operation Temperature	319.81	1031.6	-6417.6	15193	-17566	7354.5
HAZ Right	Room Temperature	214.23	-229.91	5997.4	-18738	20373	-7704.8
	Operation Temperature	258.00	-200.21	5312.8	-17142	18583	-6881.4

Table 17 Coefficients for normal stress along paths for weld case II.2.

Position	Temperature	c ₀	c ₁	c ₂	c ₃	c ₄	c ₅
HAZ Left	Room Temperature	218.61	313.27	3286.7	-22781	33342	-14648
	Operation Temperature	252.08	-409.16	2680.6	-12551	16737	-6918.8
Center Line	Room Temperature	488.89	-1257.7	4260.0	-13013	13917	-4792.0
	Operation Temperature	406.82	-716.41	2613.3	-10779	12889	-4753.1
HAZ Right	Room Temperature	237.39	703.34	-6575.7	14551	-16180	7167.1
	Operation Temperature	229.98	691.73	-6556.2	14433	-15536	6625.8

The weld residual stresses across the thickness for weld case II.3 is described by a 5th degree polynomial. The corresponding coefficients for hoop stress and normal stress are given in Table 18 and Table 19, respectively.

$$\sigma = c_0 + c_1\left(\frac{u}{t}\right) + c_2\left(\frac{u}{t}\right)^2 + c_3\left(\frac{u}{t}\right)^3 + c_4\left(\frac{u}{t}\right)^4 + c_5\left(\frac{u}{t}\right)^5 \quad [\text{MPa}]$$

Table 18 Coefficients for hoop stress along paths for weld case II.3.

Position	Temperature	c ₀	c ₁	c ₂	c ₃	c ₄	c ₅
HAZ Left	Room Temperature	326.29	69.22	-1609.5	4240.5	-5273.7	2322.6
	Operation Temperature	275.36	-2233.6	14278	-30344	26009	-7868.4
Center Line	Room Temperature	333.01	-190.20	3096.0	-10264	10976	-4014.4
	Operation Temperature	370.20	-52.31	2618.4	-9368.1	9597.1	-3227.4
HAZ Right	Room Temperature	359.78	373.21	-1038.6	-1686.4	4577.1	-2627.2
	Operation Temperature	403.13	378.53	-1695.5	657.35	1247.0	-1012.9

Table 19 Coefficients for normal stress along paths for weld case II.3.

Position	Temperature	c ₀	c ₁	c ₂	c ₃	c ₄	c ₅
HAZ Left	Room Temperature	218.31	1155.7	-6935.8	9648.2	-5250.4	924.01
	Operation Temperature	263.32	-1007.0	5705.5	-18032	20964	-8098.0
Center Line	Room Temperature	448.58	-1364.3	3884.9	-9712.4	9401.3	-3045.4
	Operation Temperature	359.16	-848.23	3340.6	-10683	11358	-3862.7
HAZ Right	Room Temperature	245.83	104.47	-4551.5	12260	-14612	6415.8
	Operation Temperature	238.21	95.79	-3964.9	9832.3	-11070	4720.7

The weld residual stresses across the thickness for weld case II.4 is described by a 5th degree polynomial. The corresponding coefficients for hoop stress and normal stress are given in Table 20 and Table 21, respectively.

$$\sigma = c_0 + c_1\left(\frac{u}{t}\right) + c_2\left(\frac{u}{t}\right)^2 + c_3\left(\frac{u}{t}\right)^3 + c_4\left(\frac{u}{t}\right)^4 + c_5\left(\frac{u}{t}\right)^5 \quad [\text{MPa}]$$

Table 20 Coefficients for hoop stress along paths for weld case II.4.

Position	Temperature	c ₀	c ₁	c ₂	c ₃	c ₄	c ₅
HAZ Left	Room Temperature	343.76	-245.46	-5273.1	24184	-33973	15302
	Operation Temperature	195.84	-361.68	3835.8	-5997.7	2015.9	616.90
Center Line	Room Temperature	272.71	-1379.2	6434.4	-5172.5	-3853.7	3892.8
	Operation Temperature	291.11	-1005.6	4509.0	-870.37	-8133.4	5356.6
HAZ Right	Room Temperature	251.98	77.49	-1030.4	9045.6	-15667	7541.2
	Operation Temperature	286.77	9.33	-1114.3	9823.1	-16900	8112.2

Table 21 Coefficients for normal stress along paths for weld case II.4.

Position	Temperature	c ₀	c ₁	c ₂	c ₃	c ₄	c ₅
HAZ Left	Room Temperature	187.64	158.88	-13765	49560	-61461	25339
	Operation Temperature	124.63	-253.52	-6156.2	24977	-32002	13249
Center Line	Room Temperature	270.93	-2059.9	-2834.0	29773	-45599	20290
	Operation Temperature	159.21	-866.10	-6383.0	35061	-50040	21871
HAZ Right	Room Temperature	104.63	-1684.4	2073.1	11509	-24542	12444
	Operation Temperature	105.51	-1524.8	1837.3	10950	-23440	11954

6.3 Weld type III

The geometry and material configuration for weld type III is shown in Figure 11. Arrows in red colour represent the paths evaluated at the positions HAZ Left, Center Line and HAZ Right. The dimensions and welding parameters are tabulated in Table 22.

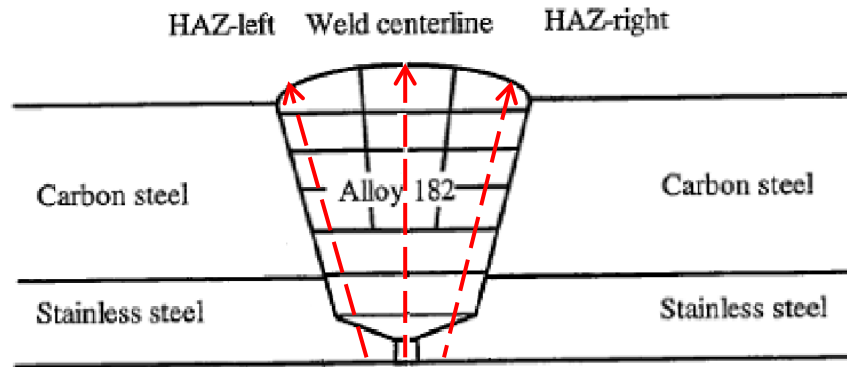


Figure 11 The geometry of weld type III.

Table 22 Dimensions and welding parameters of weld type III.

Type	Inner radius [mm]	Thickness [mm]	Passes	Arc energy [MJ/m]	Welding process
III.1	300.0	35.0	46	1.30	MMA

The weld residual stresses across the thickness for weld case III.1 is described by a 5th degree polynomial. The corresponding coefficients for hoop stress and normal stress are given in Table 23 and Table 24, respectively.

$$\sigma = c_0 + c_1\left(\frac{u}{t}\right) + c_2\left(\frac{u}{t}\right)^2 + c_3\left(\frac{u}{t}\right)^3 + c_4\left(\frac{u}{t}\right)^4 + c_5\left(\frac{u}{t}\right)^5 \quad [\text{MPa}]$$

Table 23 Coefficients for hoop stress along paths for weld case III.1.

Position	Temperature	c ₀	c ₁	c ₂	c ₃	c ₄	c ₅
HAZ Left	Room Temperature	305	-4909	27170	-58068	57964	-22209
	Operation Temperature	29.454	-3584.5	26810	-65575	70699	-28187
Center Line	Room Temperature	269.92	-3893.6	21670	-44044	40593	-14230
	Operation Temperature	173.84	-2845.9	16316	-32505	29465	-10269
HAZ Right	Room Temperature	323.98	-4844	25411	-51250	47415	-16709
	Operation Temperature	45.092	-3456.4	24682	-57747	58830	-22054

Table 24 Coefficients for normal stress along paths for weld case III.1.

Position	Temperature	c ₀	c ₁	c ₂	c ₃	c ₄	c ₅
HAZ Left	Room Temperature	352.16	-6319.5	24330	-43257	40430	-15467
	Operation Temperature	161.4	-5085.2	24608	-52323	54361	-21697
Center Line	Room Temperature	391.69	-7129.8	27742	-48225	42017	-14549
	Operation Temperature	116.36	-3697.4	14309	-23807	20798	-7492.1
HAZ Right	Room Temperature	344.81	-5587.4	18105	-22569	11022	-920.87
	Operation Temperature	152.21	-4371.4	18658	-32611	26324	-7814.9

6.4 Weld type IV

The geometry and material configuration for weld type IV is shown in Figure 12. Arrows in red colour represent the paths evaluated at the positions HAZ Left, Center Line, HAZ Right and in the buttering. The dimensions and welding parameters are tabulated in Table 25.

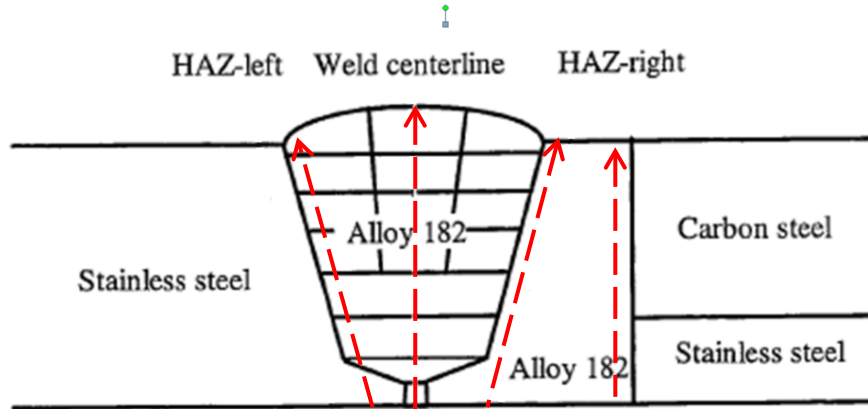


Figure 12 The geometry of weld type IV.

Table 25 Dimensions and welding parameters of weld type IV.

Type	Inner radius [mm]	Thickness [mm]	Passes	Arc energy [MJ/m]	Welding process
IV.1	300.0	40.0	48	1.50	MMA
IV.2	52.5	15.5	17	1.00	MMA
IV.3	151.0	42.0	54	1.00	MMA
IV.4	66.0	21.5	20	1.00	MMA

The weld residual stresses across the thickness for weld case IV.1 is described by a 5th degree polynomial. The corresponding coefficients for hoop stress and normal stress are given in Table 26 and Table 27, respectively.

$$\sigma = c_0 + c_1\left(\frac{u}{t}\right) + c_2\left(\frac{u}{t}\right)^2 + c_3\left(\frac{u}{t}\right)^3 + c_4\left(\frac{u}{t}\right)^4 + c_5\left(\frac{u}{t}\right)^5 \quad [\text{MPa}]$$

Table 26 Coefficients for hoop stress along paths for weld case IV.1.

Position	Temperature	c ₀	c ₁	c ₂	c ₃	c ₄	c ₅
HAZ Left	Room Temperature	161.53	-379.2	-2587.1	14888	-19502	7723.3
	Operation Temperature	-29.239	2031.1	-9136.3	21403	-20691	6782
Center Line	Room Temperature	122.83	-1043.9	6398.1	-14990	19044	-9262.1
	Operation Temperature	160.14	-431.06	3272.1	-8408.4	12905	-7231.1
HAZ Right	Room Temperature	144.64	-2391.1	12873	-24595	23318	-9063
	Operation Temperature	184.34	-2302.2	12794	-24972	23940	-9350.1
Buttering	Room Temperature	141	-3380.9	4968.8	941.17	-757.43	-1521.1
	Operation Temperature	179.78	-3078.7	3681.3	3161.1	-2779.4	-756.98

Table 27 Coefficients for normal stress along paths for weld case IV.1.

Position	Temperature	c ₀	c ₁	c ₂	c ₃	c ₄	c ₅
HAZ Left	Room Temperature	203.04	-4069.3	14255	-21335	16940	-5862.1
	Operation Temperature	119.89	-2744.1	9048.7	-12413	9621.7	-3529.8
Center Line	Room Temperature	279.31	-5342.2	21146	-40519	41737	-17271
	Operation Temperature	125.7	-2891.6	10124	-18318	21173	-10278
HAZ Right	Room Temperature	370.07	-6730.7	26785	-49309	46978	-18044
	Operation Temperature	256.08	-5231.2	21231	-38983	37135	-14420
Buttering	Room Temperature	447.18	-6654.6	20564	-24737	12209	-1419.1
	Operation Temperature	295.32	-4959.6	16170	-20824	11681	-2040.7

The weld residual stresses across the thickness for weld case IV.2 is described by a 5th degree polynomial. The corresponding coefficients for hoop stress and normal stress are given in Table 28 and Table 29, respectively.

$$\sigma = c_0 + c_1\left(\frac{u}{t}\right) + c_2\left(\frac{u}{t}\right)^2 + c_3\left(\frac{u}{t}\right)^3 + c_4\left(\frac{u}{t}\right)^4 + c_5\left(\frac{u}{t}\right)^5 \quad [\text{MPa}]$$

Table 28 Coefficients for hoop stress along paths for weld case IV.2.

Position	Temperature	c ₀	c ₁	c ₂	c ₃	c ₄	c ₅
HAZ Left	Room Temperature	273.21	-146.94	-3548.9	18339	-27180	12448
	Operation Temperature	106.32	-1049.8	11368	-24786	20751	-6169
Center Line	Room Temperature	18.367	371.51	-7151.9	34541	-49400	21859
	Operation Temperature	51.326	1073.1	-10419	40996	-55300	23838
HAZ Right	Room Temperature	-38.48	-1491.8	4799.1	5782.8	-21340	12769
	Operation Temperature	32.712	-1641	5704.6	2623.8	-17174	10935
Buttering	Room Temperature	-267.13	1679.2	-18950	57747	-64244	24283
	Operation Temperature	-235.23	1985.5	-20228	60038	-66537	25249

Table 29 Coefficients for normal stress along paths for weld case IV.2.

Position	Temperature	c ₀	c ₁	c ₂	c ₃	c ₄	c ₅
HAZ Left	Room Temperature	82.26	-170.99	-10208	45959	-63699	27960
	Operation Temperature	13.398	-568.23	-3400.3	24555	-38677	18008
Center Line	Room Temperature	189.25	-1352.3	-6939.8	39107	-53955	22876
	Operation Temperature	-1.0514	708.26	-14079	51256	-64207	26192
HAZ Right	Room Temperature	200.2	-4553.5	20053	-38081	34068	-11538
	Operation Temperature	144.99	-3990.7	18473	-35285	30953	-10174
Buttering	Room Temperature	12.963	-1298.1	-2553.4	22906	-34836	16268
	Operation Temperature	-87.555	-404.12	-3366.3	20092	-29700	13887

The weld residual stresses across the thickness for weld case IV.3 is described by a 5th degree polynomial. The corresponding coefficients for hoop stress and normal stress are given in Table 30 and Table 31, respectively.

$$\sigma = c_0 + c_1\left(\frac{u}{t}\right) + c_2\left(\frac{u}{t}\right)^2 + c_3\left(\frac{u}{t}\right)^3 + c_4\left(\frac{u}{t}\right)^4 + c_5\left(\frac{u}{t}\right)^5 \quad [\text{MPa}]$$

Table 30 Coefficients for hoop stress along paths for weld case IV.3.

Position	Temperature	c ₀	c ₁	c ₂	c ₃	c ₄	c ₅
HAZ Left	Room Temperature	89.982	-451.6	-601.26	6745.6	-7792	2295.1
	Operation Temperature	- 144.01	2844	-10748	20014	-14825	3194.6
Center Line	Room Temperature	32.254	-1489	10364	-26383	32506	-14721
	Operation Temperature	84.844	-604.06	5565.7	-15299	21137	-10649
HAZ Right	Room Temperature	8.208	-2136.3	13540	-28657	29400	-11843
	Operation Temperature	71.961	-2067.2	13687	-29494	30211	-12135
Buttering	Room Temperature	- 197.17	-3689.7	18170	-41917	47009	-19082
	Operation Temperature	- 147.28	-2905.3	13675	-31443	35905	-14760

Table 31 Coefficients for normal stress along paths for weld case IV.3.

Position	Temperature	c ₀	c ₁	c ₂	c ₃	c ₄	c ₅
HAZ Left	Room Temperature	189.74	-3674.6	13657	-21617	17298	-5770.5
	Operation Temperature	63.333	-2020.8	6974	-9678.7	7342	-2585.5
Center Line	Room Temperature	268.72	-5495.1	24235	-49795	51556	-20811
	Operation Temperature	53.452	-2283.1	9152.5	-17932	20881	-9972.5
HAZ Right	Room Temperature	301.3	-6331.5	27392	-53215	51571	-19727
	Operation Temperature	155.46	-4536.6	20547	-39872	38438	-14787
Buttering	Room Temperature	267.98	-5643.8	20937	-31915	22770	-6071
	Operation Temperature	86.399	-3006.4	10526	-13327	6881.8	-880.77

The weld residual stresses across the thickness for weld case IV.4 is described by a 5th degree polynomial. The corresponding coefficients for hoop stress and normal stress are given in Table 32 and Table 33, respectively.

$$\sigma = c_0 + c_1\left(\frac{u}{t}\right) + c_2\left(\frac{u}{t}\right)^2 + c_3\left(\frac{u}{t}\right)^3 + c_4\left(\frac{u}{t}\right)^4 + c_5\left(\frac{u}{t}\right)^5 \quad [\text{MPa}]$$

Table 32 Coefficients for hoop stress along paths for weld case IV.4.

Position	Temperature	c ₀	c ₁	c ₂	c ₃	c ₄	c ₅
HAZ Left	Room Temperature	126.8	-730.3	-2217.3	23329	-38507	18249
	Operation Temperature	-74.599	210.93	1980.6	3513.5	-12522	7164.2
Center Line	Room Temperature	-129	69.4	-2305.8	19582	-30608	13661
	Operation Temperature	-97.215	1016.9	-7387.7	30671	-41516	17576
HAZ Right	Room Temperature	-66.015	-2172.9	5746.7	10406	-30723	17252
	Operation Temperature	0.25635	-2263.6	6313.5	8123.4	-27632	15900
Buttering	Room Temperature	-362.37	1480.9	-19942	65164	-74511	28495
	Operation Temperature	-315.83	1727.4	-21225	67532	-76752	29371

Table 33 Coefficients for normal stress along paths for weld case IV.4.

Position	Temperature	c ₀	c ₁	c ₂	c ₃	c ₄	c ₅
HAZ Left	Room Temperature	60.101	-94.782	-13740	58810	-78541	33457
	Operation Temperature	-44.124	298.03	-10983	45974	-61759	26476
Center Line	Room Temperature	127.14	-1213.7	-7278.5	37912	-49490	19924
	Operation Temperature	-79.134	1407.1	-17665	57455	-67146	25945
HAZ Right	Room Temperature	176.45	-4687.6	18732	-30654	23462	-6794.1
	Operation Temperature	122.36	-4057.1	16958	-27765	20479	-5545
Buttering	Room Temperature	10.913	-1852.4	-379.67	20082	-33184	15841
	Operation Temperature	-103.1	-344.78	-4623.7	24372	-34382	15512

6.5 Weld type V

The geometry and material configuration for weld type V is shown in Figure 13. Arrows in red colour represent the paths evaluated at the positions HAZ Left, Center Line and HAZ Right. The dimensions and welding parameters are tabulated in Table 34.

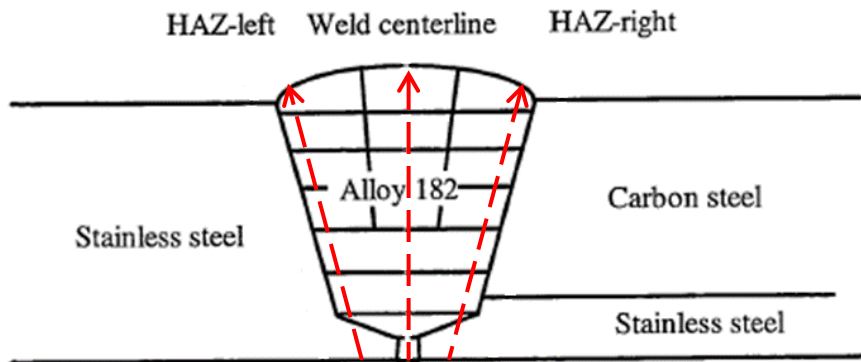


Figure 13 The geometry of weld type V.

Table 34 Dimensions and welding parameters of weld type V.

Type	Inner radius [mm]	Thickness [mm]	Passes	Arc energy [MJ/m]	Welding process
V.1	300.0	67.0	90	1.30	MMA

The weld residual stresses across the thickness for weld case V.1 is described by a 5th degree polynomial. The corresponding coefficients for hoop stress and normal stress are given in Table 35 and Table 36, respectively.

$$\sigma = c_0 + c_1\left(\frac{u}{t}\right) + c_2\left(\frac{u}{t}\right)^2 + c_3\left(\frac{u}{t}\right)^3 + c_4\left(\frac{u}{t}\right)^4 + c_5\left(\frac{u}{t}\right)^5 \quad [\text{MPa}]$$

Table 35 Coefficients for hoop stress along paths for weld case V.1.

Position	Temperature	c ₀	c ₁	c ₂	c ₃	c ₄	c ₅
HAZ Left	Room Temperature	49.683	-1673.2	10322	-25381	30350	-13387
	Operation Temperature	-134.25	2911.8	-12615	23725	-16755	3216
Center Line	Room Temperature	136.44	-4223.6	25772	-57131	56660	-20804
	Operation Temperature	122.28	-2498.1	16532	-36441	35769	-13063
HAZ Right	Room Temperature	114.71	-4551.7	30946	-76622	82722	-32321
	Operation Temperature	-56.923	-302.12	8274.3	-26107	32353	-13831

Table 36 Coefficients for normal stress along paths for weld case V.1.

Position	Temperature	c ₀	c ₁	c ₂	c ₃	c ₄	c ₅
HAZ Left	Room Temperature	213.17	-5692.6	29695	-68698	74667	-30186
	Operation Temperature	55.156	-1988.9	9807.8	-24141	29522	-13227
Center Line	Room Temperature	382.23	-8466.4	41246	-86965	84431	-30290
	Operation Temperature	67.139	-2473.6	10854	-20813	19559	-6968.1
HAZ Right	Room Temperature	351.24	-8377.4	41964	-89246	86312	-30709
	Operation Temperature	144.43	-4020.4	20082	-42177	40082	-13859

6.6 Weld type VI

The geometry and material configuration for weld type VI is shown in Figure 14. Arrows in red colour represent the paths evaluated at the positions HAZ Left, Center Line, HAZ Right and in the buttering. The dimensions and welding parameters are tabulated in Table 37. The bead sequence adopted for this weld type is shown in Figure 15.

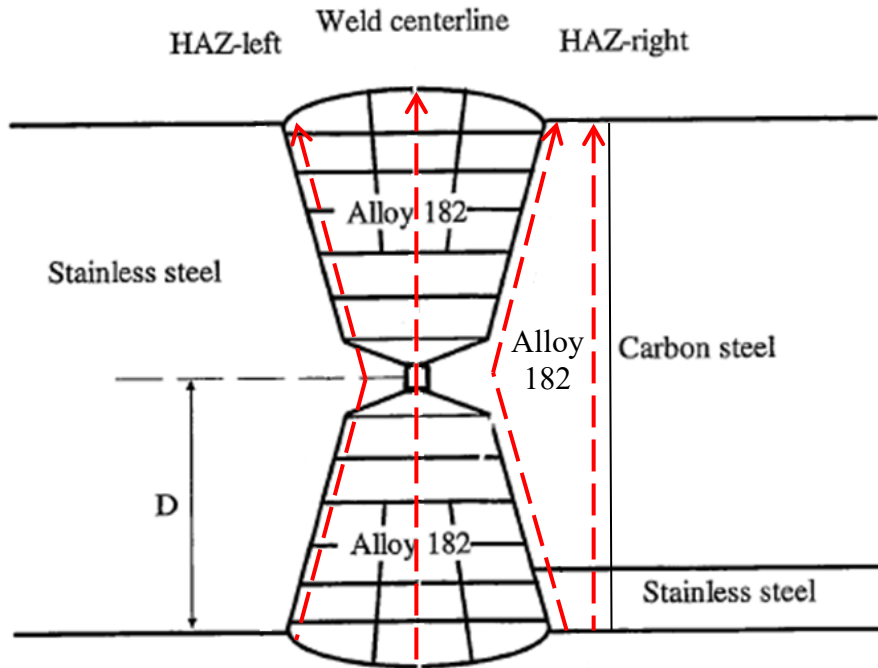


Figure 14 The geometry of weld type VI.

Table 37 Dimensions and welding parameters of weld type VI.

Type	Inner radius [mm]	Thickness [mm]	Passes	Arc energy [MJ/m]	Welding process
VI.1	348.5	79.5	96	1.50	MMA

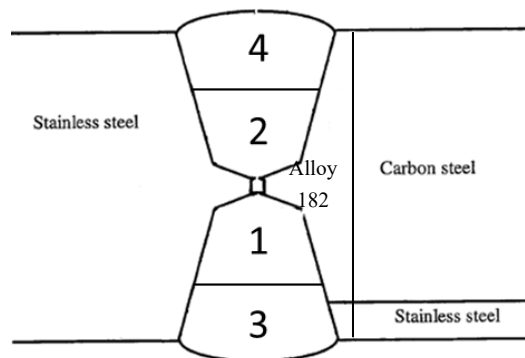


Figure 15 Bead sequence adopted for weld type VI.

The weld residual stresses across the thickness for weld case VI.1 is described by a 5th degree polynomial. The corresponding coefficients for hoop stress and normal stress are given in Table 38 and Table 39, respectively.

$$\sigma = c_0 + c_1\left(\frac{u}{t}\right) + c_2\left(\frac{u}{t}\right)^2 + c_3\left(\frac{u}{t}\right)^3 + c_4\left(\frac{u}{t}\right)^4 + c_5\left(\frac{u}{t}\right)^5 \quad [\text{MPa}]$$

Table 38 Coefficients for hoop stress along paths for weld case VI.1.

Position	Temperature	c ₀	c ₁	c ₂	c ₃	c ₄	c ₅
HAZ Left	Room Temperature	42.839	9696.6	-56952	1.1374e+05	-90238	23977
	Operation Temperature	39.555	9103	-54491	1.0996e+05	-88143	23796
Center Line	Room Temperature	106.78	8652	-49700	92260	-63362	12291
	Operation Temperature	76.537	8654.4	-50403	94109	-64955	12739
HAZ Right	Room Temperature	75.523	10734	-63306	1.2316e+05	-92543	22115
	Operation Temperature	21.616	11005	-65046	1.2688e+05	-95735	23093
Buttering	Room Temperature	377.01	-179.65	-7494.8	19558	-18000	6326.1
	Operation Temperature	310.97	576.98	-12037	29415	-27031	9333.1

Table 39 Coefficients for normal stress along paths for weld case VI.1.

Position	Temperature	c ₀	c ₁	c ₂	c ₃	c ₄	c ₅
HAZ Left	Room Temperature	225.5	5888.4	-47437	1.0309e+05	-86111	24596
	Operation Temperature	187.32	5718	-45140	97115	-79906	22259
Center Line	Room Temperature	323.17	5275.1	-44997	94692	-73388	18349
	Operation Temperature	262.1	5452.9	-44392	92336	-70828	17426
HAZ Right	Room Temperature	125.28	7631.4	-54496	1.1122e+05	-85531	21158
	Operation Temperature	28.135	8704.8	-58862	1.1969e+05	-93277	23824
Buttering	Room Temperature	317.33	3312.9	-34409	78989	-68766	20987
	Operation Temperature	130.66	5599.7	-44023	97679	-85706	26755

7. Conclusions

Residual stresses in nickel-based dissimilar metal pipe butt-welds have been analysed by numerical welding simulation. Detailed welding simulations have been performed for a set of cases with nickel-based welds in Swedish nuclear power plants. The nickel-based welds were grouped in different weld types based on the design of materials constituting the joint, including the buttering configuration. Each weld type contains several weld cases encompassing different thickness, pipe radius, number of weld passes, arc energy and welding process.

The modelling method used for the 2D axisymmetric numerical simulations in this report has been developed and validated within different projects, see for example [9], [10] and [11].

The effect from the individual simulation steps (i.e. buttering welding process, PWHT, pressure testing and machining) has been illustrated and discussed.

Recommended weld residual stress profiles have been developed for all weld cases. As a basis, the results are predicted from analyses with typical heat input data. Typical data has been used for influencing parameters with the aim to establish realistic through-thickness stress distributions. Sensitivity analyses with reduction in heat input show that residual stress levels and profiles for medium thick pipes are most sensitive to this change in heat input. This was accounted for when developing the recommended weld residual stress profiles.

Each weld case has been evaluated along paths in the weld centreline, HAZ regions and in the buttering when present. The recommended weld residual stress profiles are given as 5th order polynomials.

Welds deviating from the conditions assumed in this report are recommended to be handled with individual simulations. Examples of such deviations are (but not limited to); geometries other than straight pipes, different weld joint geometries, circumferential welds closer than $2.5\sqrt{Rt}$, effect from severe operational transients, or influence from welding start/stop positions.

The results also need to be generally updated if significant improvements in numerical modelling or experimental measurements are confirmed as well as if information regarding parameters critical to the weld residual stress state is revealed.

The weld residual stress profiles in this report are best-estimate predictions using typical data. It is increasingly important to perform sensitivity studies as part of a defect tolerance assessment since these profiles are best-estimate predictions rather than upper-bound estimates.

8. Suggested further work

During the course of the project, a few areas have been identified where work can be performed to further improve the results.

Additional sensitivity analyses for medium thick pipes

The heat source modelling used in this report implies challenges regarding sensitivity analysis since temperature control is applied. In addition, the 2D axisymmetric approximation makes it difficult to properly model thermal effects in the welding direction. Further, the sensitivity analysis needs to be performed with realistic ranges of welding parameters which would ensure acceptable weld quality for a given bead size. Heat input outside this range requires corresponding changes regarding bead size. It is suggested to perform additional sensitivity analyses regarding heat input, in particular for medium thick pipe welds.

Review of weld machining

The effect from machining of welds is noticeable for thickness reductions in the order of 20 % or more. This report contains analyses for two weld cases. A detailed review of the weld documentation is suggested to investigate the degree of machining for all weld cases, and to perform additional analyses for weld cases identified with extensive machining.

Validation of nickel-base welds to experimental measurements

In this report, only one reference with experimental weld residual stress measurements was found similar to the current weld cases (i.e. buttering, weld joint geometry, and bead sequence from the outside only). It is suggested to search for further references with experimental measurements for weld cases similar to the conditions for the welds in the current report. If no relevant cases are found, it is further suggested that relevant validation cases are proposed. This serve as a basis for the possibility to manufacture mock-ups and perform experimental weld residual stress measurements with detailed documentation.

9. Acknowledgments

This work has been financially supported by the Swedish Radiation Safety Authority (SSM), and the utilities OKG Aktiebolag and Ringhals AB. The support is gratefully acknowledged.

10. References

- [1] Dillström P, Gunnars J, von Unge P, Mångård D, "Procedure for Safety Assessment of Components with Defects - Handbook Edition 5 - SSM 2018:18," Swedish Radiation Safety Authority.
- [2] B. Brickstad och L. Josefson, "A Parametric Study of Residual Stresses in Multipass Butt-Welded Stainless Steel Pipes".
- [3] P. Delfin, B. Brickstad och L. Josefson, "Residual Stresses in Multi-Pass Butt-Welded Bimetallic Piping, Part I".
- [4] P. Delfin, B. Brickstad och J. Gunnars, "Residual Stresses in Multi-Pass Butt-Welded Bimetallic Piping, Part II".
- [5] J. Gunnars och M. Andersson, "Residual stresses in heat treated bi-metallic pipe weld – NESC III / ADIMEW," 2004.
- [6] M. Smith och A. Smith, "NeT bead-on-plate round robin: Comparison of transient thermal predictions and measurements," *International Journal of Pressure Vessels and Piping*, vol. 86, pp. 96-109, 2009.
- [7] P. Bouchard, "The NeT Bead-on-plate benchmark for weld residual stress simulation," *International Journal of Pressure Vessels and Piping*, vol. 86, pp. 31-42, 2009.
- [8] M. Smith och A. Smith, "NeT bead-on-plate round robin: Comparison of residual stress prediction and measurements," *International Journal of Pressure Vessels and Piping*, vol. 86, pp. 79-95, 2009.
- [9] W. Zang, J. Gunnars, P. Dong och J. Hong, "Improvement and Validation of Weld Residual Stress Modelling Procedure," 2009.
- [10] J. Mullins och J. Gunnars, "Influence of Hardening Model on Weld Residual Stress Distribution," 2009.
- [11] J. Mullins and J. Gunnars, "Validation of Weld Residual Stress Modeling in the NRC International Round Robin Study - SSM 2013:01," Swedish Radiation Safety Authority.
- [12] E. Bonnaud and J. Gunnars, "Effect of weld repairs on residual stresses in nickel base dissimilar metal welds - SSM 2017:22," Swedish Radiation Safety Authority.
- [13] J.H. Argyris, J. Szimmat and K. William, "Finite element analysis of arc-welding process," i *Numerical methods in thermal problems – Proceedings of the third International Conference*, 1983.
- [14] D. Rosenthal, "Mathematical theory of heat distribution during welding and cutting," *Welding Journal*, vol. 20, pp. 220-234, 1941.
- [15] E. Friedman, "Thermomechanical Analysis of the Welding Process using the Finite Element Method," *Journal of Pressure Vessel Technology*, vol. 97, pp. 206-213, 1975.
- [16] J. Goldak, A. Chakravarti och M. Bibby, "A New Finite Element Model for Welding Heat Sources," *Met. Trans. B*, vol. 15, pp. 299-305, 1984.

- [17] Taylor, G.A. et al., "Finite volume methods applied to the computational modelling of welding phenomena," i *Proceedings of Int. Conf. on CFD in the Minerals and Process Industries, CSIRO*, Melbourne, Australia, 1999.
- [18] T. Eagar och N. Tsai, "Temperature Fields Produced by Traveling Distributed Heat Sources," *Welding Research Supplement*, pp. 346-355, 1983.
- [19] J. Price, A. Ziara-Paradowska, S. Joshi, T. Finlayson, C. Semetay och H. Nied, "Comparison of experimental and theoretical residual stresses in welds: The issue of gauge volume," *Int. J. Mechanical Sciences*, vol. 50, pp. 513-521, 2008.
- [20] P. Dong och e. al, "JIP on Residual Stress Estimate and Post-Weld Heat Treatment," 2002-2005.
- [21] P. Dong och J. Hong, "Recommendations on Residual Stress Estimate for Fitness-for-Service Assessment".
- [22] J. Mullins and J. Gunnars, "Deformation Histories Relevant to Multipass Girth Welds: Temperature, Stress and Plastic Strain Histories," *Materials Science Forum*, vol. 681, pp. 61-66, 2011.
- [23] J. Mullins and J. Gunnars, "PVP2012-78599: WELDING SIMULATION: RELATIONSHIP BETWEEN WELDING GEOMETRY AND DETERMINATION OF HARDENING MODEL," i *Proceedings of the ASME 2012 Pressure Vessels and Piping Conference*, July 15-19, 2012, Toronto, Canada.
- [24] Edwards, L., et al., "Advances in Residual Stress Modeling and Measurement for the Structural Integrity Assessment of Welded Thermal Power Plant," *Advanced Materials Research*, Vol. %1 av %241-42, pp. 391-400, 2008.
- [25] M. Kartal et al., "Determination of Weld Metal Mechanical Properties Utilising Novel Tensile Testing Methods," *Applied Mechanics and Materials*, Vol. %1 av %27-8, pp. 127-132, 2007.
- [26] Y. Xinghua et. al, "PVP2014-28869 High Temperature Dynamics Strain Hardening Behavior in Stainless Steels and Nickel Alloys," i *Proceedings of the ASME 2014 Pressure Vessels & Piping Conference*, July 20-24, 2014, Anaheim, California, USA.
- [27] EPRI, "Materials Reliability Program: Finite-Element Model Validation for Dissimilar Metal Butt-Welds (MRP-316 Revision 1): Volumes 1 and 2," 2015.

Table of Revisions

Rev. No.	Cause	Handled by	Date
0	First issue.	Etienne Bonnaud, Daniel Mångård, Jens Gunnars	2014-05-03
1	Updated results to include buttering welding simulation and PWHT.	Etienne Bonnaud, Daniel Mångård, Jens Gunnars	2015-01-22
2	Updated results to include the effect of extensive machining for some nozzles.	Etienne Bonnaud	2016-07-15
3	Text in all sections revised based on review comments.	Daniel Mångård, Jens Gunnars	2024-02-28

Appendix A – Material properties

Numerical welding simulation requires thermal, physical and mechanical properties as function of temperature. This appendix summarises the temperature dependent material properties used in the current work for nickel based alloy 82, austenitic stainless steel 316 and ferritic steel 508 Class 3.

Thermal and physical properties

The temperature dependent thermal and physical properties are thermal conductivity, specific heat capacity, density and latent heat.

For nickel based alloy 82 and the austenitic stainless steel 316, the temperature dependent thermal and physical properties are based on data published by the NRC [A1]. For alloy 82, the properties are obtained through testing and these properties are also very similar for other nickel-based alloys such as alloy 182 and alloy 600.

For ferritic steel 508 Class 3, the temperature dependent thermal and physical properties are based on the data published by the NRC [A4].

The thermal and physical properties are summarised in Table A1 – A3.

Table A1. Thermal and physical properties as a function of temperature for nicked-based alloy 82.

Temperature [°C]	Conductivity [W/m °C] [A1]	Specific heat [J/kg °C] [A1]
20	14.2	444
200	17.2	486
400	20.8	519
600	24.3	578
800	27.8	611
1000	31.3	645
1200	34.8	679
1400	38.2	713
Density 8470 kg/m ³ [A1].		
Latent heat at melting temperature 297 600 J/kg [A1].		

Table A2. Thermal and physical properties as a function of temperature for austenitic stainless steel 316.

Temperature [°C]	Conductivity [W/m °C] [A1]	Specific heat [J/kg °C] [A1]
20	14.7	452
200	17.2	513
400	20.0	550
600	22.2	577
800	25.2	591
1000	28.1	599
1200	30.9	607
1400	33.8	616
Density 7900 kg/m ³ [A1].		
Latent heat at melting temperature 225 600 J/kg [A1].		

Table A3. Thermal and physical properties as a function of temperature for ferritic steel 508 Class 3.

Temperature [°C]	Conductivity [W/m °C] [A4]	Specific heat [J/kg °C] [A4]
20	51.9	460
200	48.3	532
400	42.7	630
600	35.6	798
800	26.0	925
1000	27.2	846
1200	29.7	842
1400	-	-
Density 7850 kg/m ³ is assumed.		

Mechanical properties

The temperature dependent mechanical properties required for welding simulations are the elastic and plastic material properties as well as thermal expansion.

For nickel based alloy 82 and ferritic steel 508 Class 3, an isotropic constitutive material model was used. While, mixed isotropic-kinematic constitutive material model was used for austenitic stainless steel 316. Furthermore, material annealing was included and simulated for high temperatures.

For the nickel based alloy 82, temperature dependent mechanical properties are based upon data supplied by the NRC [A2].

For the austenitic stainless steel 316, temperature dependent mechanical properties are based upon the data supplied by the NRC [A2], NESC III [A3] as well as from the work performed in [A6-A9].

For the ferritic steel 508 Class 3, temperature dependent mechanical properties are based on the data published by the NRC [A4], NESC III [A3] and ASME II [A5].

Note that to avoid non-conservative estimates of the residual stresses, it is important to use typical values for the yield properties rather than minimum required properties.

The mechanical properties used are summarized in Table A4 – A6.

Table A4. Mechanical properties as a function of temperature for nicked-based alloy 82.

Temperature [°C]	Young's modulus [GPa] [A2]	Poisson's ratio [-] [A2]	Yield stress [MPa] [A2]	Thermal expansion [10 ⁻⁶ 1/°C] [A2]
20	214	0.29	312	12.4
200	203	0.32	280	13.6
400	192	0.36	205	14.4
600	180	0.40	164	15.3
800	164	0.40	135	16.1
1000	143	0.40	71	16.7
1200	92	0.40	64	17.3
1400	-	-	-	17.8

Table A5. Mechanical properties as a function of temperature for austenitic stainless steel 316.

Temperature [°C]	Young's modulus [GPa] [A2]	Poisson's ratio [-] [A2]	Yield stress [MPa] [A6]	Thermal expansion [10 ⁻⁶ 1/°C] [A3]
20	195	0.27	217	16.4
200	183	0.31	121	17.2
400	168	0.29	110	18.1
600	152	0.24	76	18.7
800	133	0.22	140	19.1
1000	100	0.22	50	19.3
1200	-	-	-	19.8
1400	-	-	-	18.6

Table A6. Mechanical properties as a function of temperature for ferritic steel 508 Class 3.

Temperature [°C]	Young's modulus [GPa] [A4]	Poisson's ratio [-] [A4]	Yield stress [MPa] [A3]	Thermal expansion [10 ⁻⁶ 1/°C] [A5]
20	212	0.30	393	12.6
200	204	0.30	363	13.6
400	190	0.30	318	14.4
600	155	0.30	216	15.0
800	95	0.30	58	15.3
1000	68	0.30	-	-
1200	42	0.30	-	-
1400	15	0.30	-	-

References Appendix A

- [A1] US Nuclear Regulatory Commission, "International Weld Residual Stress Round Robin Problem Statement - Version 1.0," Office of Nuclear Regulatory Research, Division of Engineering, Component Integrity Branch, 2009.
- [A2] 'Phase 2a Mockup-Materials.xls', Computer file from email communication sent from Howard Rathbun to Jonathan Mullins, 23-02-2011.
- [A3] D.E. Katsareas, NESC III Project TG6 2nd (Detailed) Computational Round Robin, NESCDOC TG6 (04) 01, IE-JRC, February 26th 2004.
- [A4] The Battelle Integrity of Nuclear Piping (BINP) Program Final Report, NUREG/CR-6837, Vol. 2, US Nuclear Regulatory Commission, 2005.
- [A5] ASME Boiler and Pressure Vessel Code 2010 Section II Materials Part D Properties (Metric).
- [A6] Mullins, J. and Gunnars, J. Welding simulation: Relationship between welding geometry and determination of hardening model, PVP2012-78599, Proc. ASME Pressure Vessels and Piping Conf., 2012
- [A7] Zang, W., Gunnars, J, Dong, P. and Hong, J.K., Improvement and validation of weld residual stress modelling procedure, SSM research report, 2009:15.
- [A8] Mullins, J., Gunnars, J. Influence of hardening model on weld residual stress distribution, SSM research report, 2009:16.
- [A9] Lindgren, L., Domkin, K., Hansson, S., Dislocations, vacancies and solute diffusion in physical based plasticity model for AISI 316L, Mechanics of Materials, Vol 40, pp 907-919, 2008.

Appendix B – Detailed results

Weld case I.1

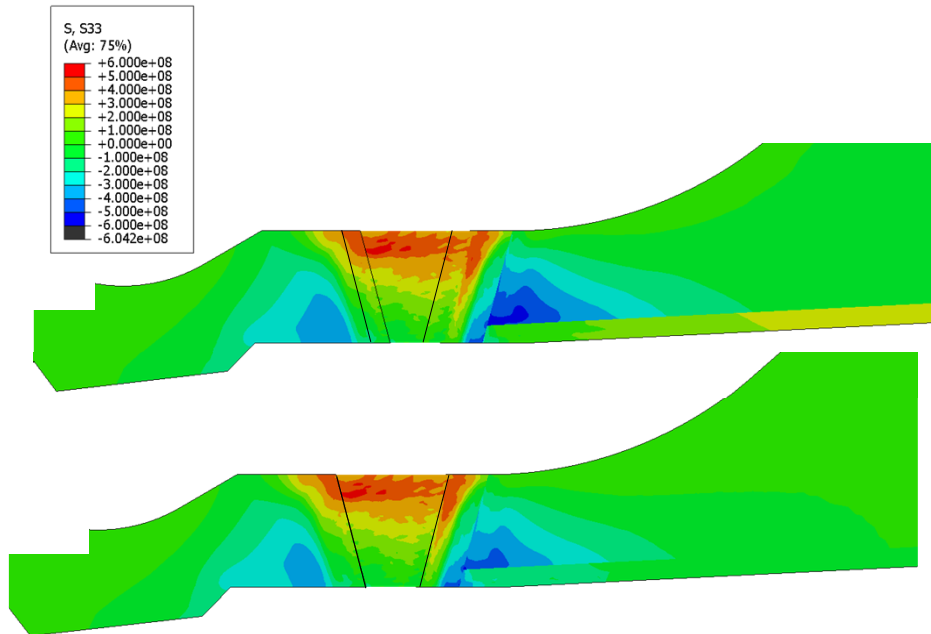


Figure 16 Hoop stress (S33) at: (a) Room Temperature (RT) and (b) Operation Temperature (OT) for weld case I.1.

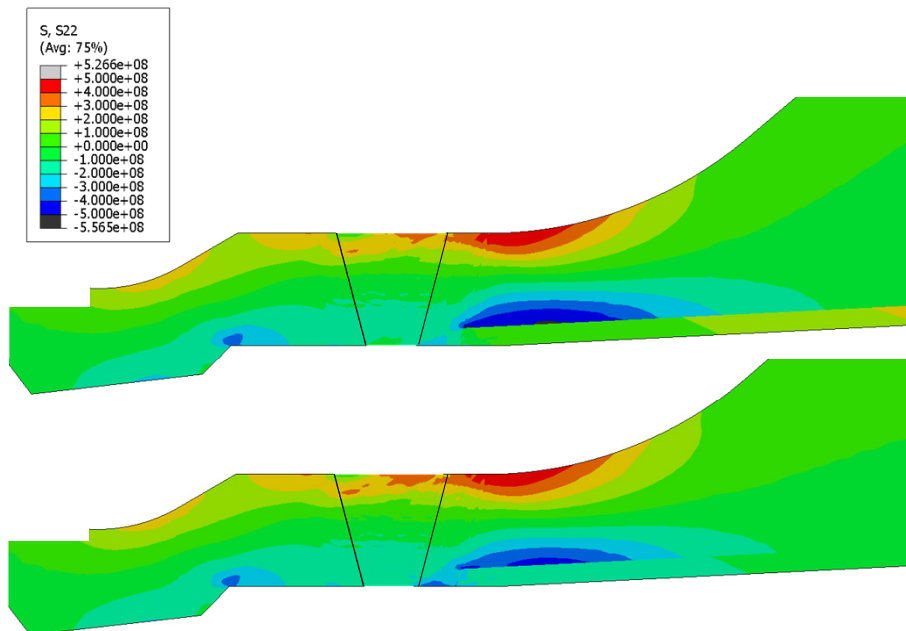


Figure 17 Axial stress (S22) at: (a) Room Temperature (RT) and (b) Operation Temperature (OT) for weld case I.1.

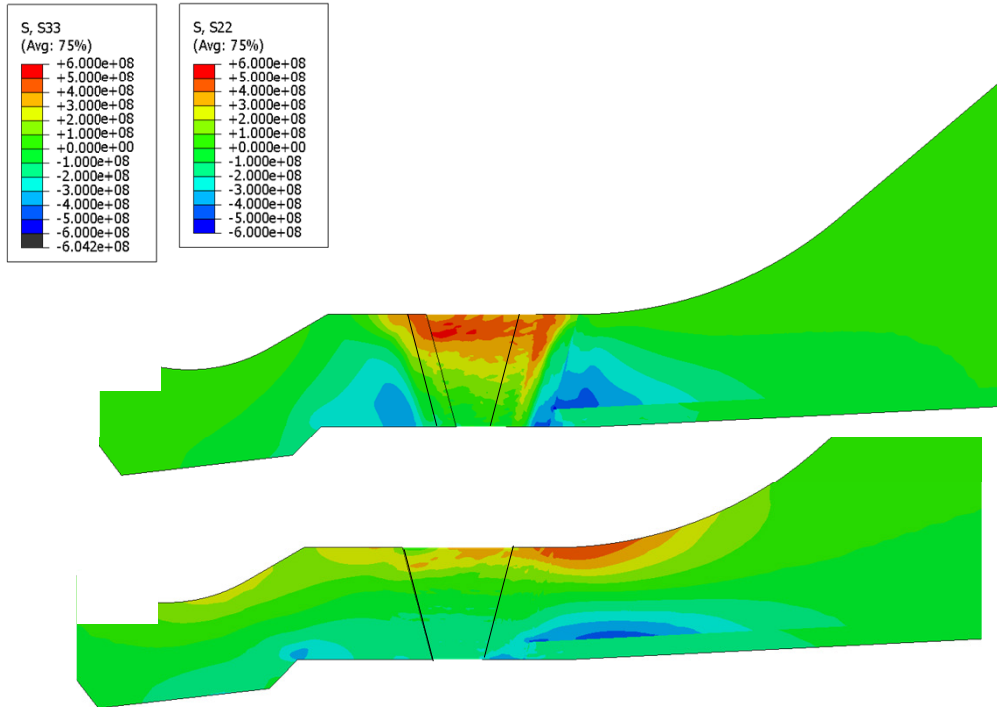


Figure 18 (a) Hoop stress S33 and (b) Axial stress S22 at Operation Temperature (OT) for weld case I.1.

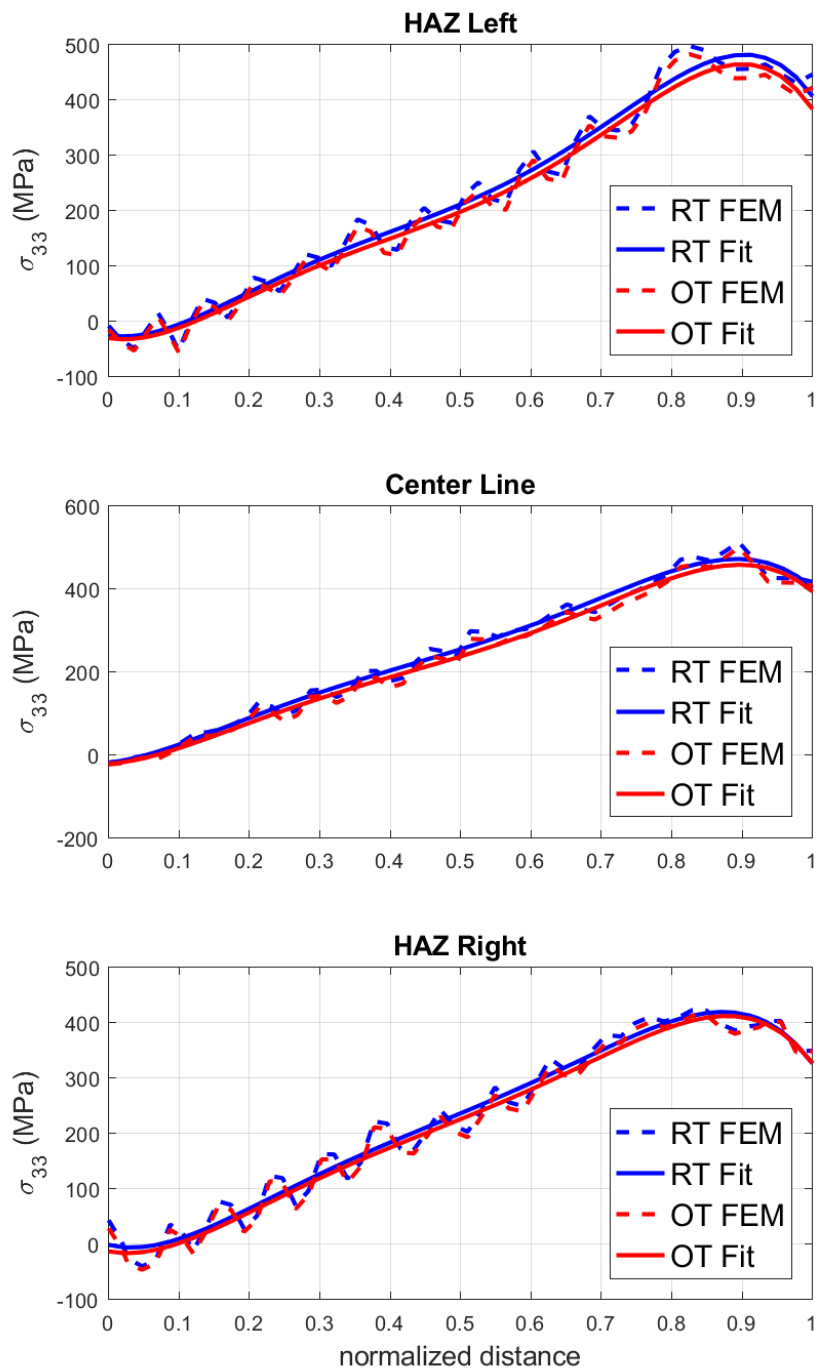


Figure 19 Hoop stress polynomial fit for weld case I.1.

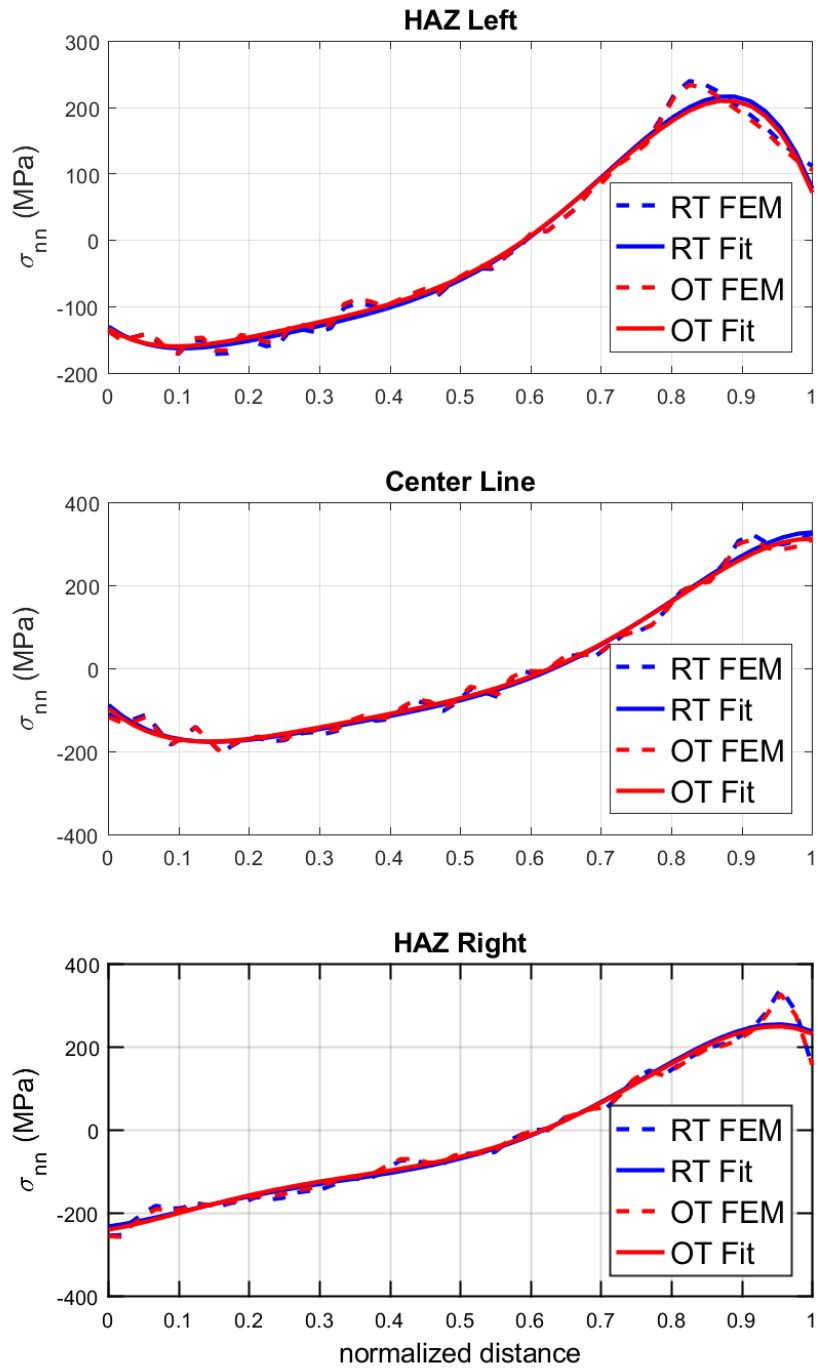


Figure 20 Normal stress polynomial fit for weld case I.1.

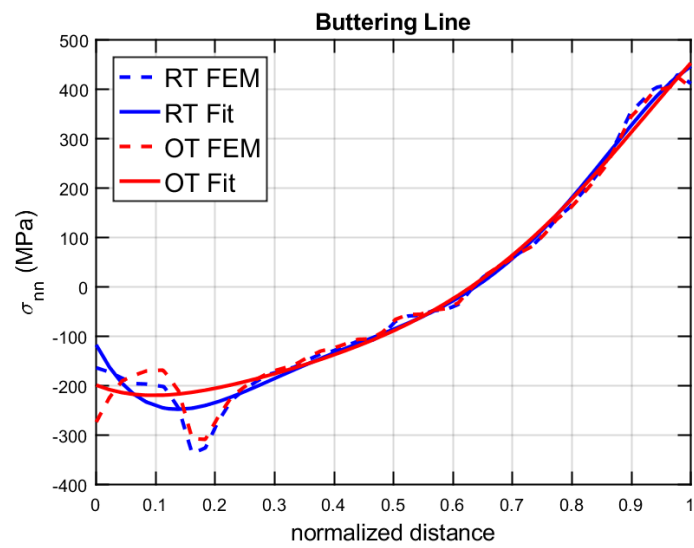
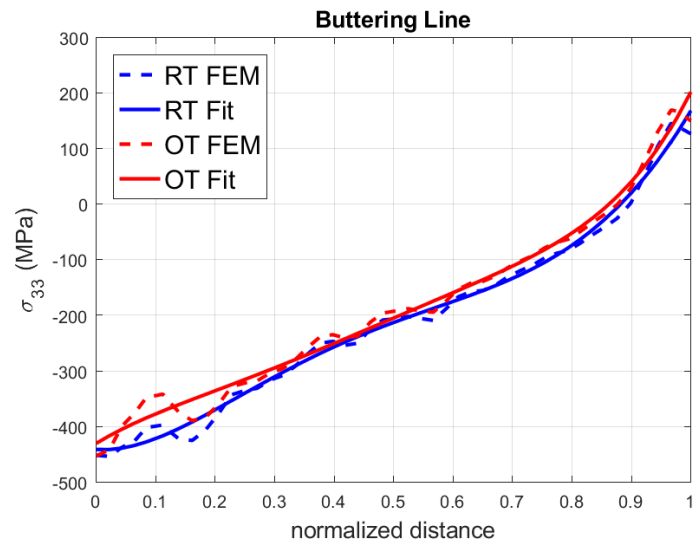


Figure 21 Hoop and normal stress polynomial fit for weld case I.1.

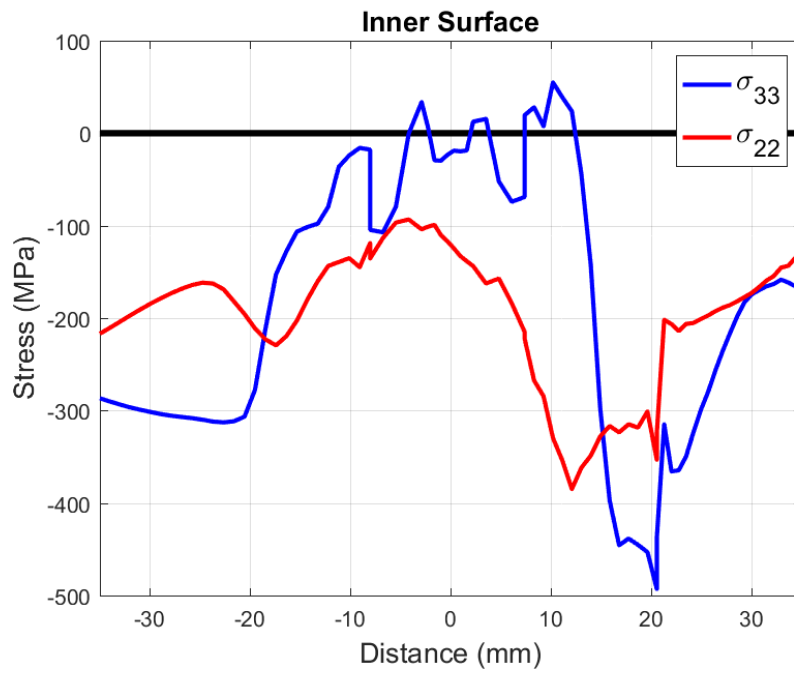


Figure 22 Hoop and axial stresses at the inner surface at Operation Temperature (OT) for weld case I.1.

Weld case I.2

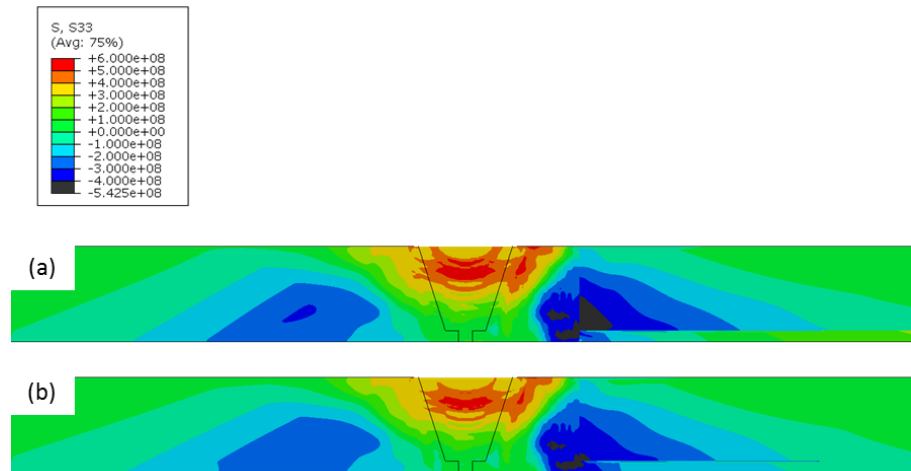


Figure 23 Hoop stress (S33) at: (a) Room Temperature (RT) and (b) Operation Temperature (OT) for weld case I.2.

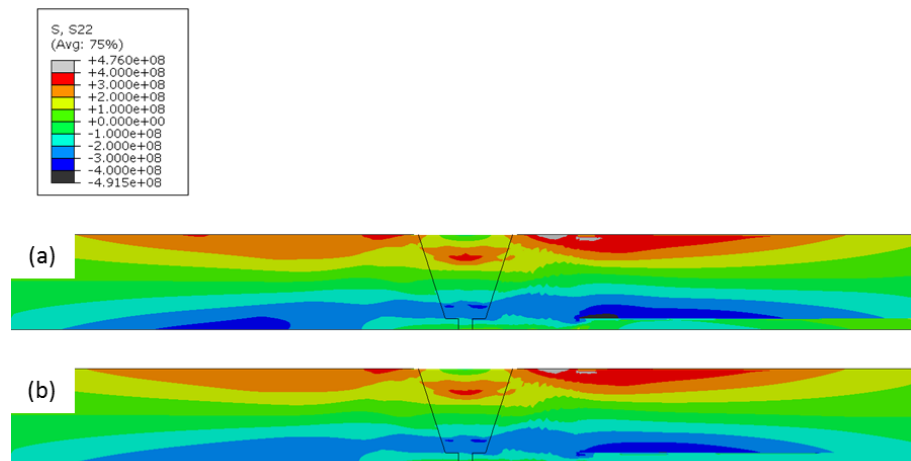


Figure 24 Axial stress (S22) at: (a) Room Temperature (RT) and (b) Operation Temperature (OT) for weld case I.2.

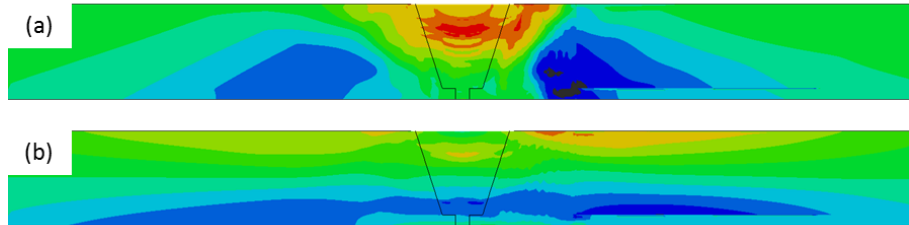
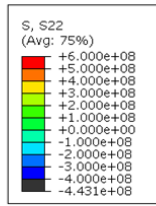
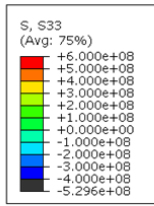


Figure 25 (a) Hoop stress S33 and (b) Axial stress S22 at Operation Temperature (OT) for weld case I.2.

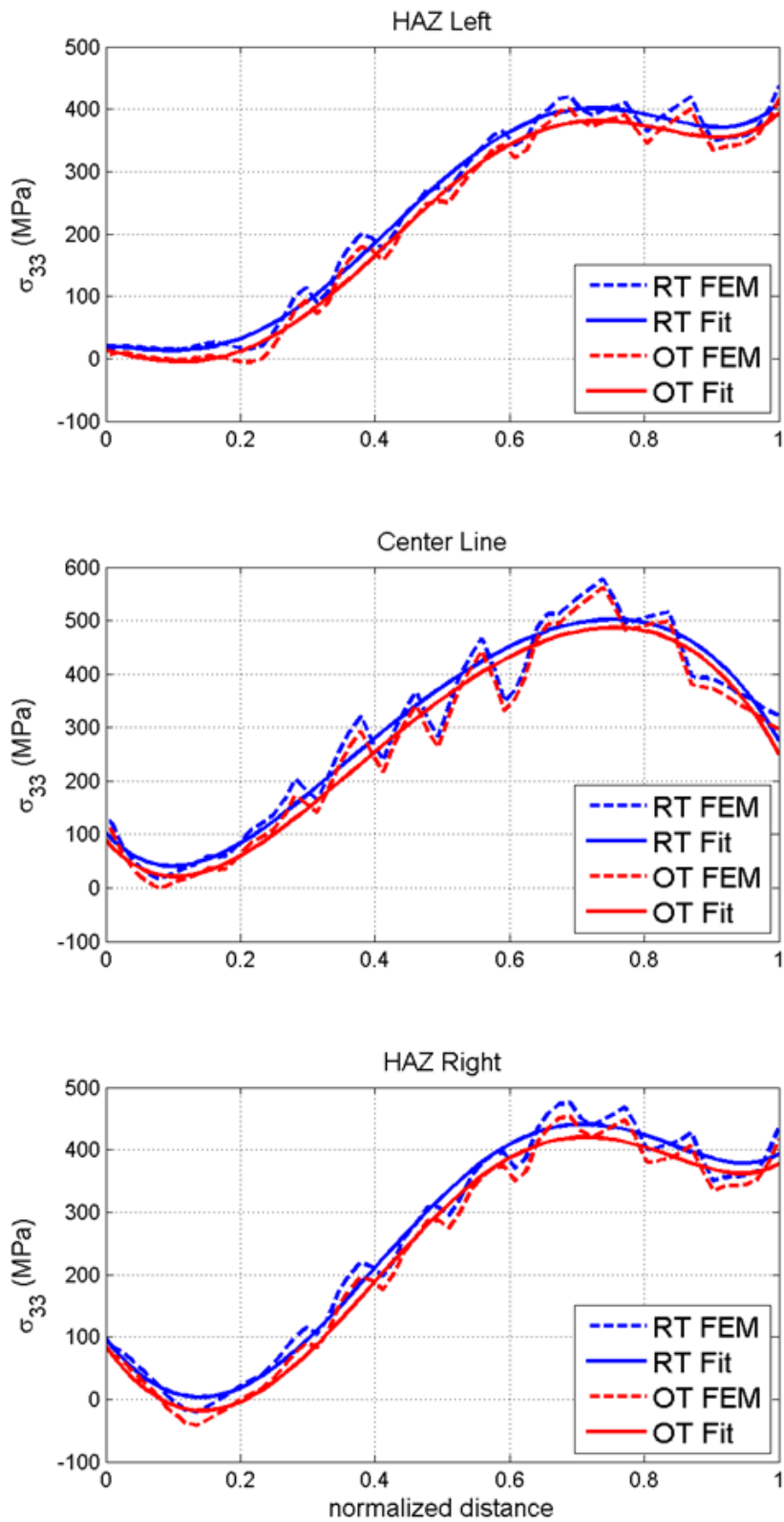


Figure 26 Hoop stress polynomial fit for weld case I.2.

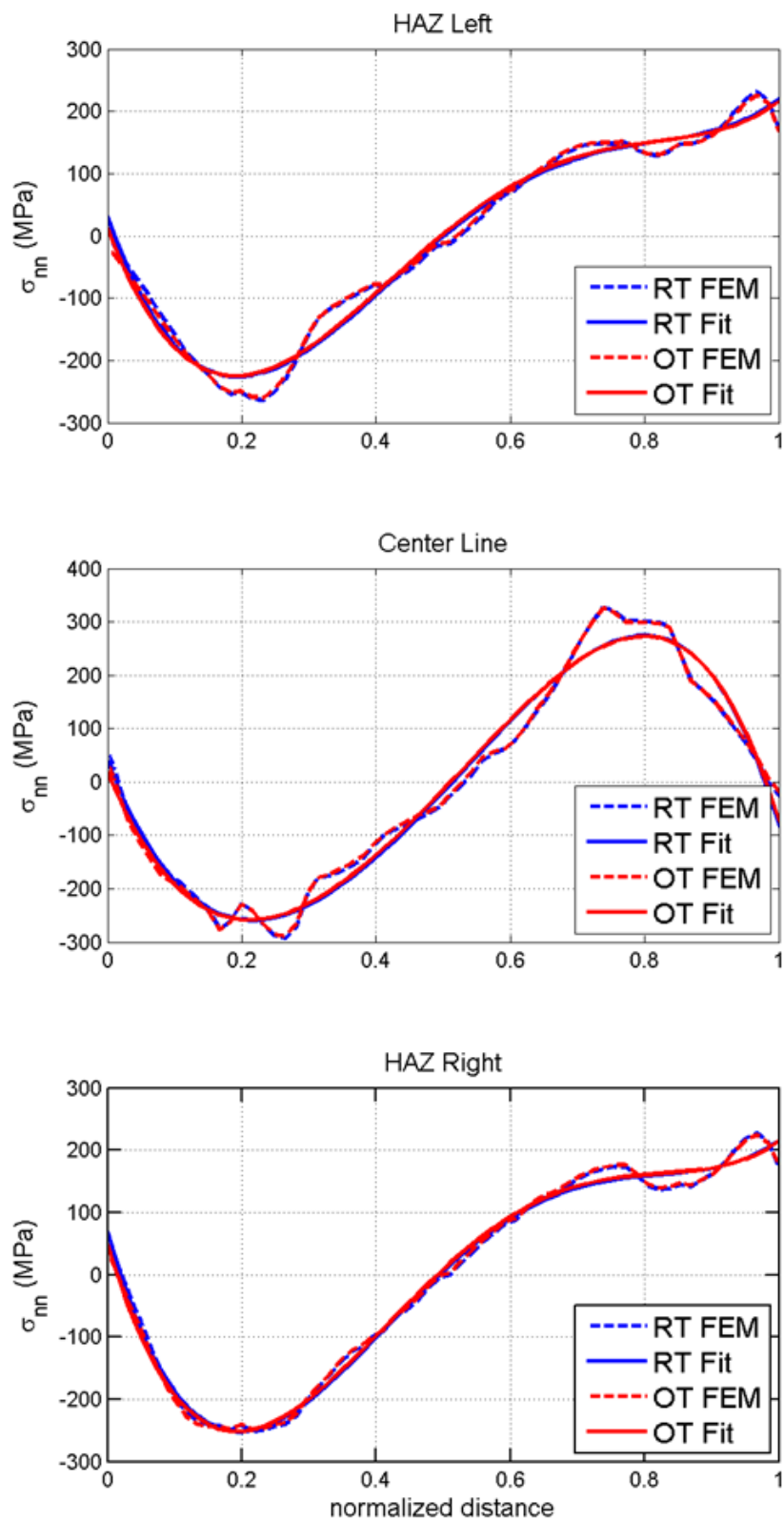


Figure 27 Normal stress polynomial fit for weld case I.2.

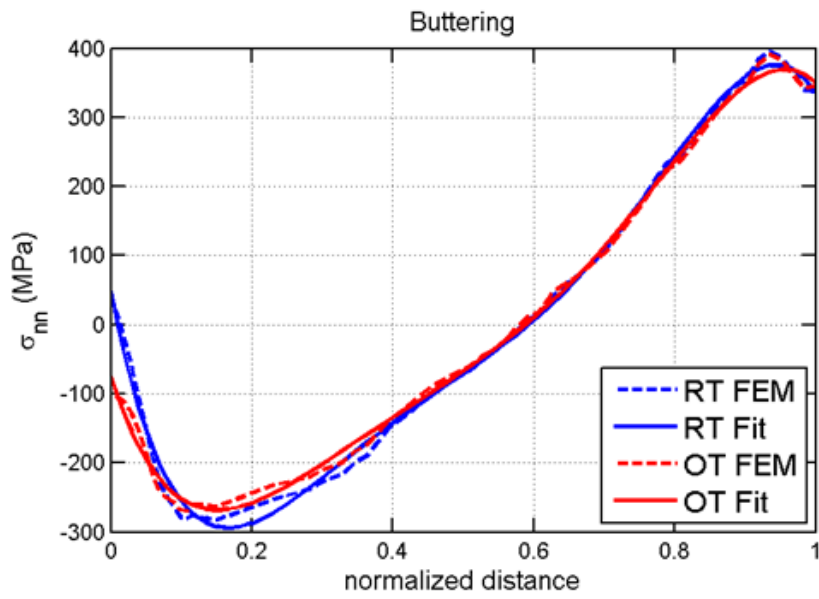
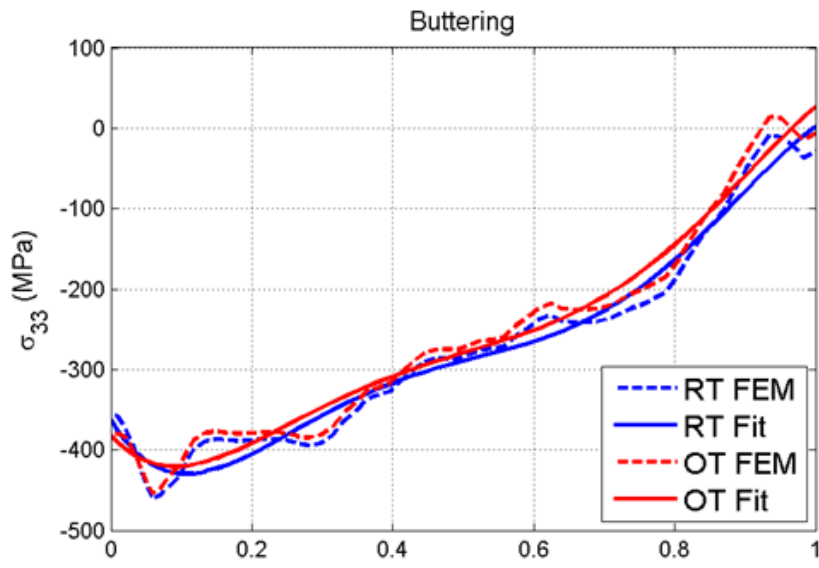


Figure 28 Hoop and normal stress polynomial fit for weld case I.2.

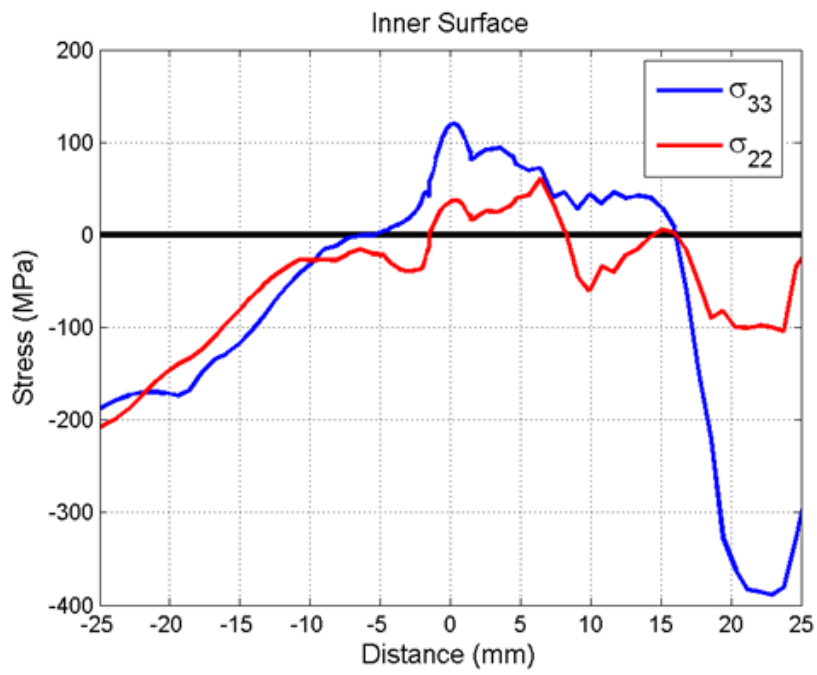


Figure 29 Hoop and axial stresses at the inner surface at Operation Temperature (OT) for weld case I.2.

Weld case I.3

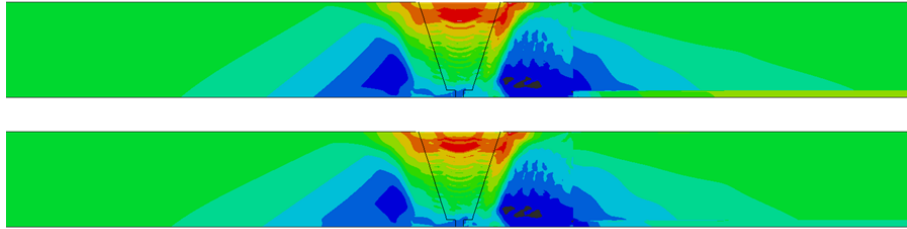
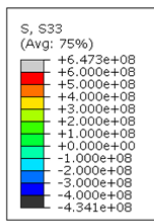


Figure 30 Hoop stress (S33) at: (a) Room Temperature (RT) and (b) Operation Temperature (OT) for weld case I.3.

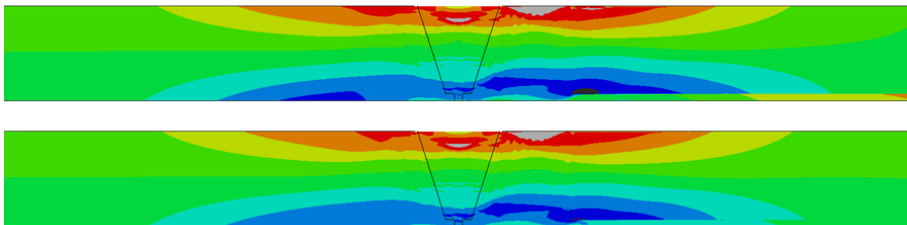
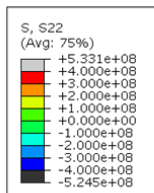


Figure 31 Axial stress (S22) at: (a) Room Temperature (RT) and (b) Operation Temperature (OT) for weld case I.3.

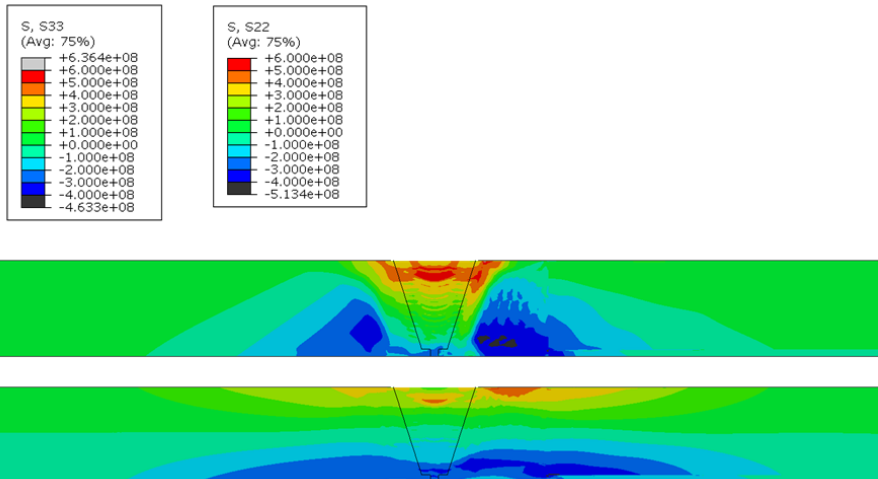


Figure 32 (a) Hoop stress S33 and (b) Axial stress S22 at Operation Temperature (OT) for weld case I.3.

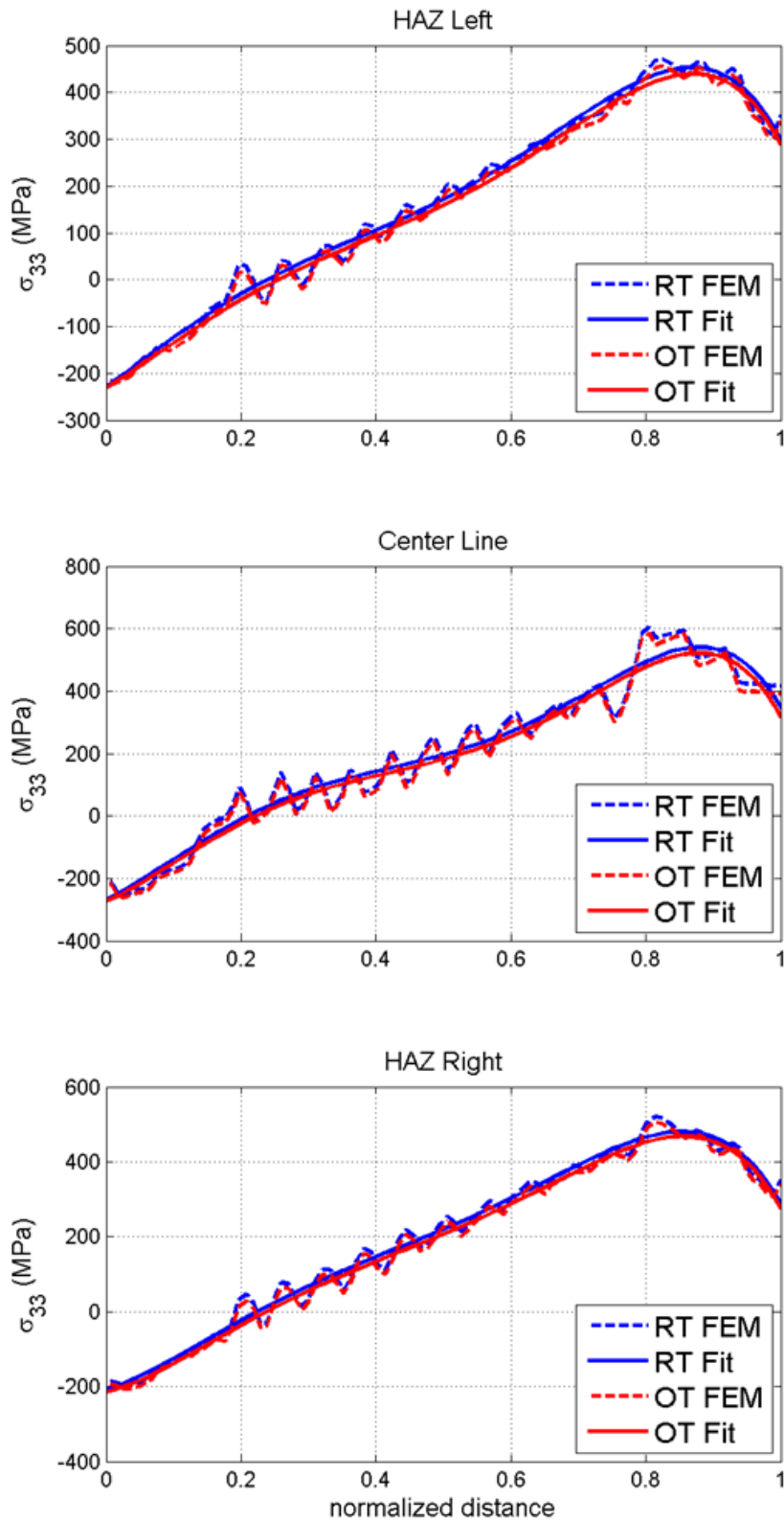


Figure 33 Hoop stress polynomial fit for weld case I.3.

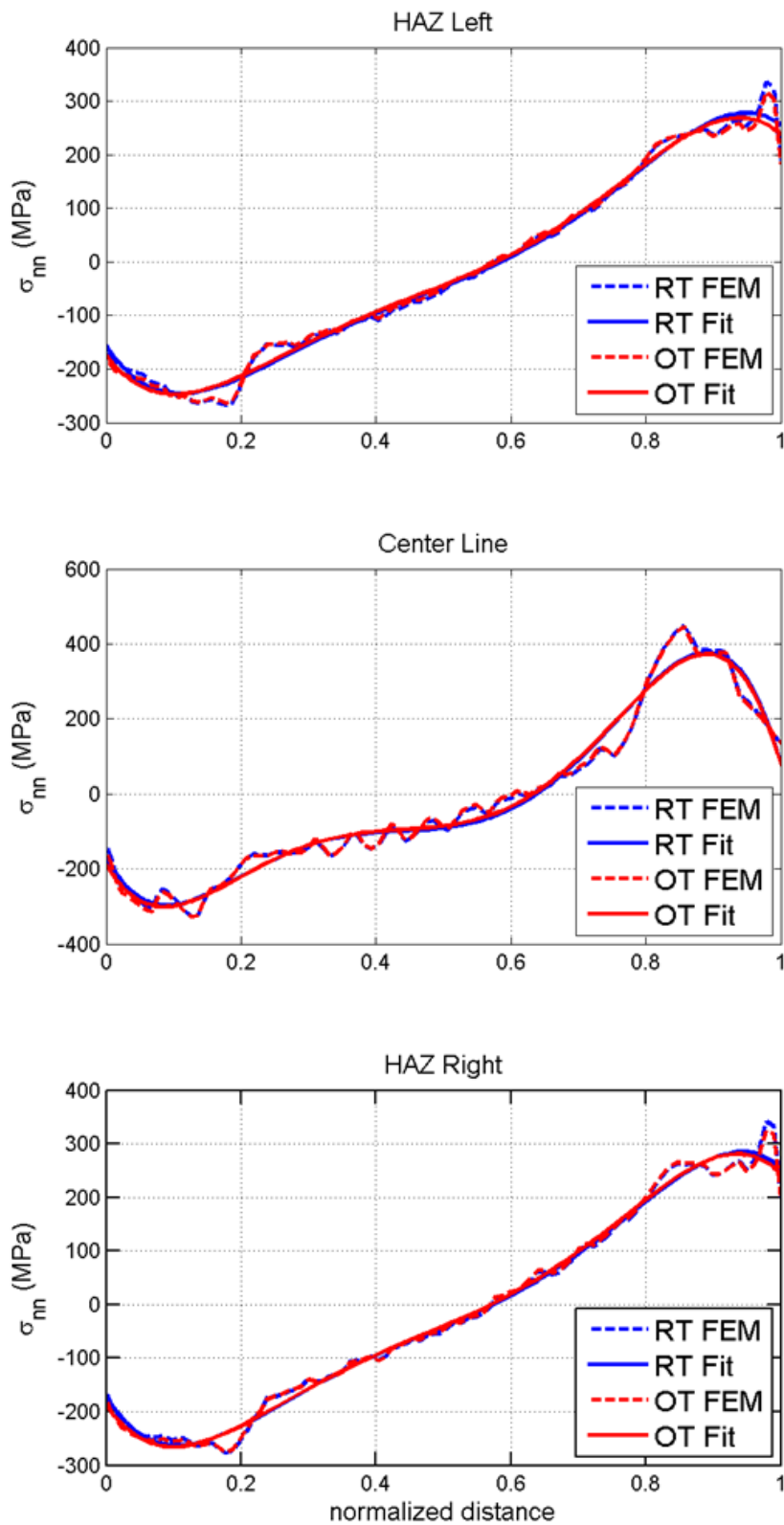


Figure 34 Normal stress polynomial fit for weld case I.3.

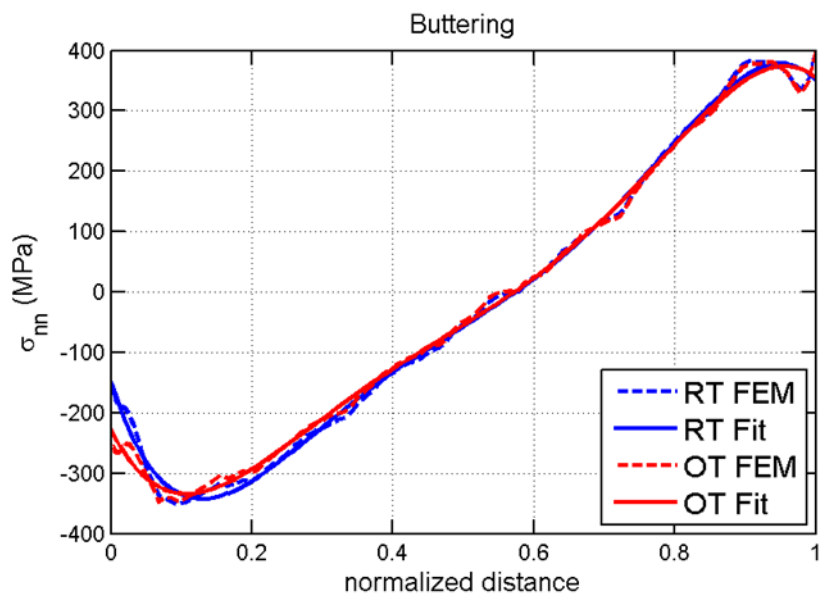
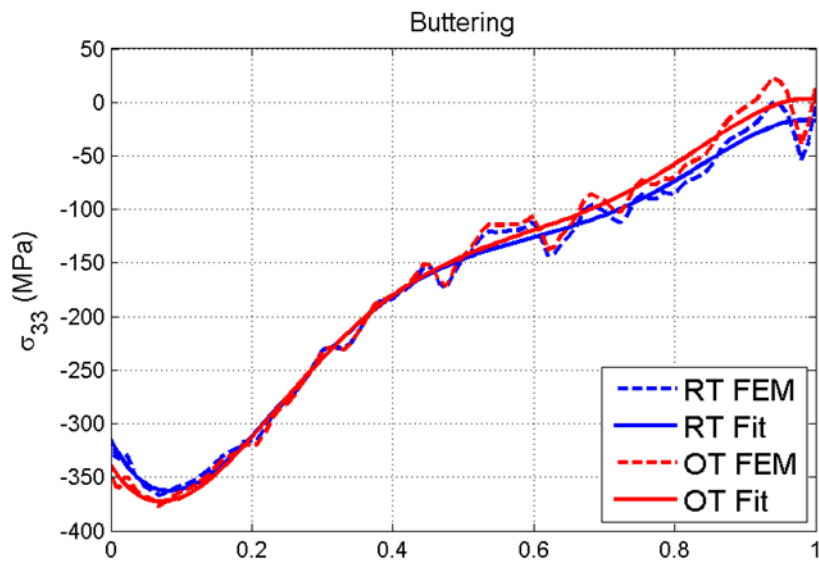


Figure 35 Hoop and normal stress polynomial fit for weld case I.3.

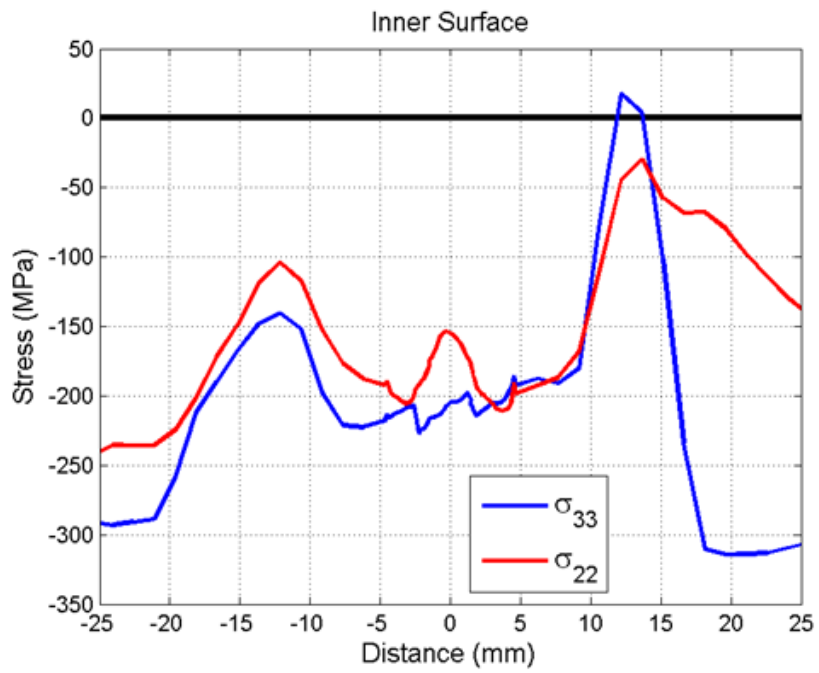


Figure 36 Hoop and axial stresses at the inner surface at Operation Temperature (OT) for weld case I.3.

Weld case I.4

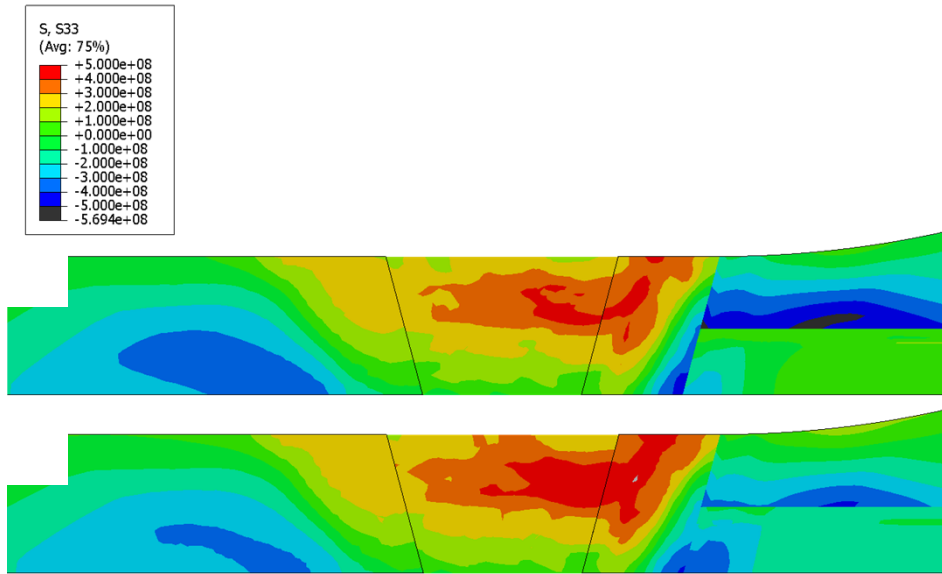


Figure 37 Hoop stress (S33) at: (a) Room Temperature (RT) and (b) Operation Temperature (OT) for weld case I.4.

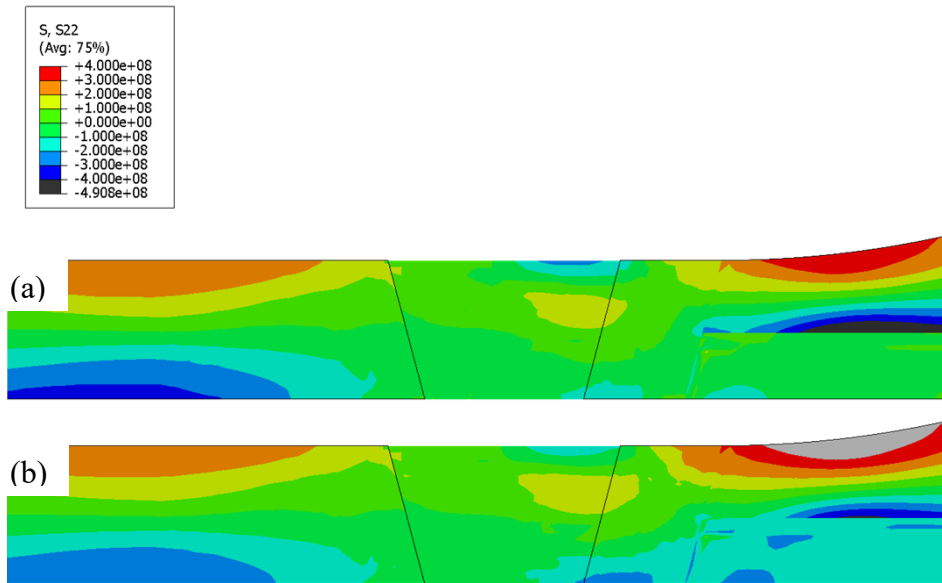


Figure 38 Axial stress (S22) at: (a) Room Temperature (RT) and (b) Operation Temperature (OT) for weld case I.4.

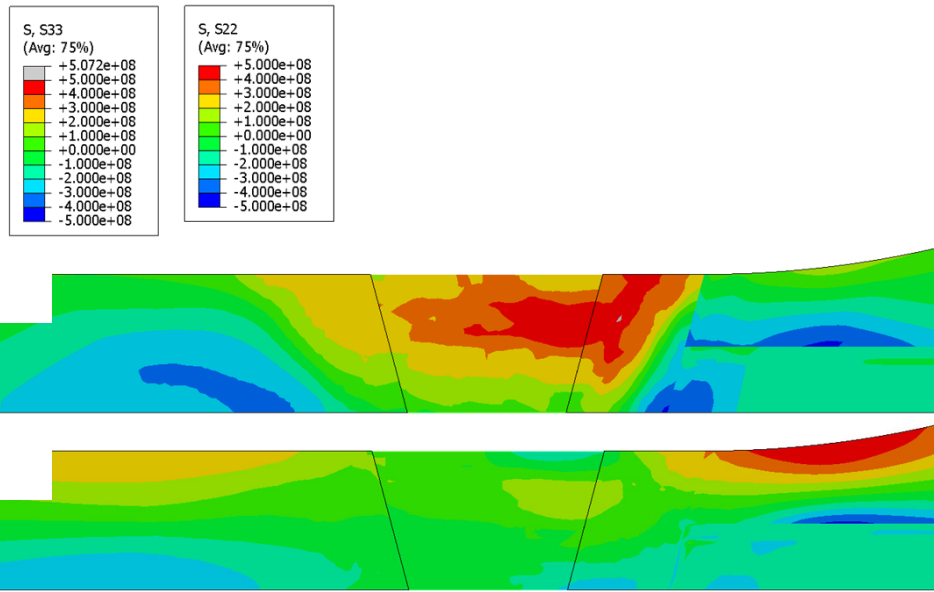


Figure 39 (a) Hoop stress S33 and (b) Axial stress S22 at Operation Temperature (OT) for weld case I.4.

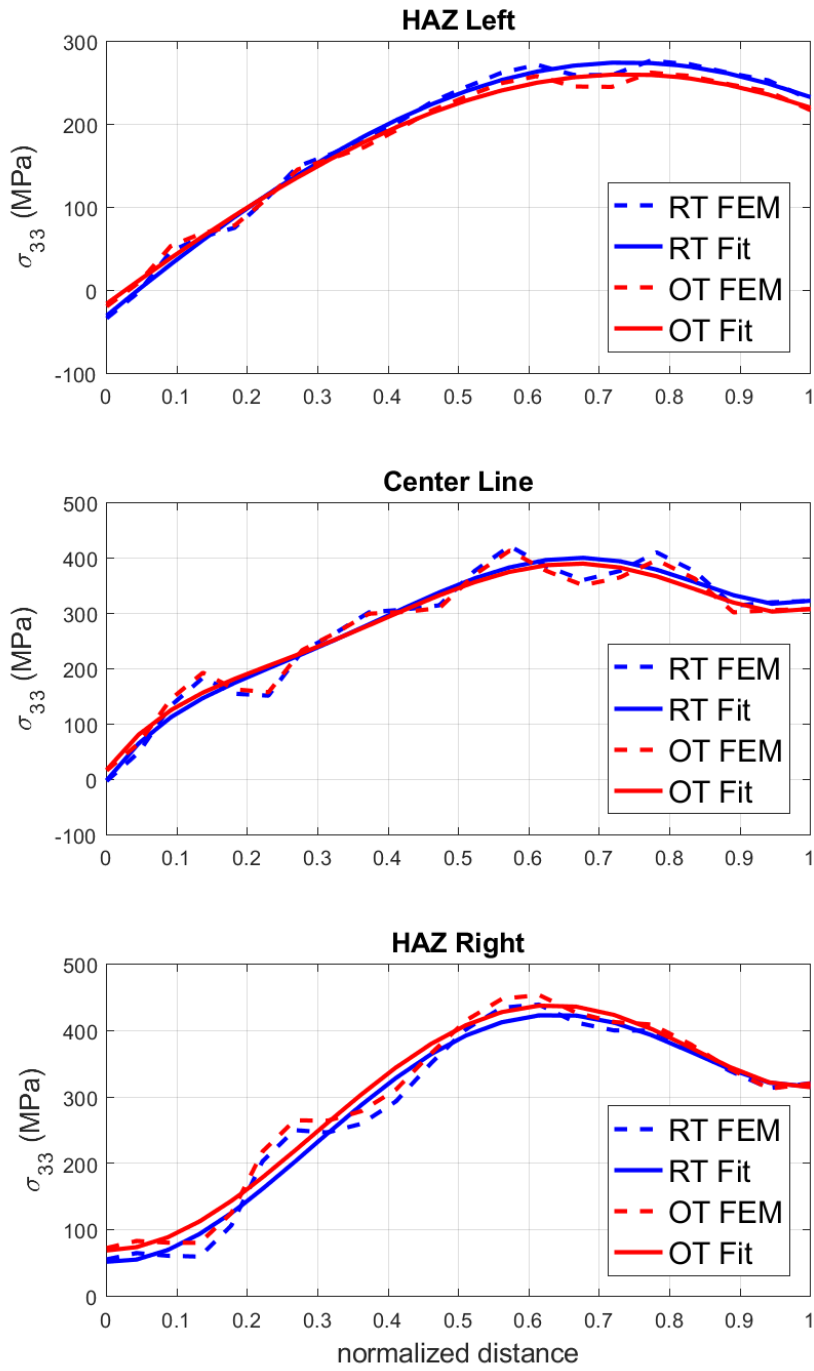


Figure 40 Hoop stress polynomial fit for weld case I.4.

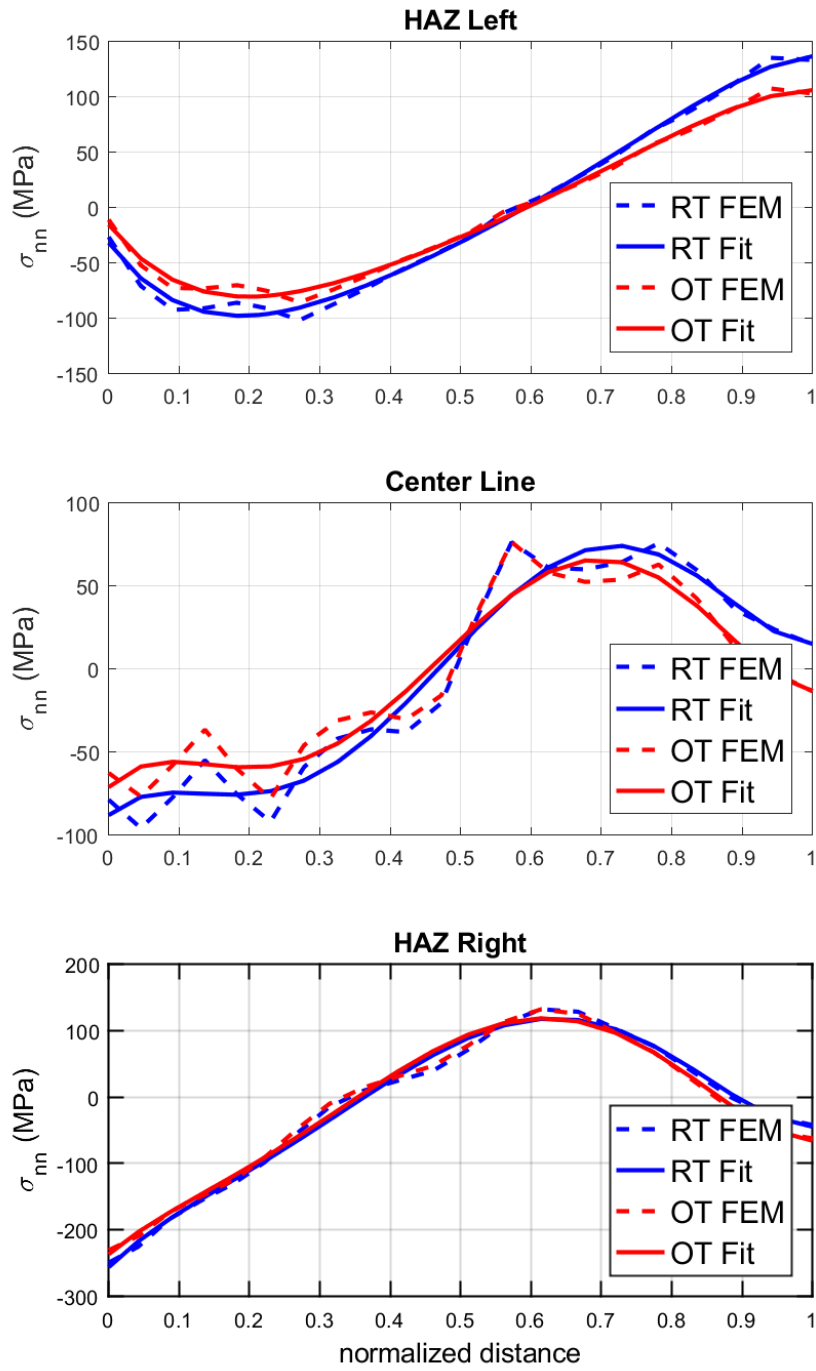


Figure 41 Normal stress polynomial fit for weld case I.4.

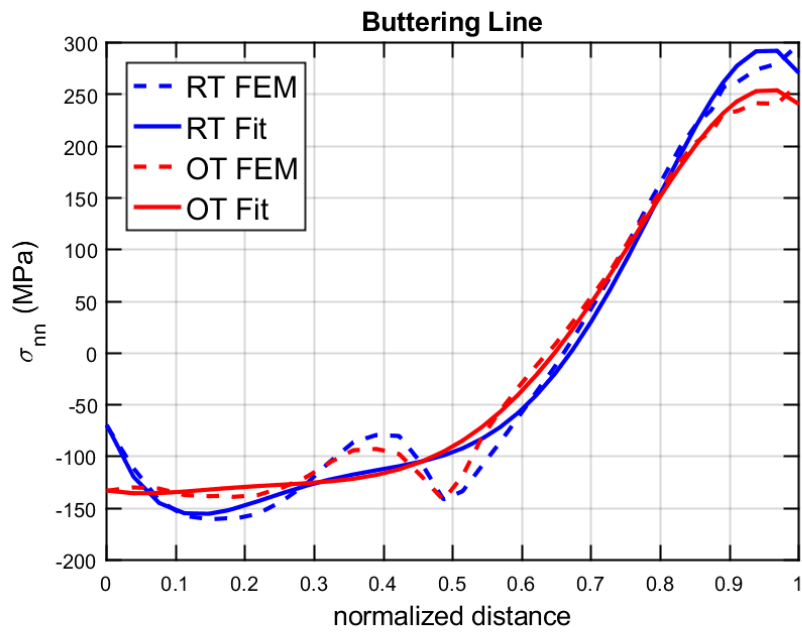
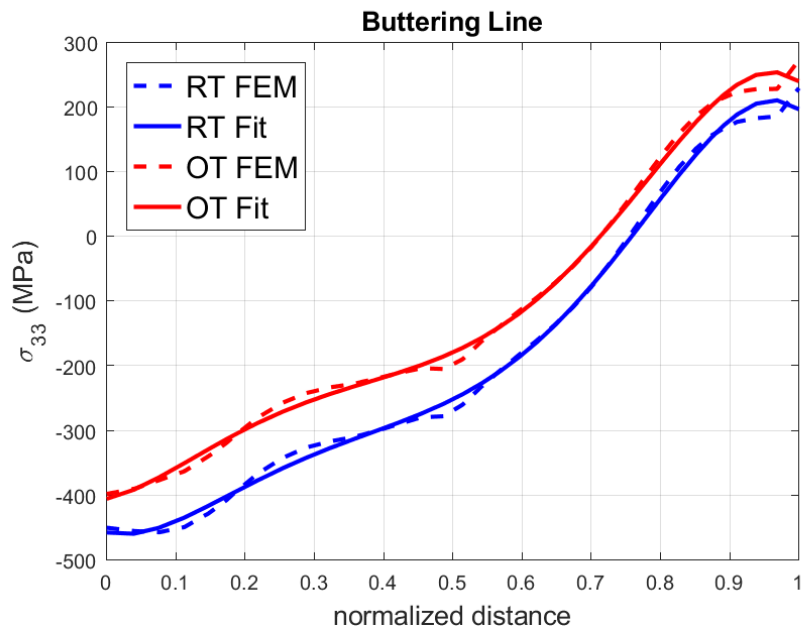


Figure 42 Hoop and normal stress polynomial fit for weld case I.4.

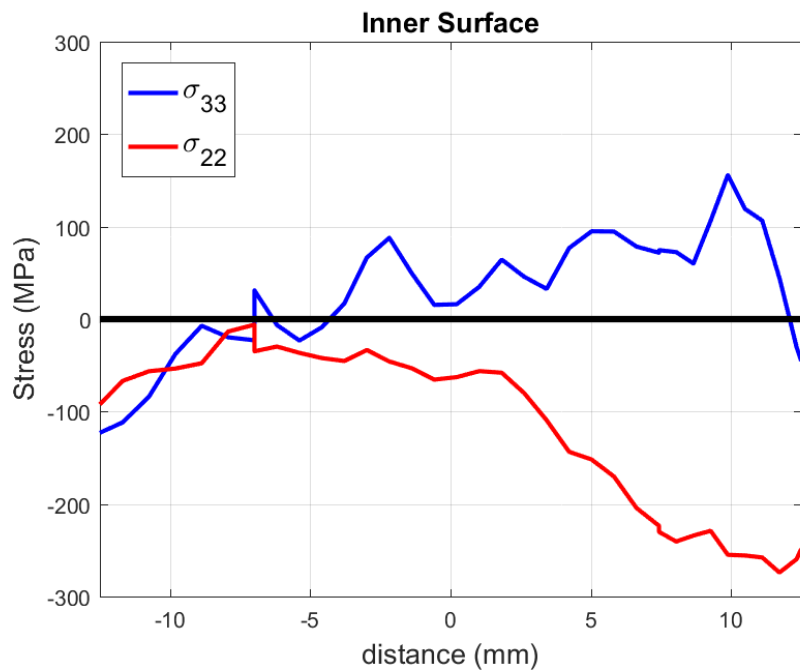


Figure 43 Hoop and axial stresses at the inner surface at Operation Temperature (OT) for weld case I.4.

Weld case II.1

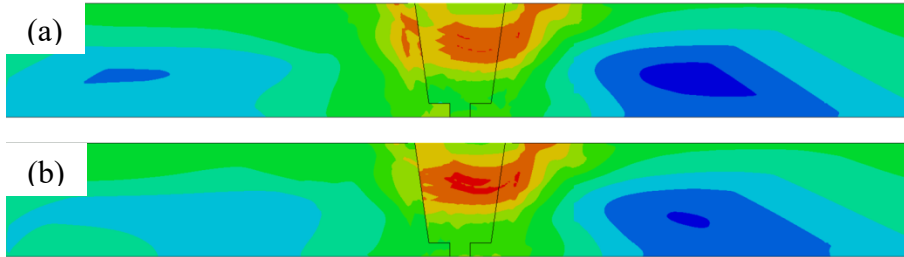
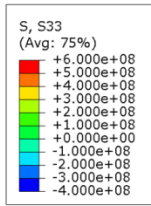


Figure 44 Hoop stress (S33) at: (a) Room Temperature (RT) and (b) Operation Temperature (OT) for weld case II.1.

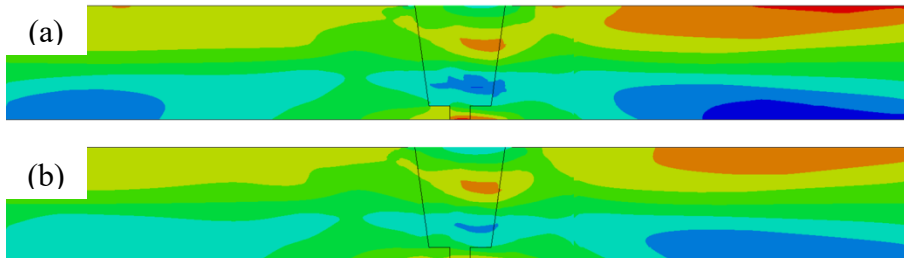
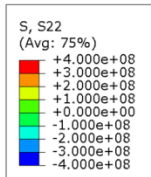


Figure 45 Axial stress (S22) at: (a) Room Temperature (RT) and (b) Operation Temperature (OT) for weld case II.1.

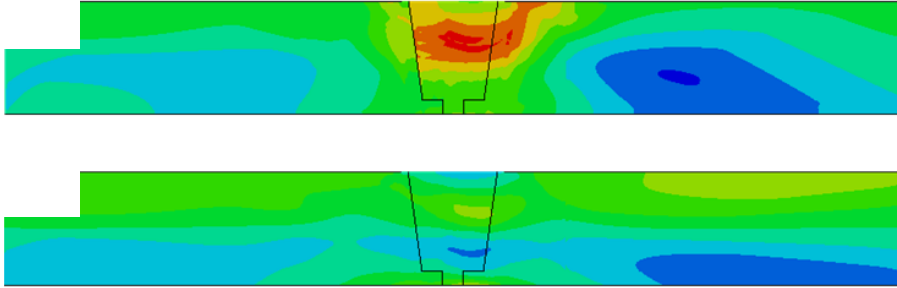
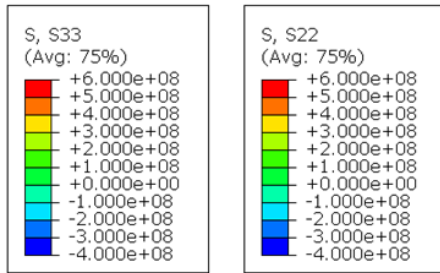


Figure 46 (a) Hoop stress S33 and (b) Axial stress S22 at Operation Temperature (OT) for weld case II.1.

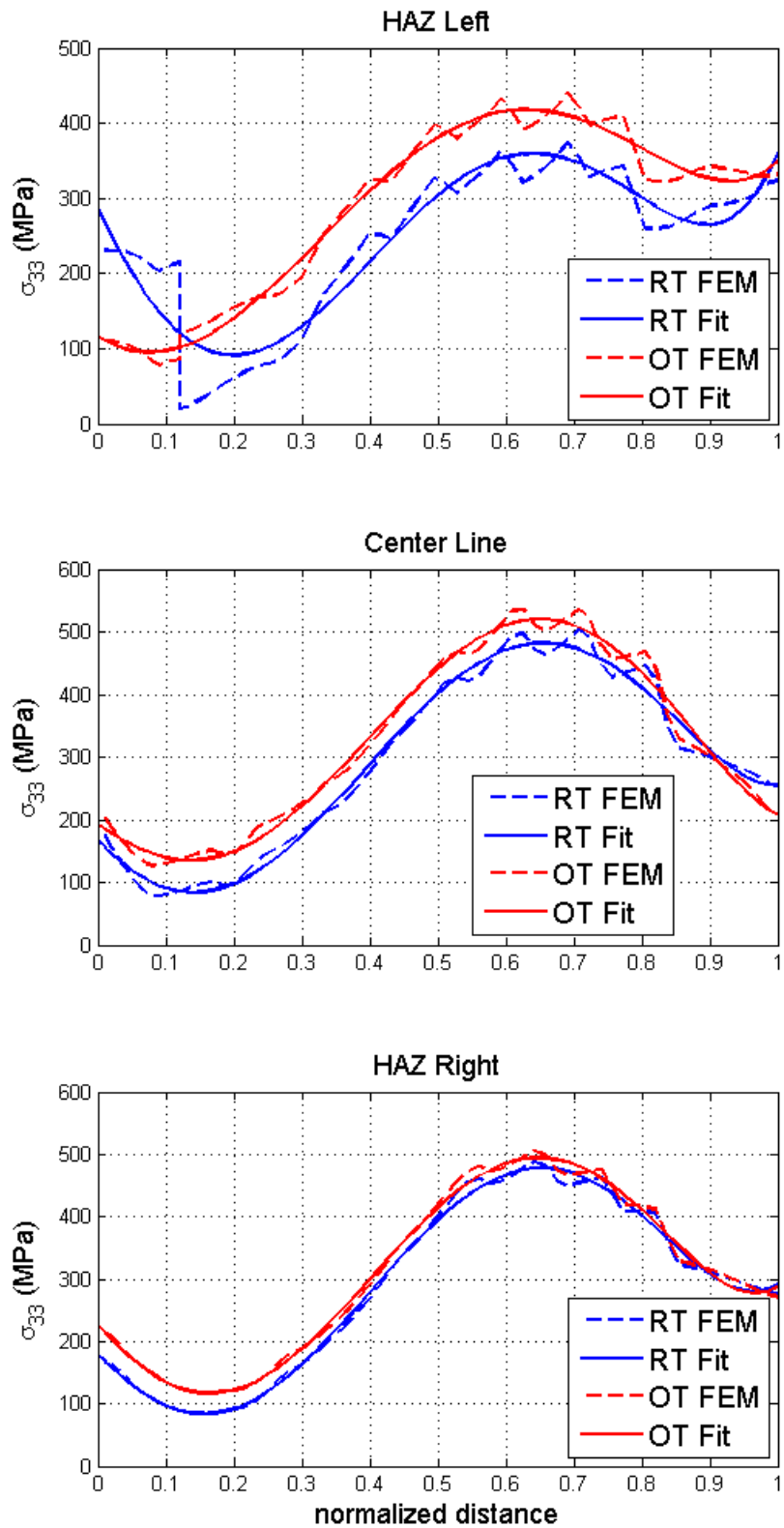


Figure 47 Hoop stress polynomial fit for weld case II.1.

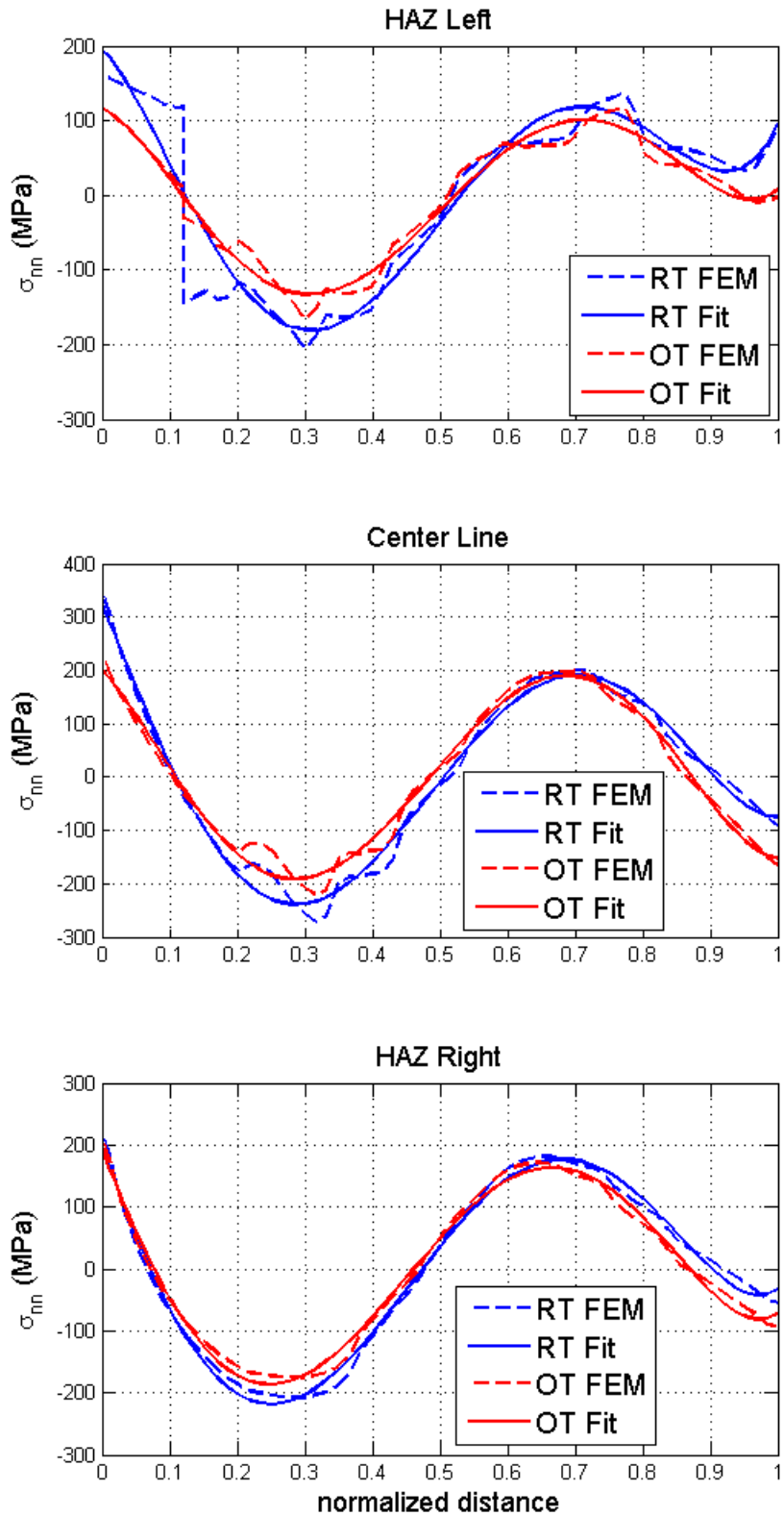


Figure 48 Normal stress polynomial fit for weld case II.1.

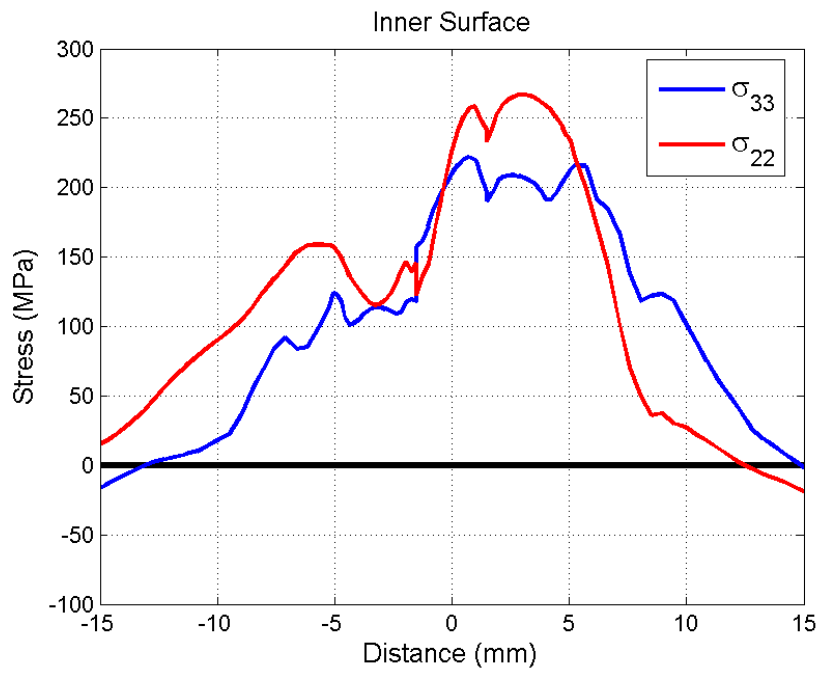


Figure 49 Hoop and axial stresses at the inner surface at Operation Temperature (OT) for weld case II.1.

Weld case II.2

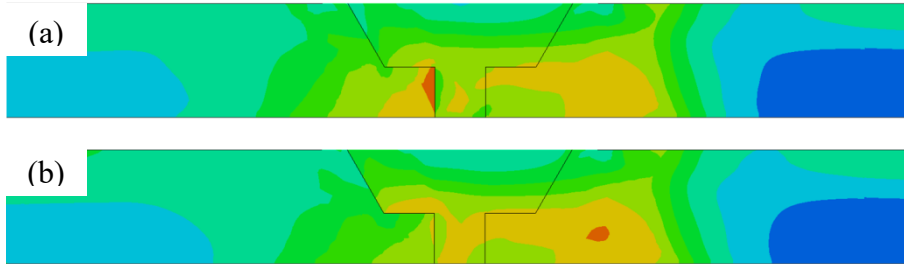
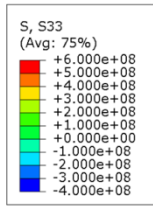


Figure 50 Hoop stress (S33) at: (a) Room Temperature (RT) and (b) Operation Temperature (OT) for weld case II.2.

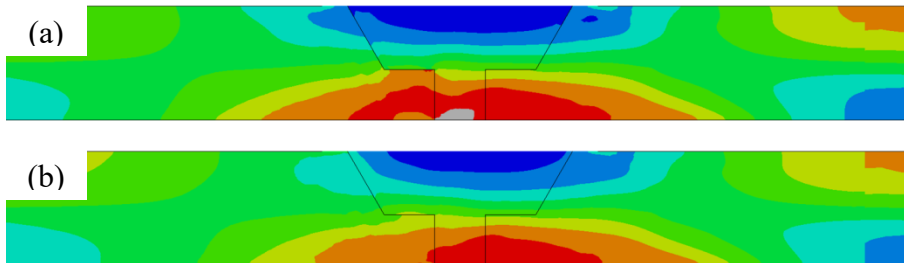
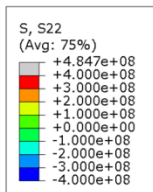


Figure 51 Axial stress (S22) at: (a) Room Temperature (RT) and (b) Operation Temperature (OT) for weld case II.2.

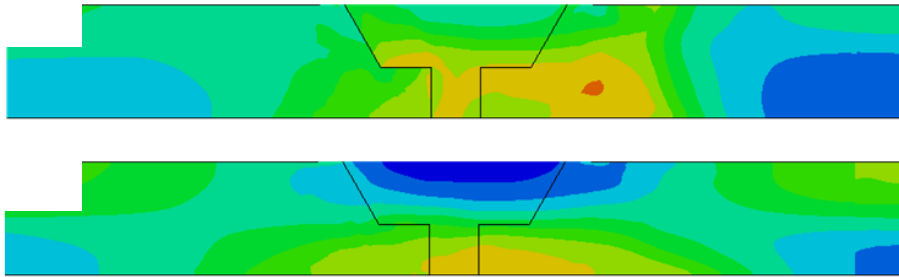
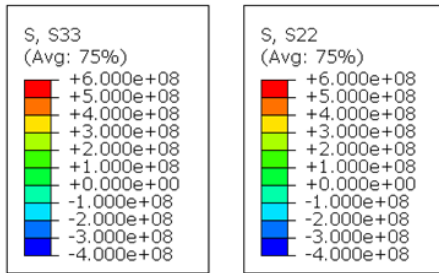


Figure 52 (a) Hoop stress S33 and (b) Axial stress S22 at Operation Temperature (OT) for weld case II.2.

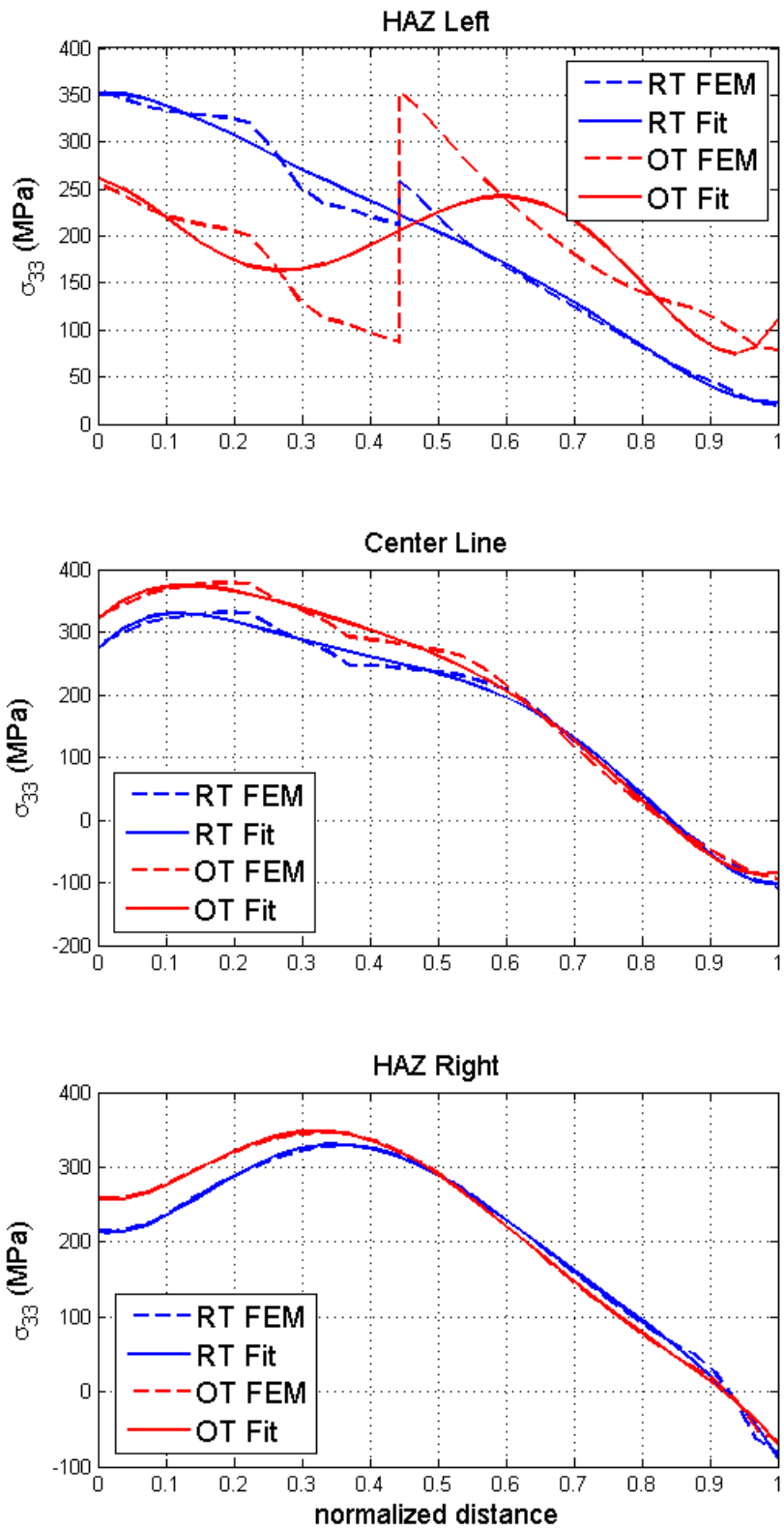


Figure 53 Hoop stress polynomial fit for weld case II.2.

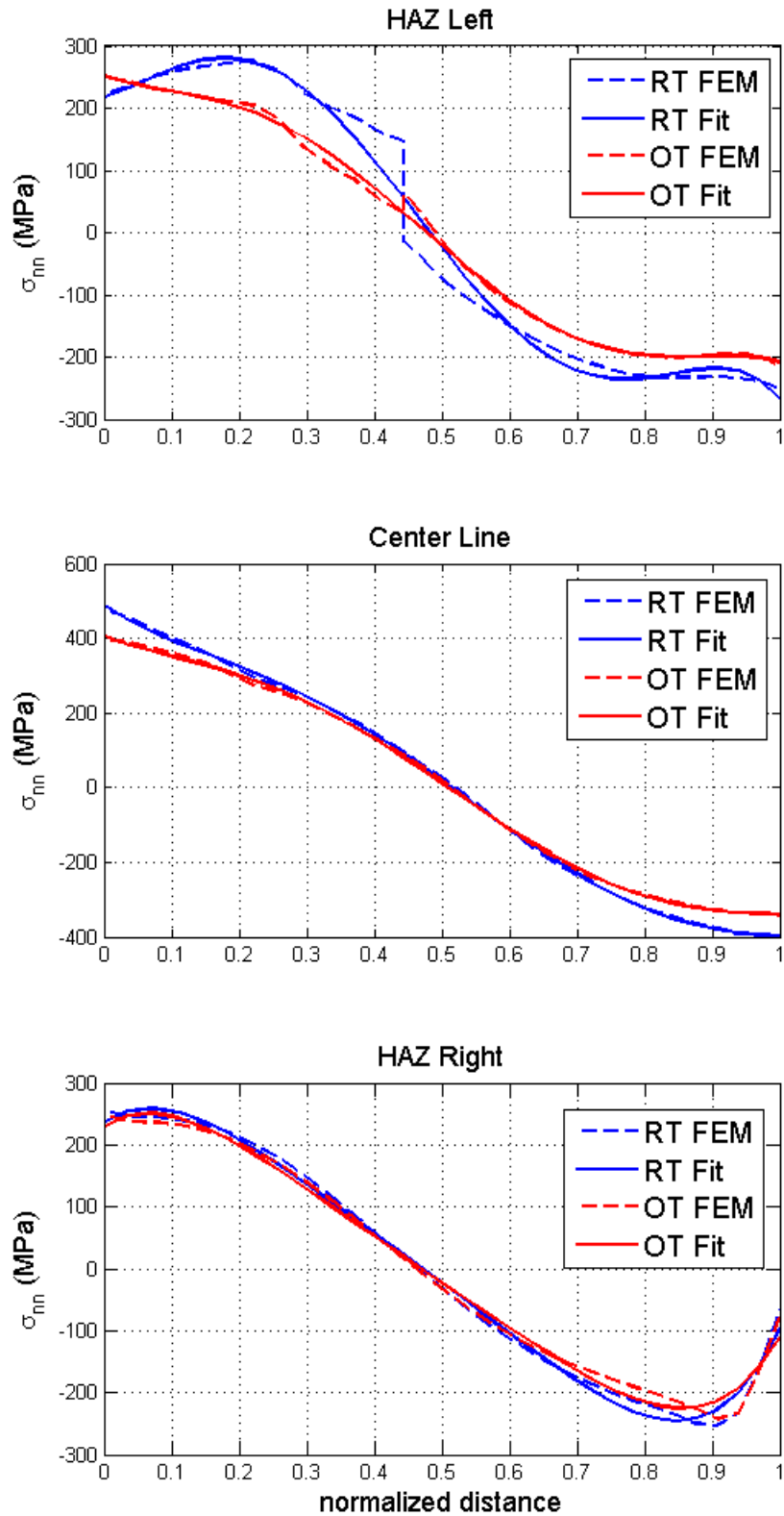


Figure 54 Normal stress polynomial fit for weld case II.2.

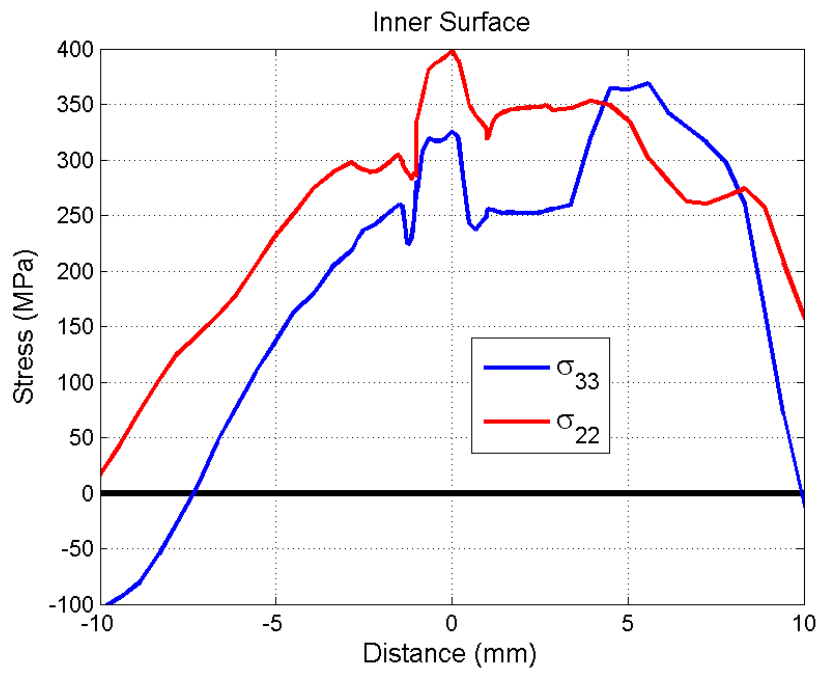


Figure 55 Hoop and axial stresses at the inner surface at Operation Temperature (OT) for weld case II.2.

Weld case II.3

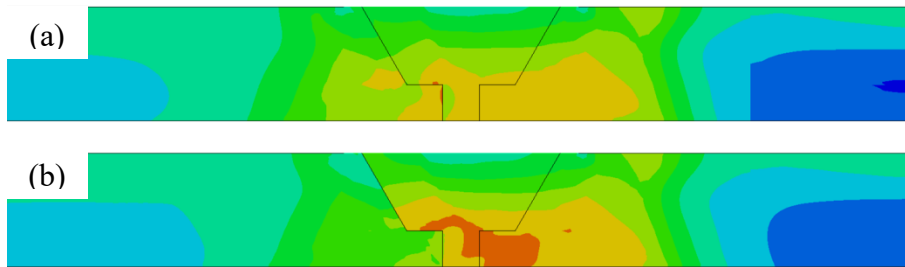
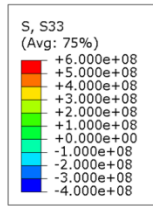


Figure 56 Hoop stress (S33) at: (a) Room Temperature (RT) and (b) Operation Temperature (OT) for weld case II.3.

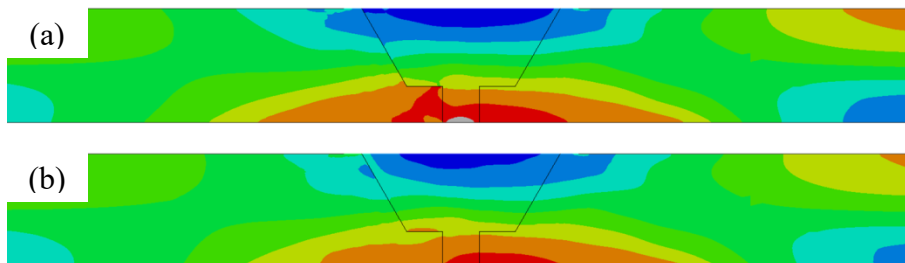
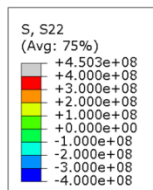


Figure 57 Axial stress (S22) at: (a) Room Temperature (RT) and (b) Operation Temperature (OT) for weld case II.3.

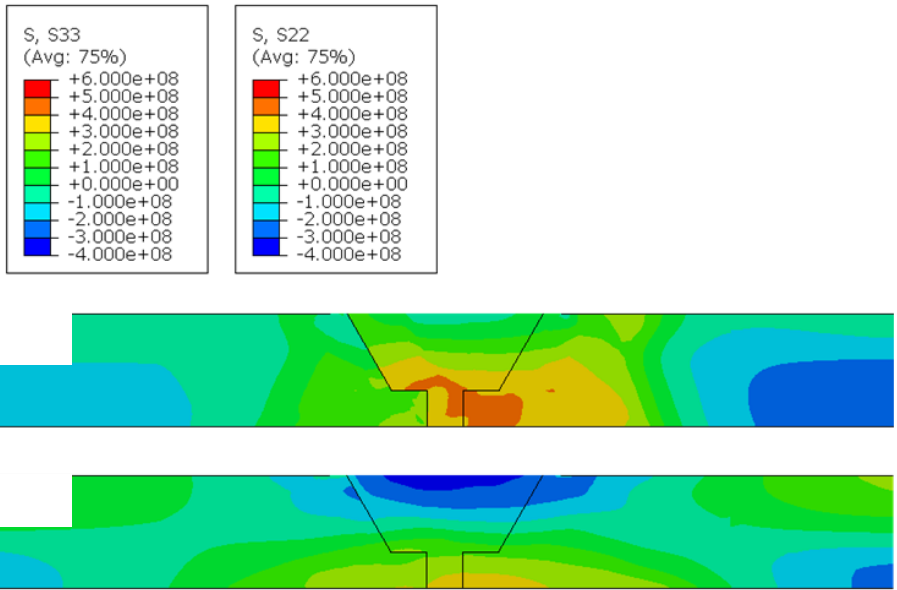


Figure 58 (a) Hoop stress S33 and (b) Axial stress S22 at Operation Temperature (OT) for weld case II.3.

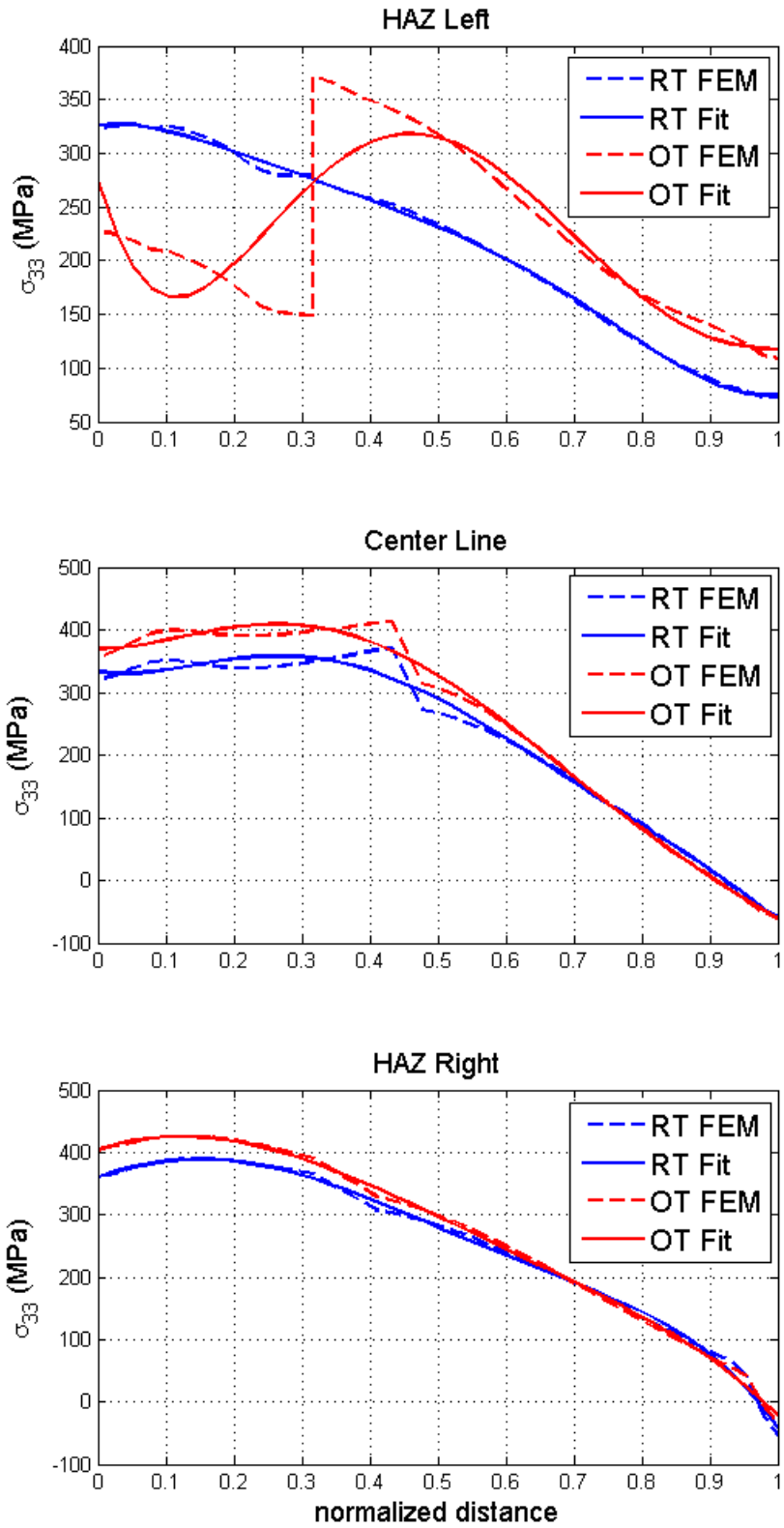


Figure 59 Hoop stress polynomial fit for weld case II.3.

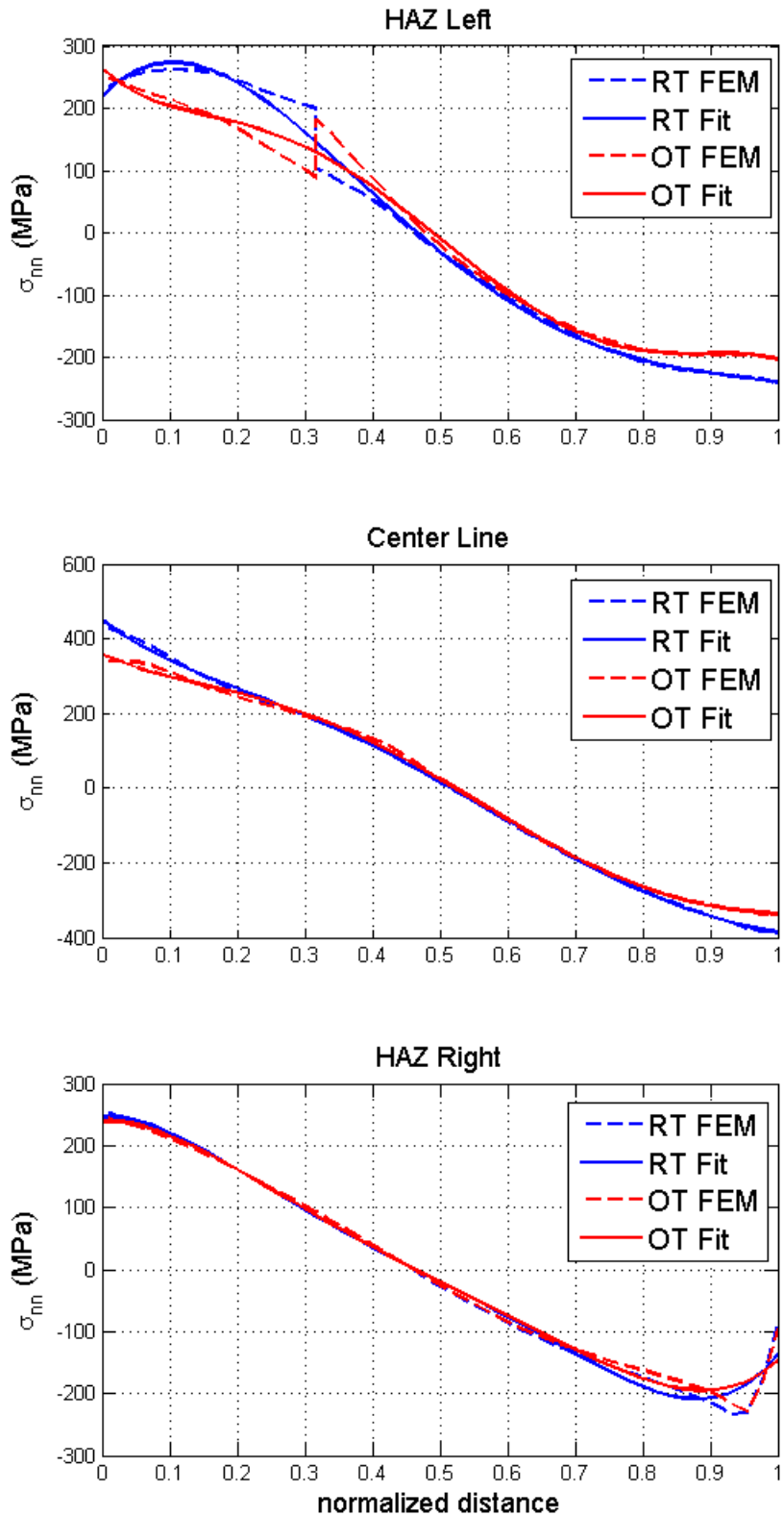


Figure 60 Normal stress polynomial fit for weld case II.3.

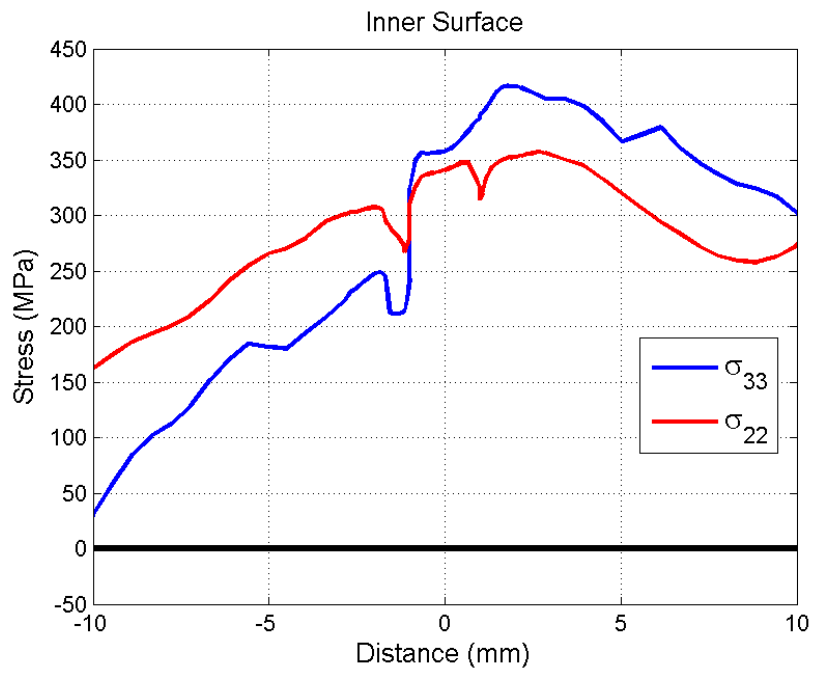


Figure 61 Hoop and axial stresses at the inner surface at Operation Temperature (OT) for weld case II.3.

Weld case II.4

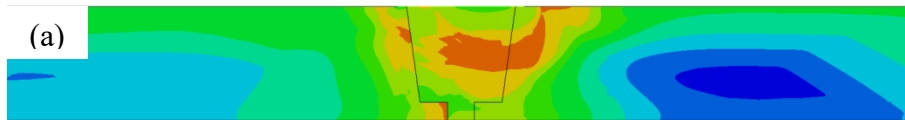
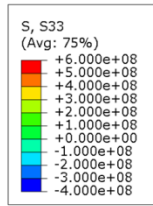


Figure 62 Hoop stress (S33) at: (a) Room Temperature (RT) and (b) Operation Temperature (OT) for weld case II.4.

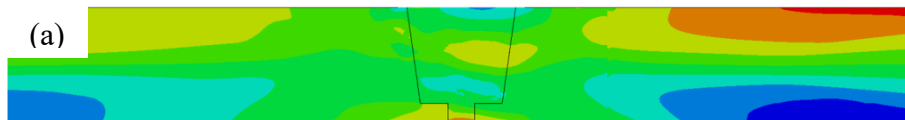
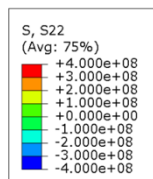


Figure 63 Axial stress (S22) at: (a) Room Temperature (RT) and (b) Operation Temperature (OT) for weld case II.4.

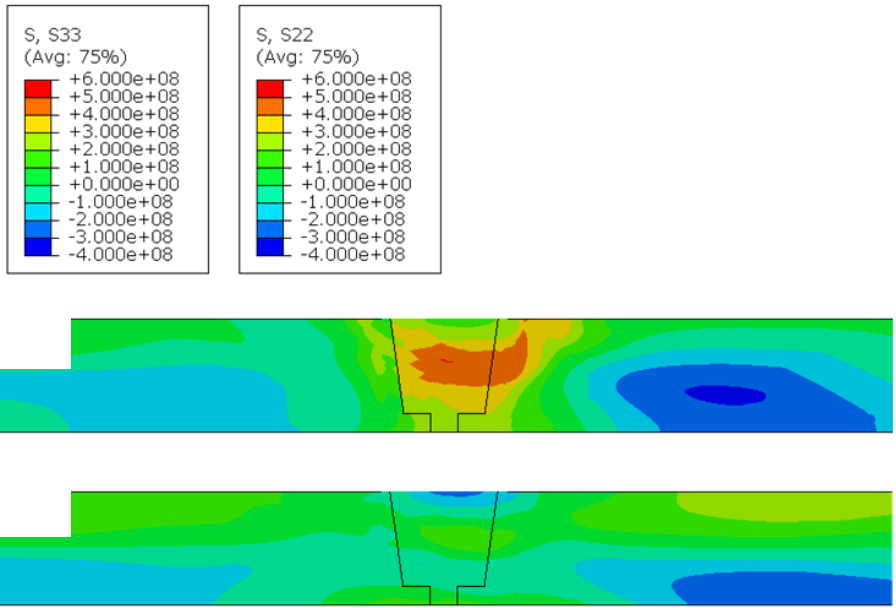
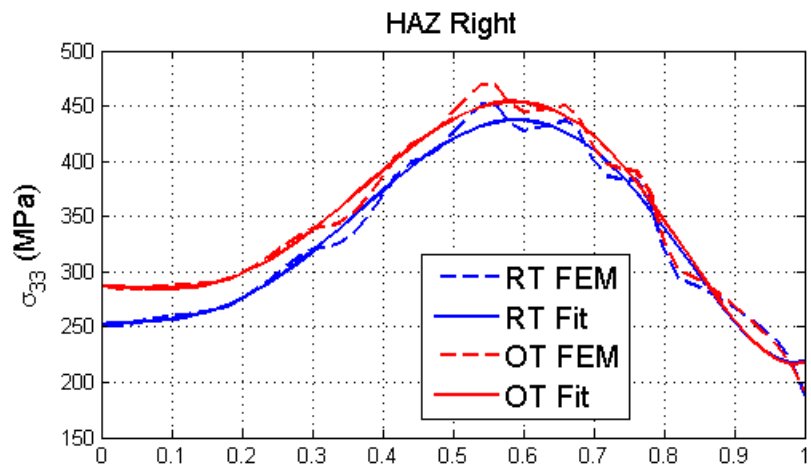
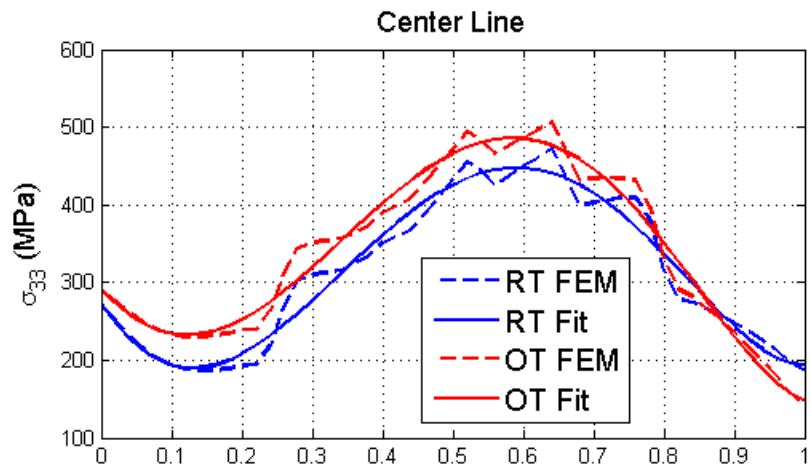
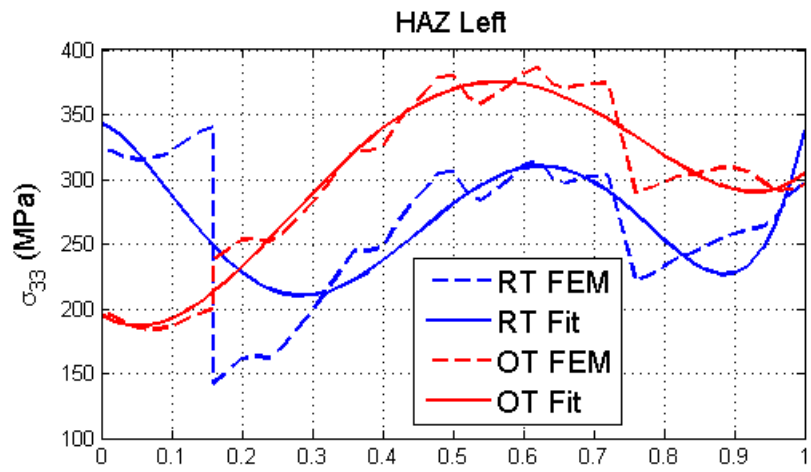


Figure 64 (a) Hoop stress S33 and (b) Axial stress S22 at Operation Temperature (OT) for weld case II.4.



normalized distance
 Figure 65 Hoop stress polynomial fit for weld case II.4.

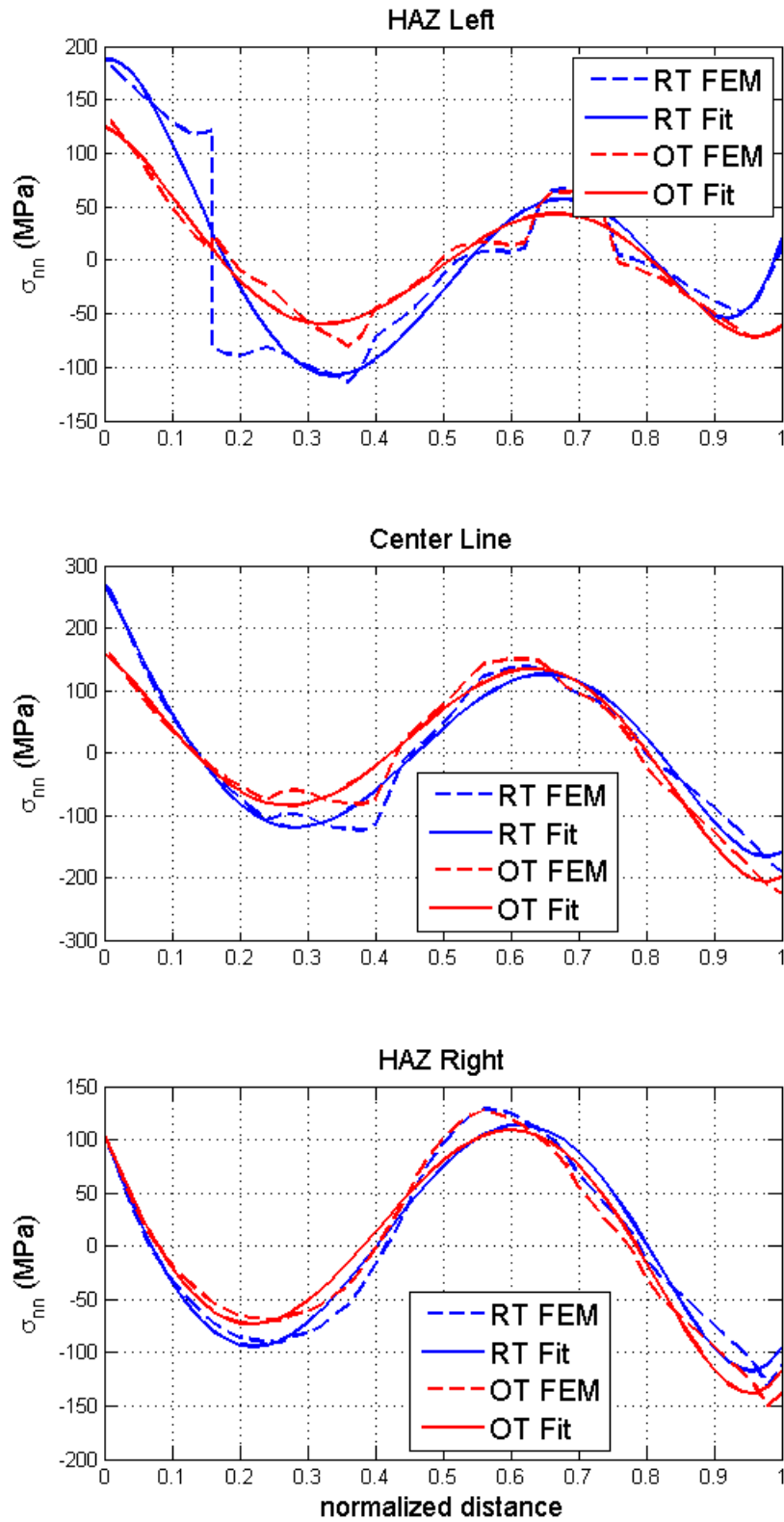


Figure 66 Normal stress polynomial fit for weld case II.4.

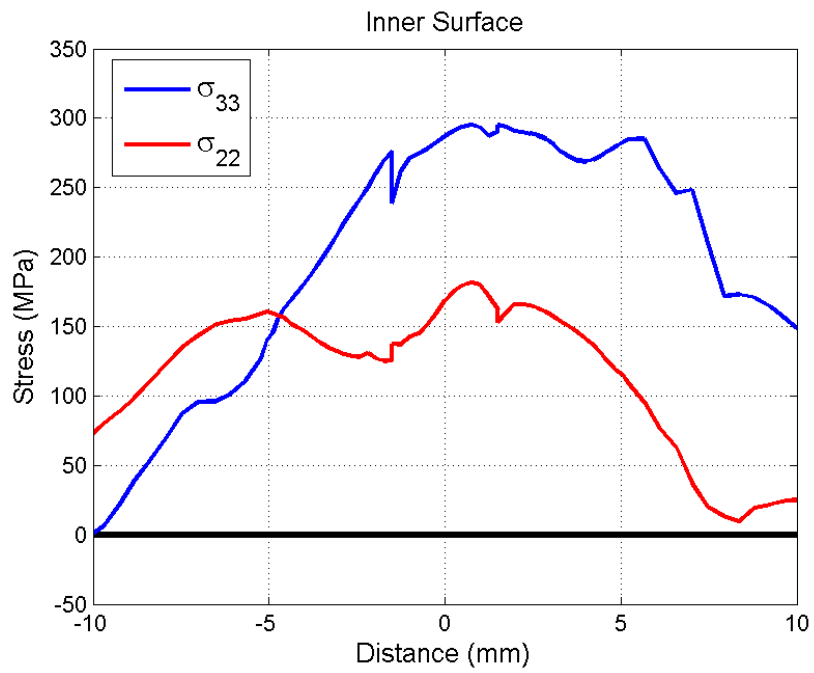


Figure 67 Hoop and axial stresses at the inner surface at Operation Temperature (OT) for weld case II.4.

Weld case III.1

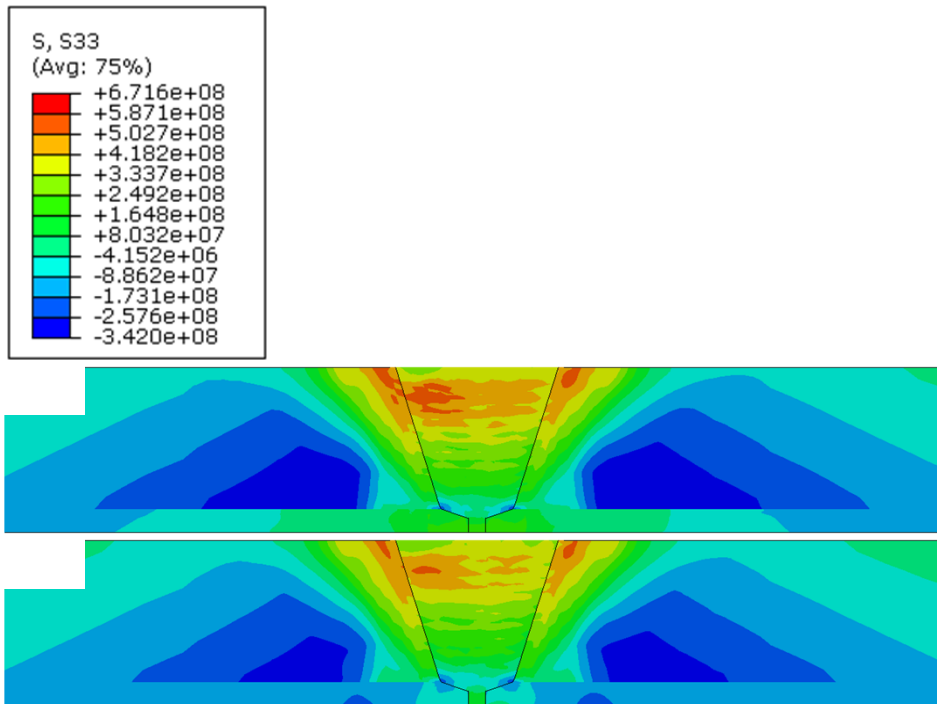


Figure 68 Hoop stress (S33) at: (a) Room Temperature (RT) and (b) Operation Temperature (OT) for weld case III.1.

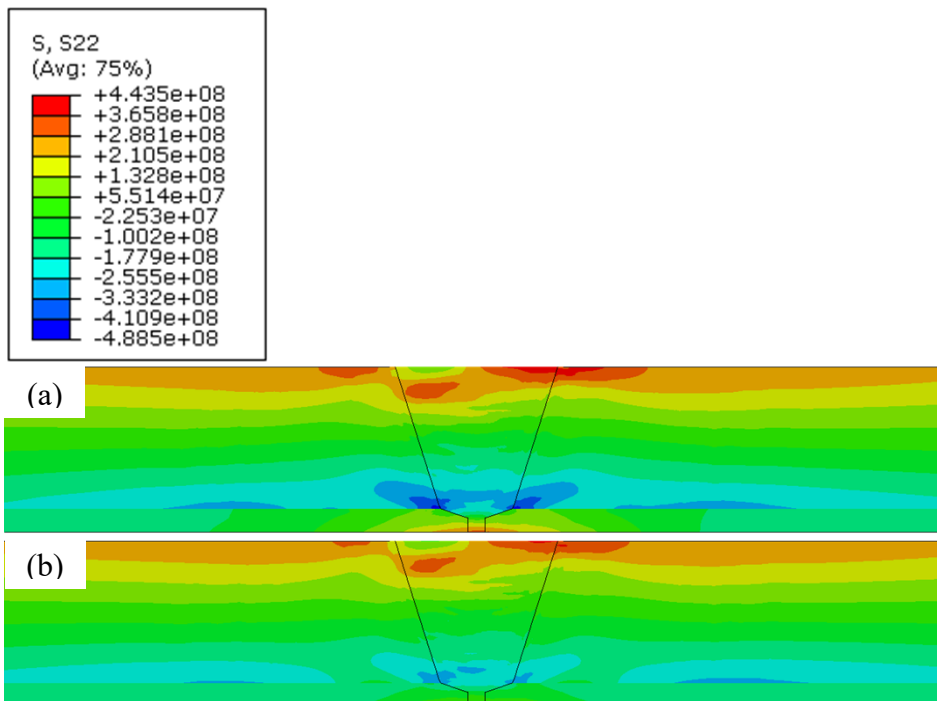


Figure 69 Axial stress S22 at: (a) Room Temperature (RT) and (b) Operation Temperature (OT) for weld case III.1.

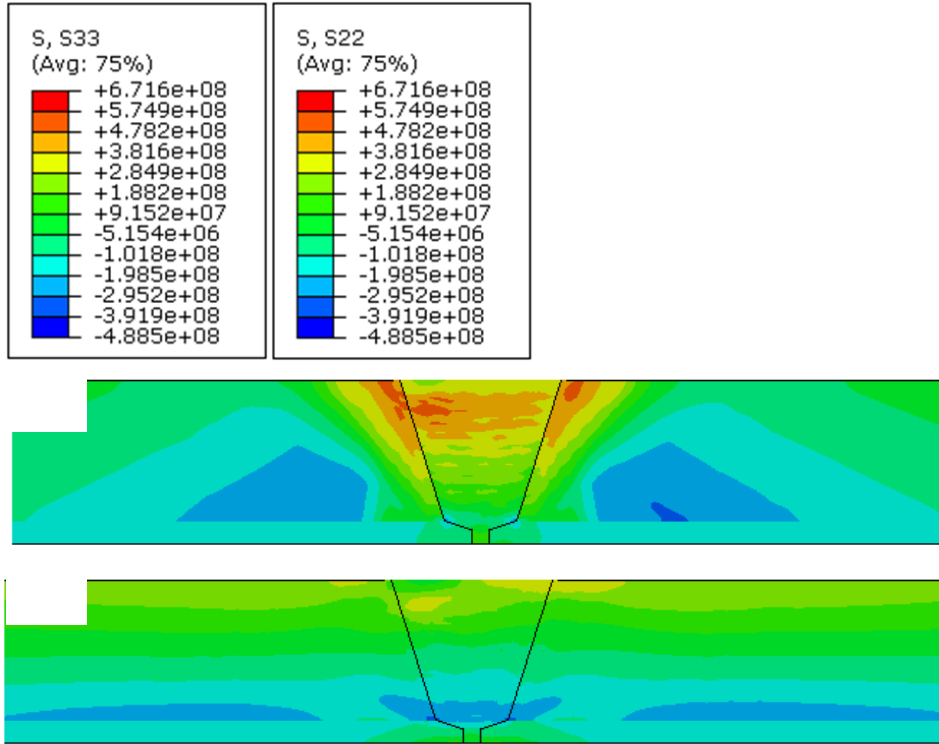


Figure 70 (a) Hoop stress S33 and (b) Axial stress S22 at Operation Temperature (OT) for weld case III.1.

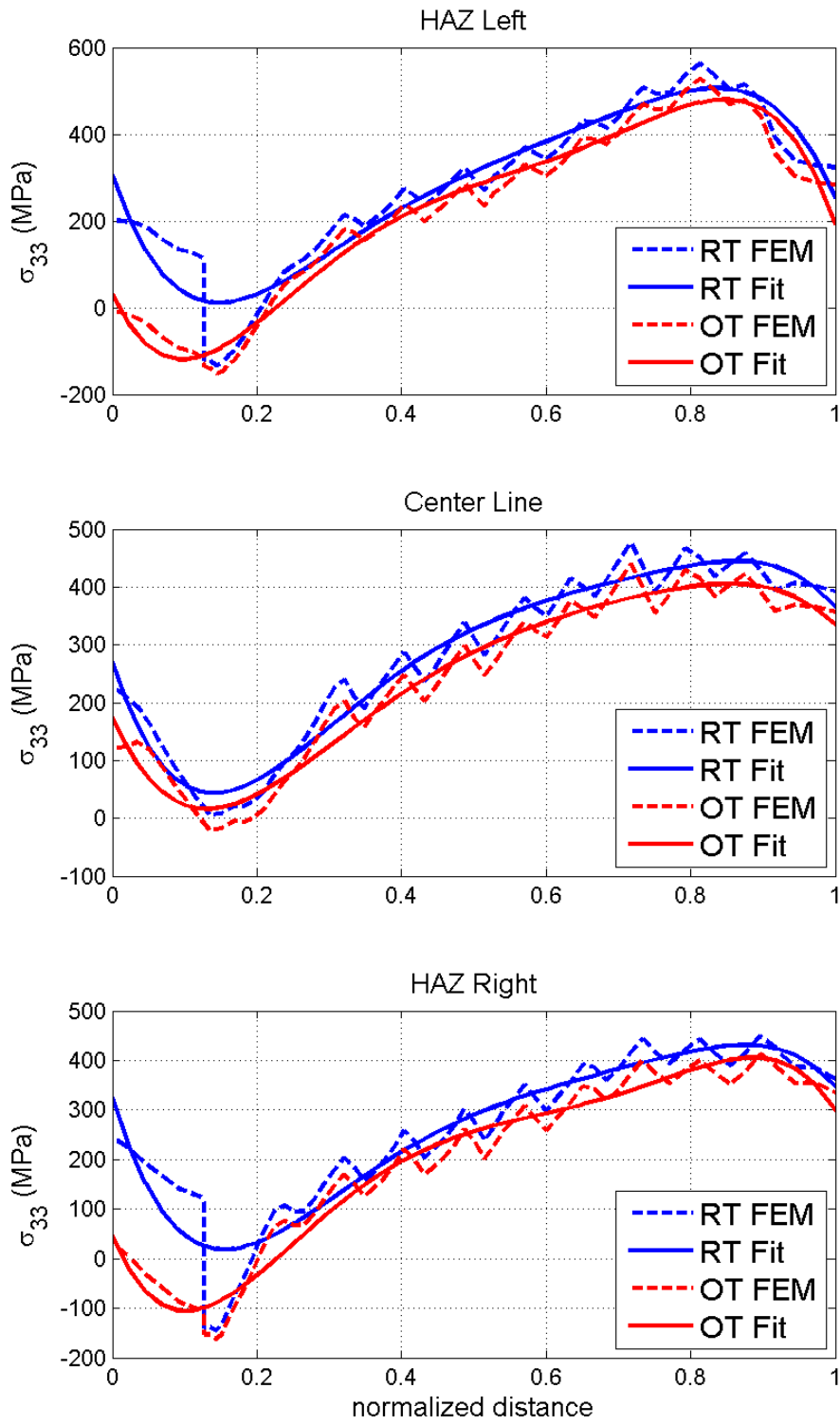


Figure 71 Hoop stress polynomial fit for weld case III.1.

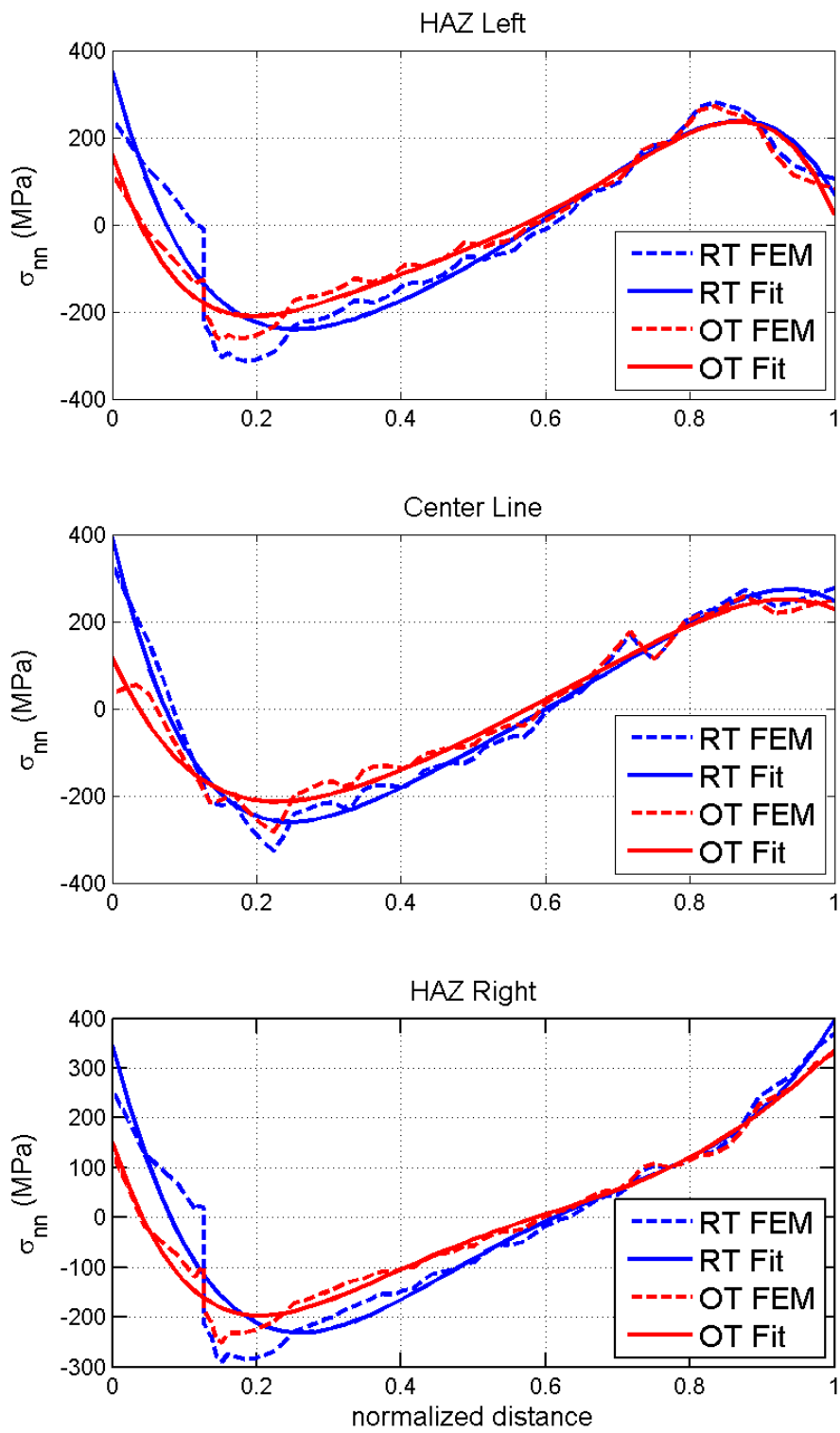


Figure 72 Normal stress polynomial fit for weld case III.1.

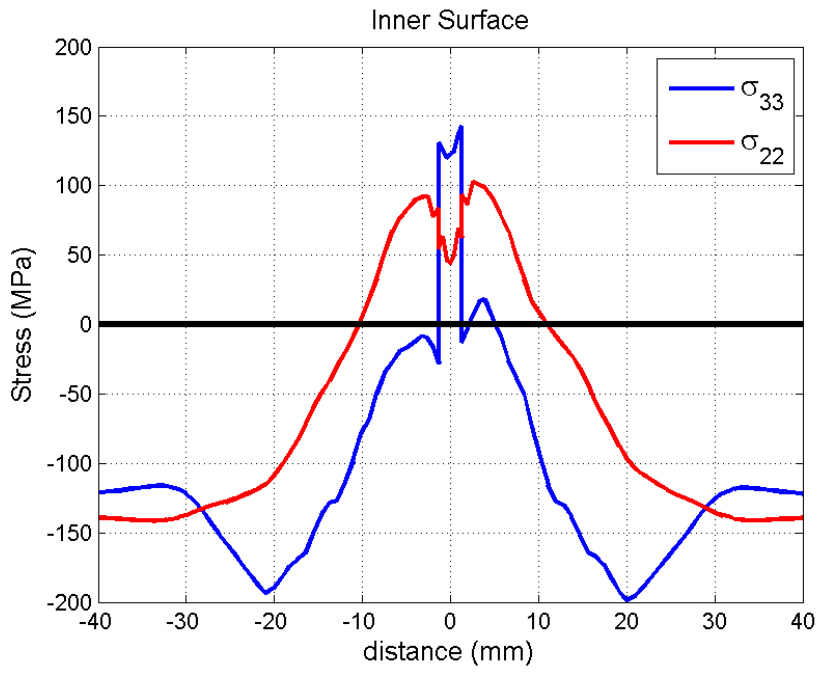


Figure 73 Hoop and axial stresses at the inner surface at Operation Temperature (OT) for weld case III.1.

Weld case IV.1

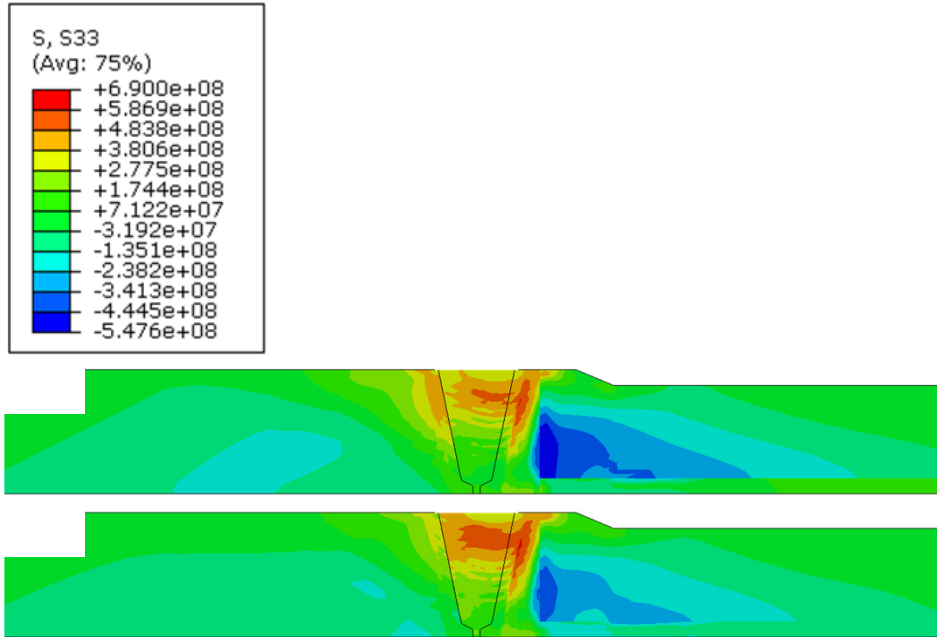


Figure 74 Hoop stress (S33) at: (a) Room Temperature (RT) and (b) Operation Temperature (OT) for weld case IV.1.

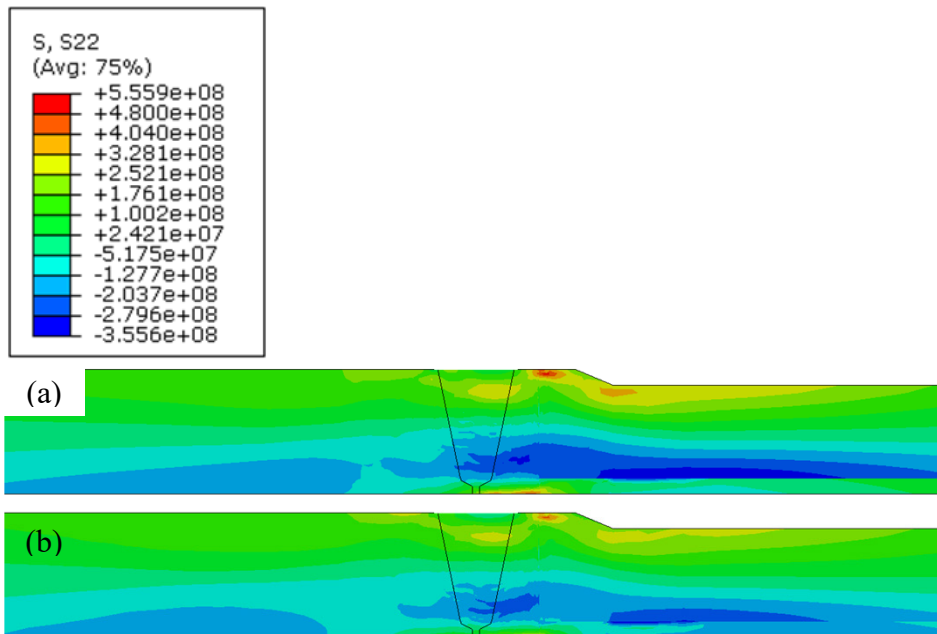


Figure 75 Axial stress S22 at: (a) Room Temperature (RT) and (b) Operation Temperature (OT) for weld case IV.1.

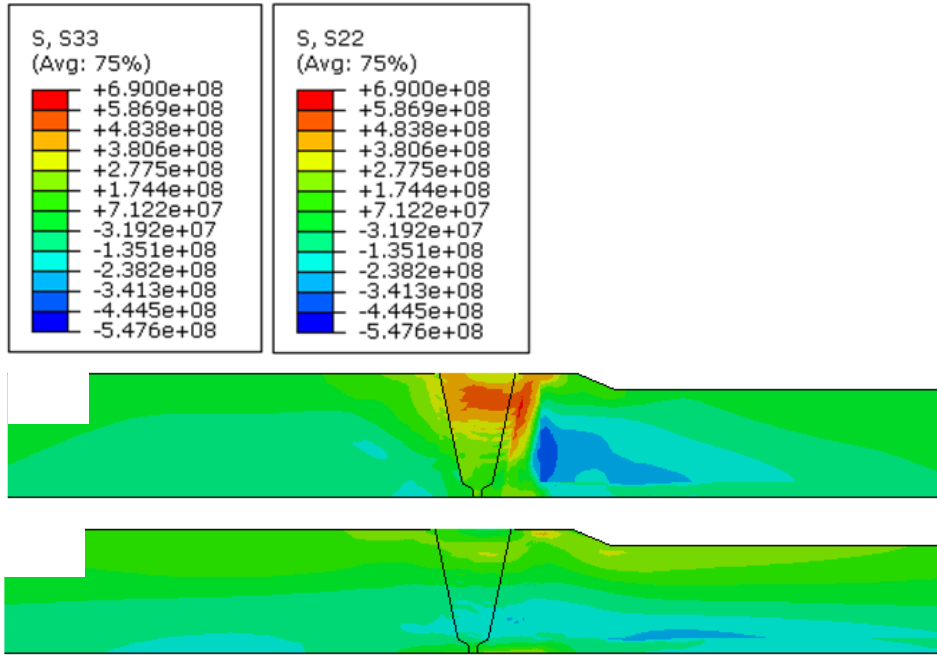


Figure 76 (a) Hoop stress S33 and (b) Axial stress S22 at Operation Temperature (OT) for weld case IV.1.

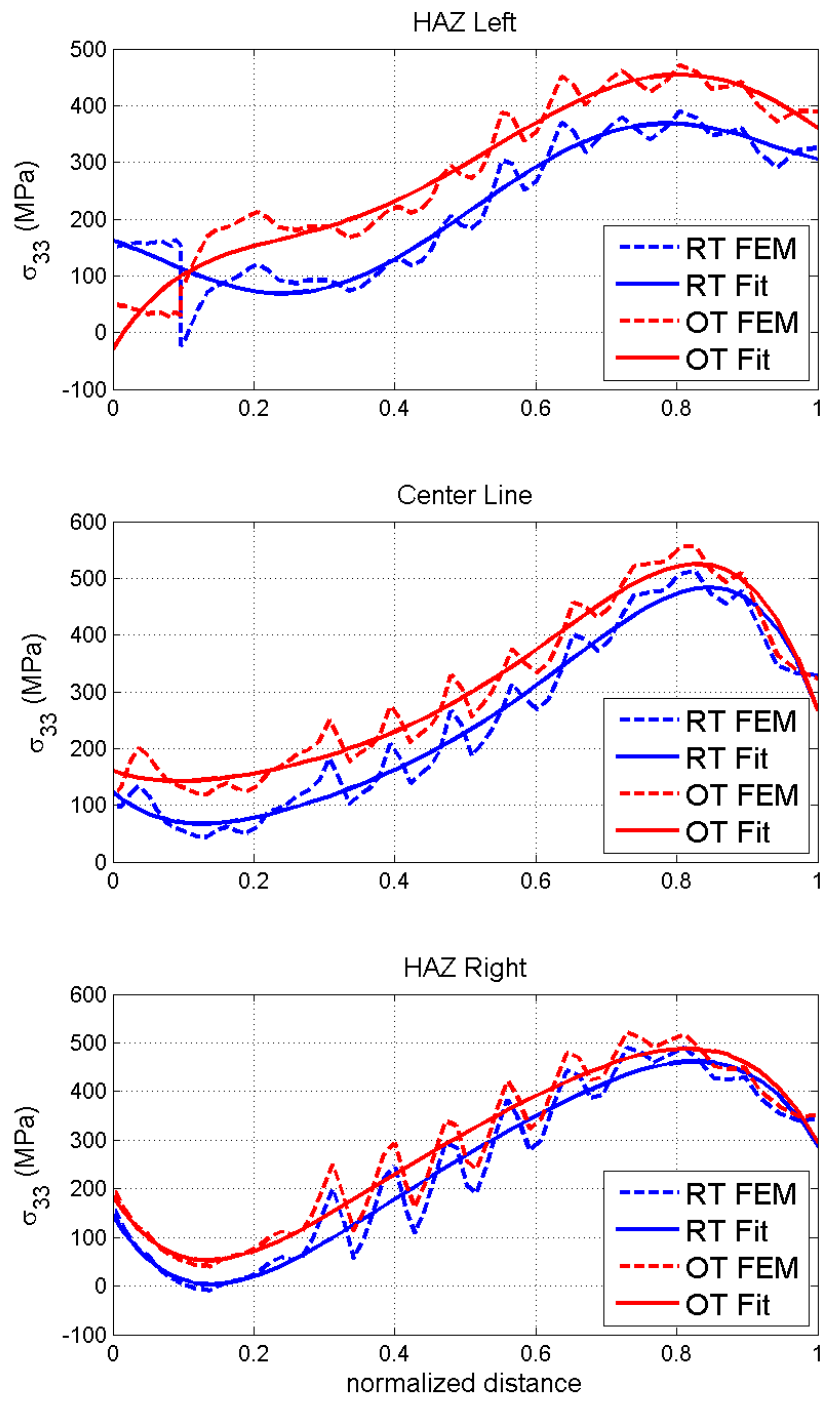


Figure 77 Hoop stress polynomial fit for weld case IV.1.

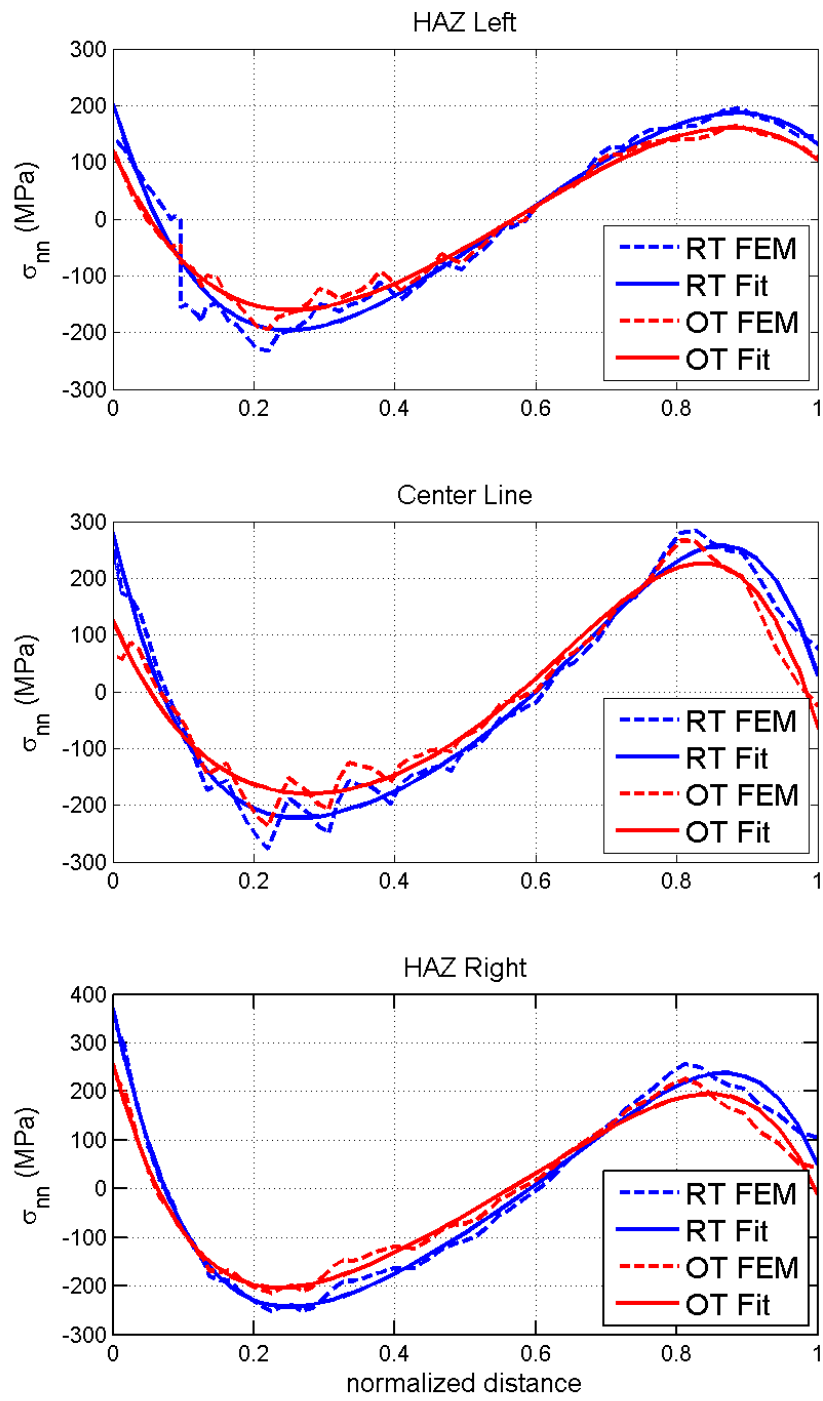


Figure 78 Normal stress polynomial fit for weld case IV.1.

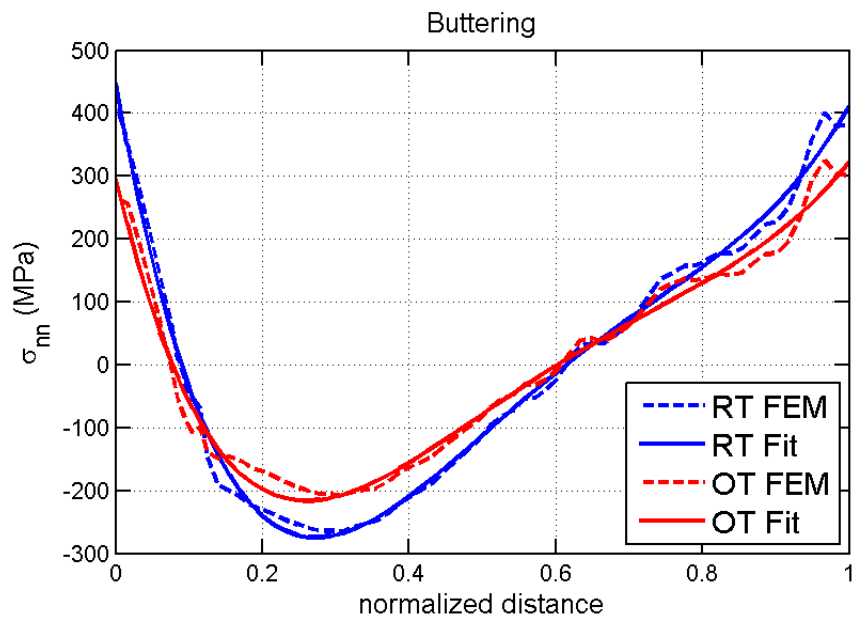
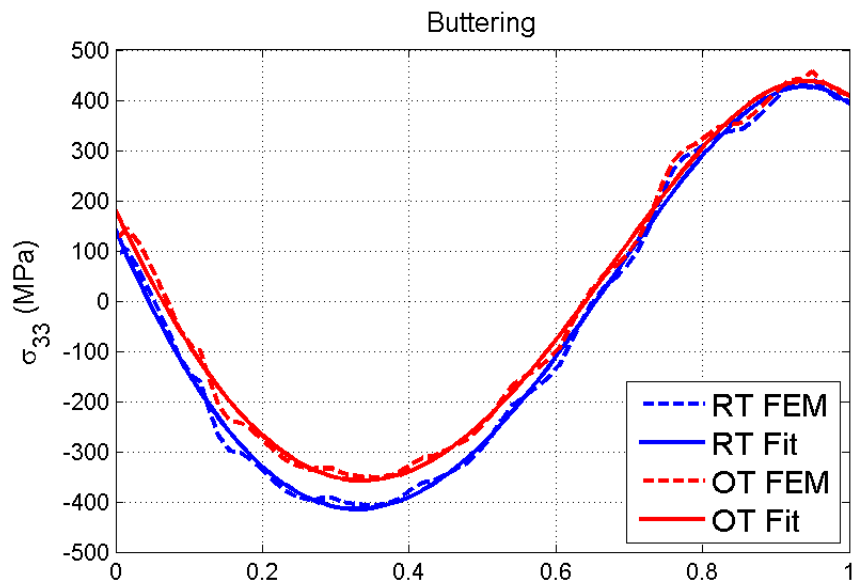


Figure 79 Hoop and normal stress polynomial fit for weld case IV.1.

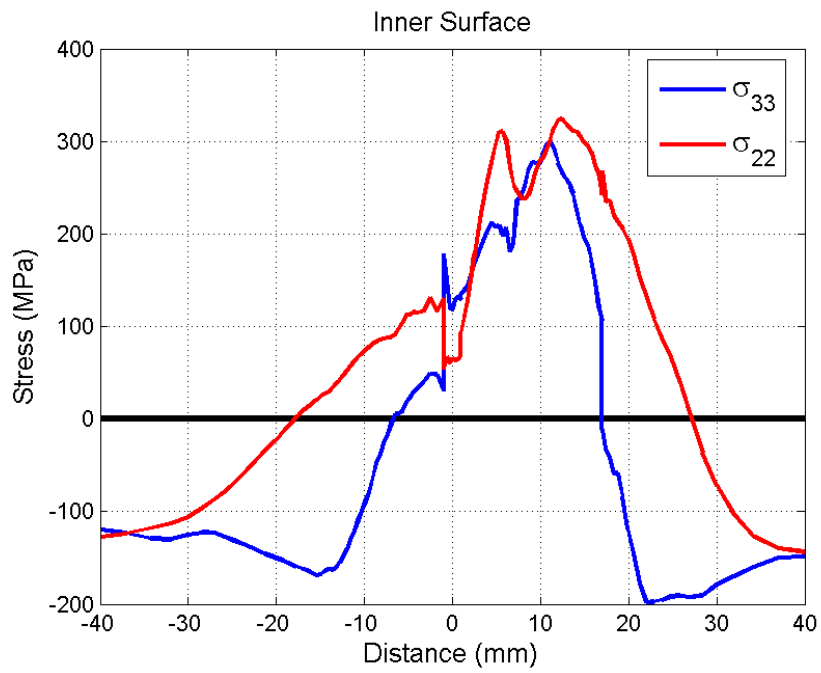


Figure 80 Hoop and axial stresses at the inner surface at Operation Temperature (OT) for weld case IV.1.

Weld case IV.2

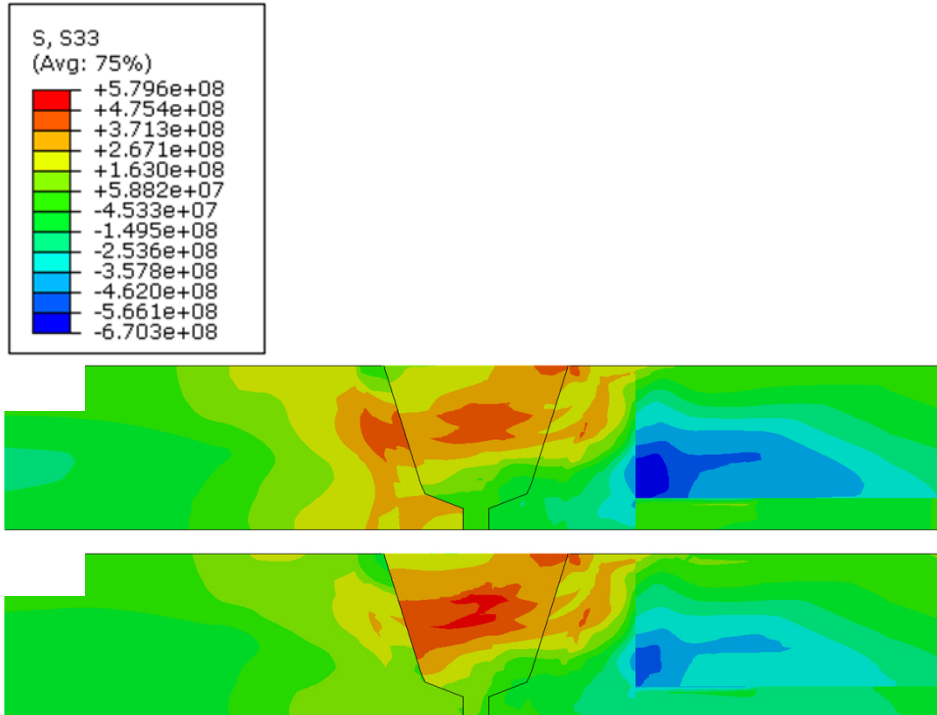


Figure 81 Hoop stress (S33) at: (a) Room Temperature (RT) and (b) Operation Temperature (OT) for weld case IV.2.

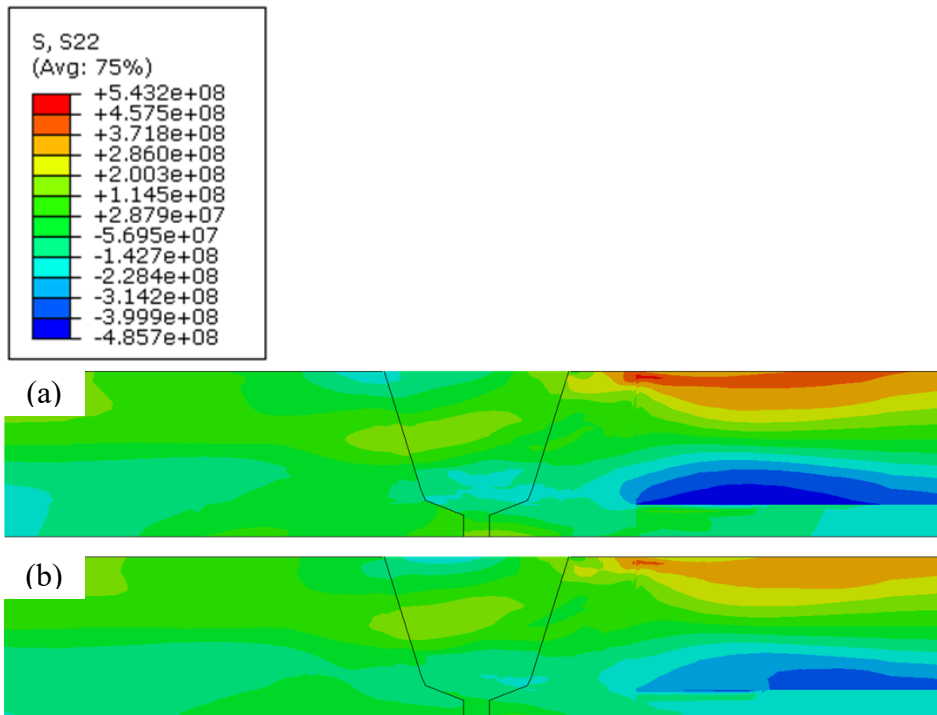


Figure 82 Axial stress S22 at: (a) Room Temperature (RT) and (b) Operation Temperature (OT) for weld case IV.2.

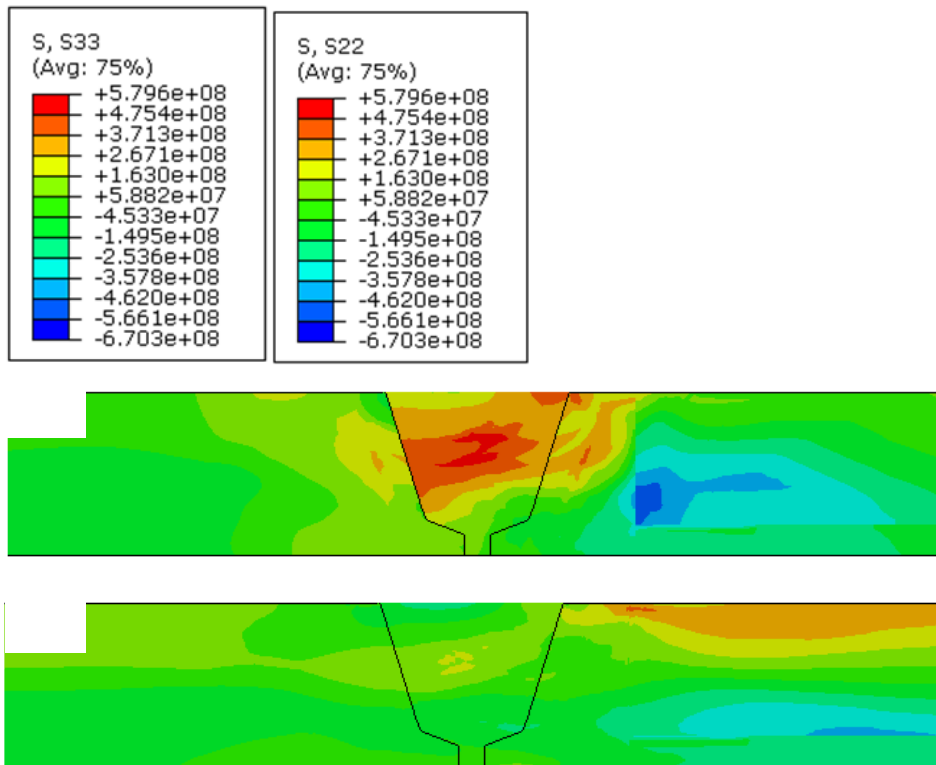


Figure 83 (a) Hoop stress S33 and (b) Axial stress S22 at Operation Temperature (OT) for weld case IV.2.

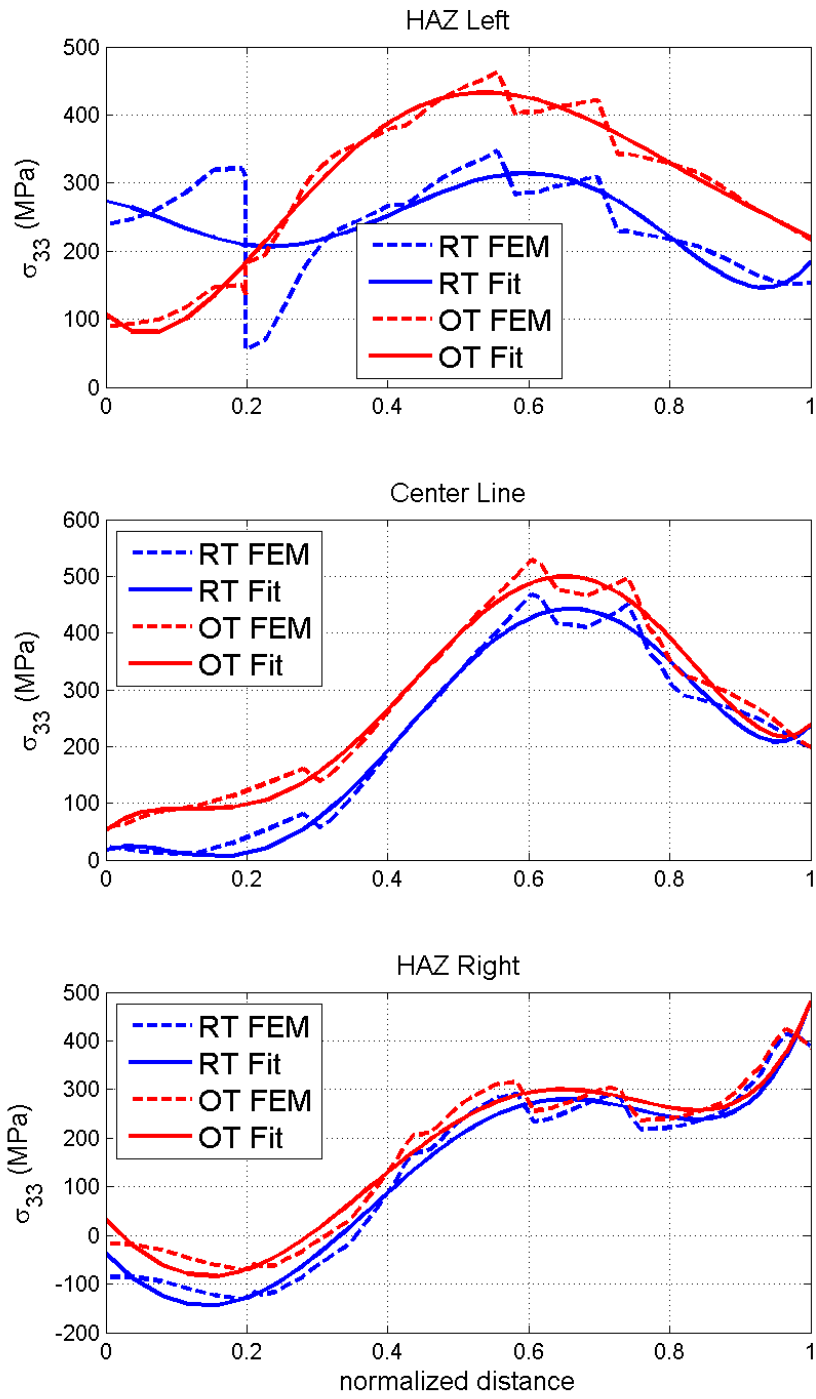


Figure 84 Hoop stress polynomial fit for weld case IV.2.

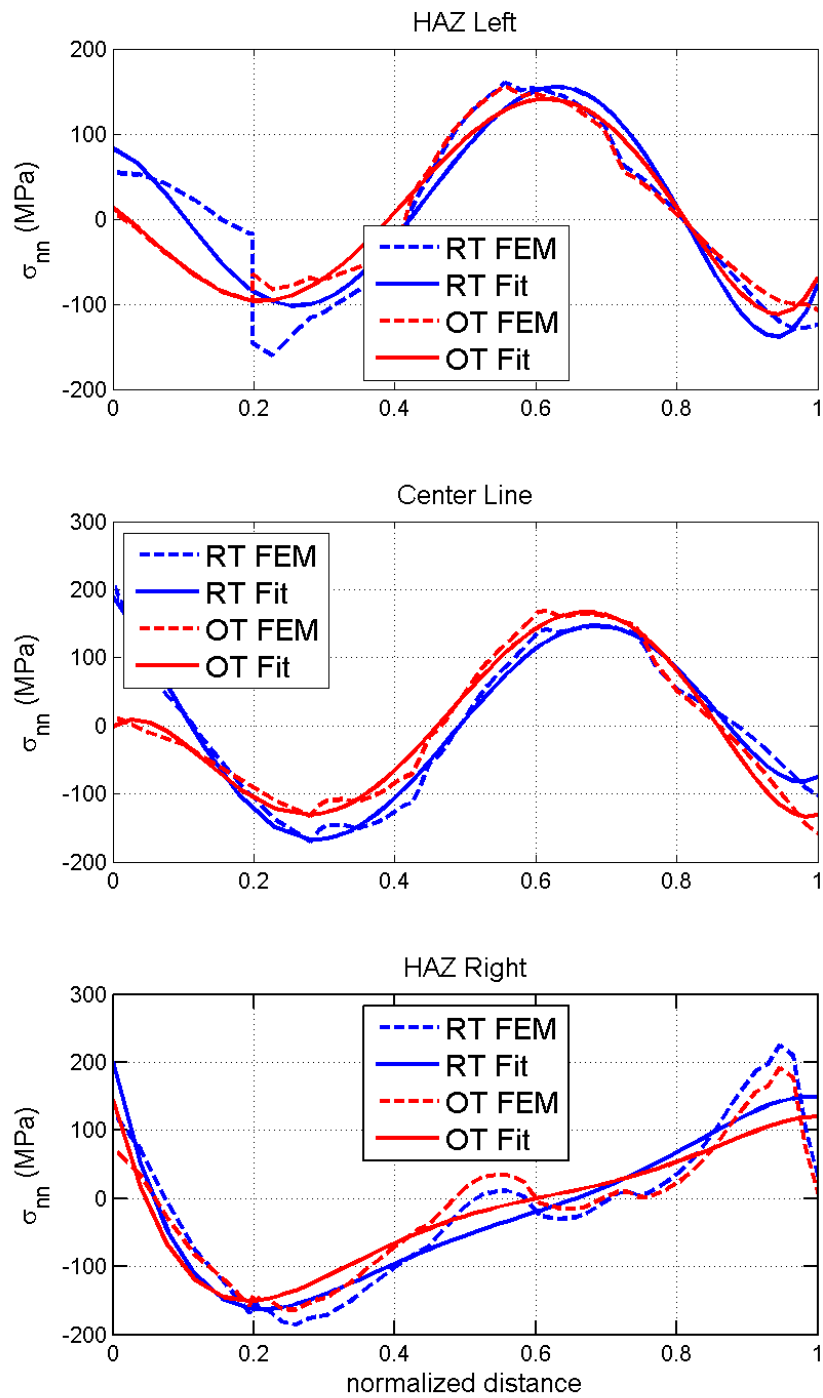


Figure 85 Normal stress polynomial fit for weld case IV.2.

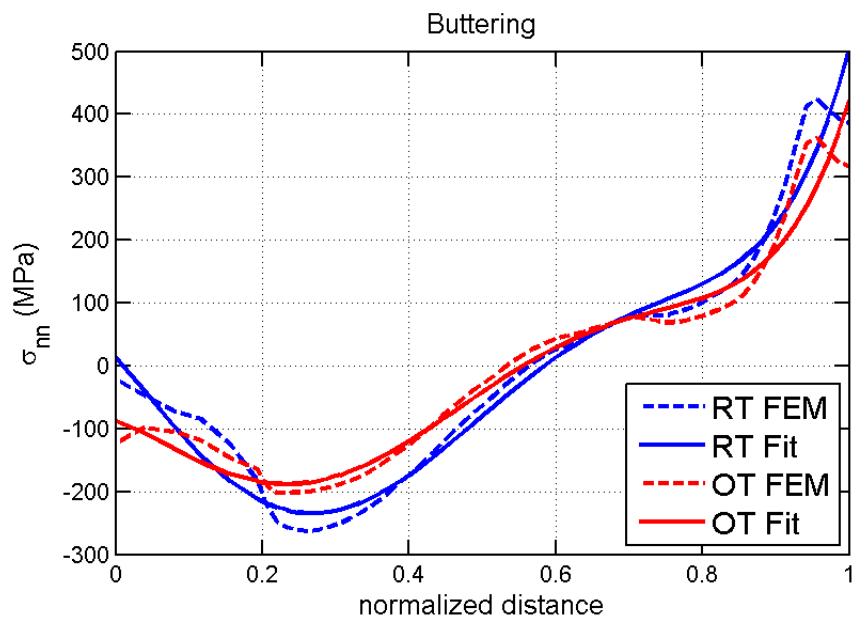
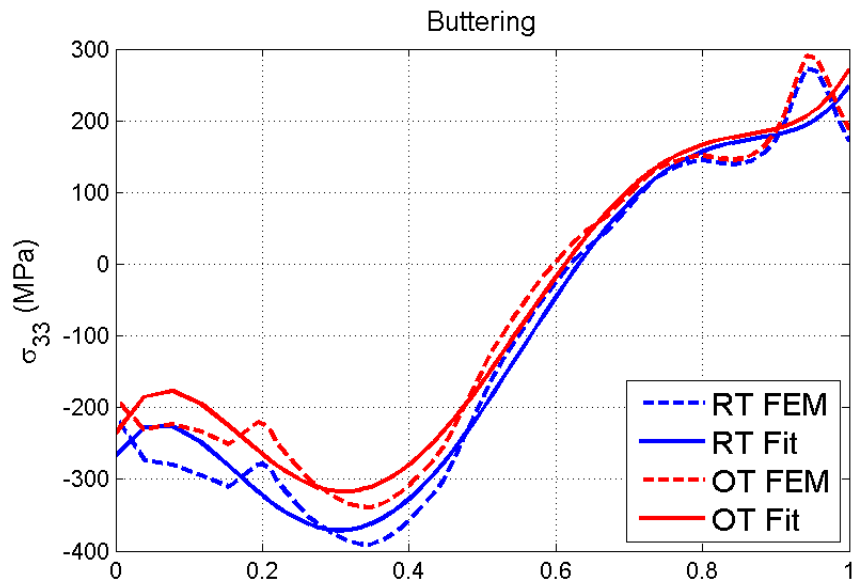


Figure 86 Hoop and normal stress polynomial fit for weld case IV.2.

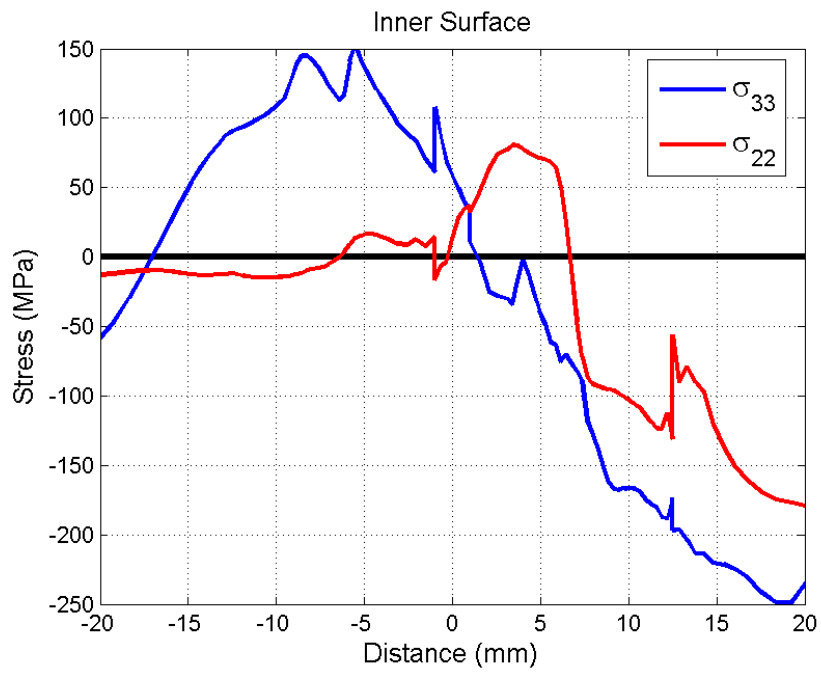


Figure 87 Hoop and axial stresses at the inner surface at Operation Temperature (OT) for weld case IV.2.

Weld case IV.3

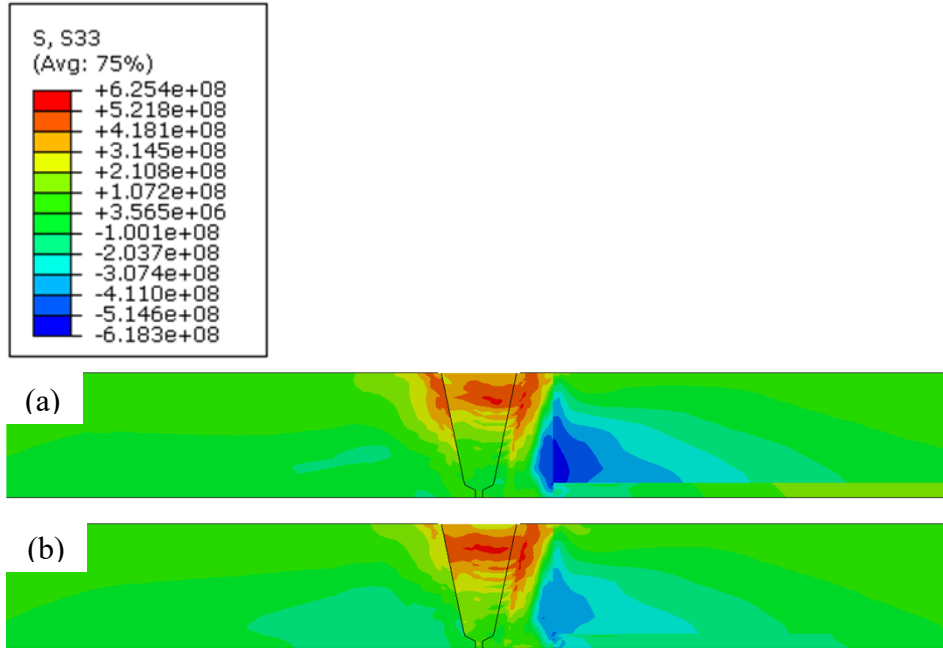


Figure 88 Hoop stress (S33) at: (a) Room Temperature (RT) and (b) Operation Temperature (OT) for weld case IV.3.

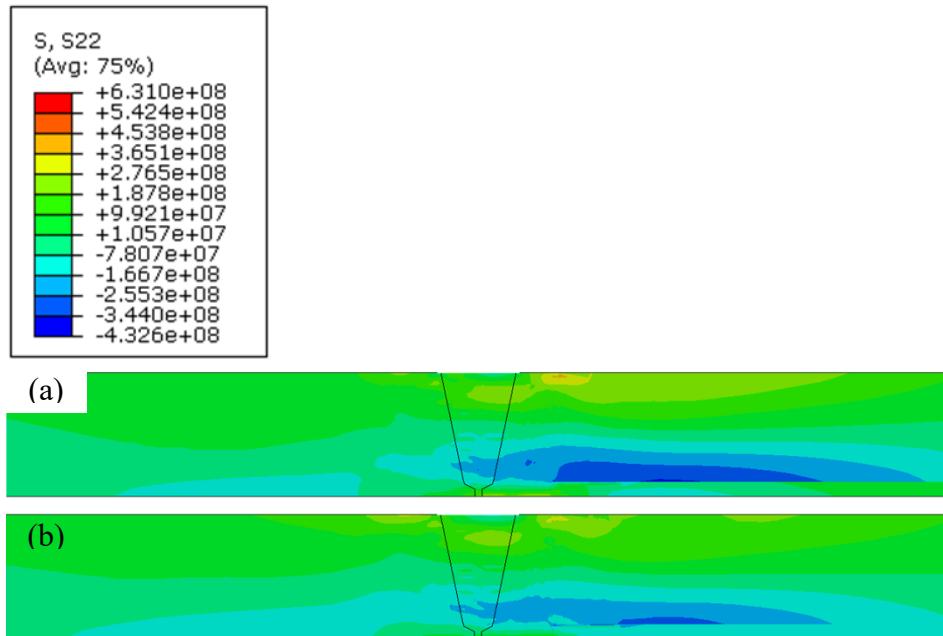


Figure 89 Axial stress S22 at: (a) Room Temperature (RT) and (b) Operation Temperature (OT) for weld case IV.3.

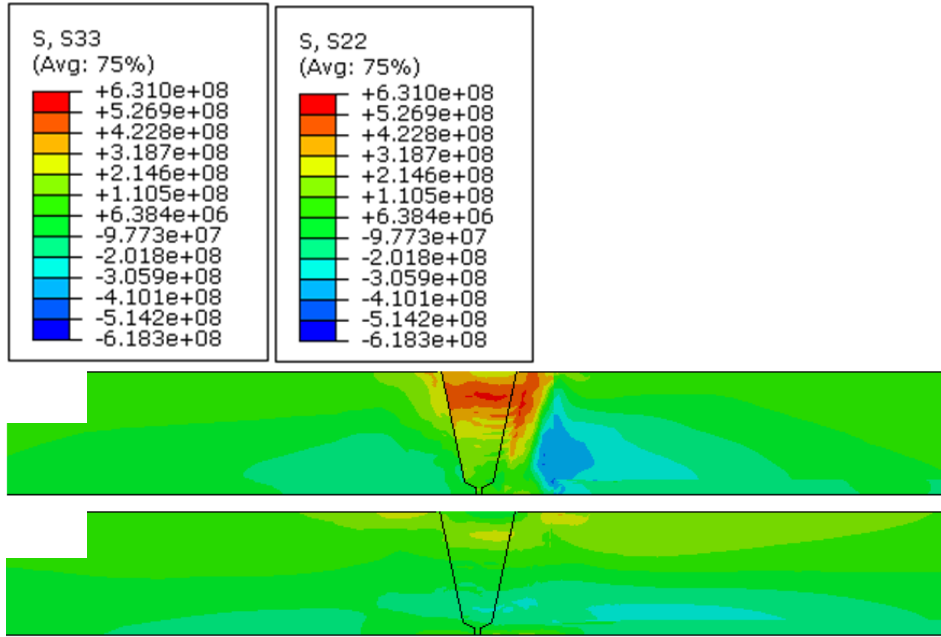


Figure 90 (a) Hoop stress S33 and (b) Axial stress S22 at Operation Temperature (OT) for weld case IV.3.

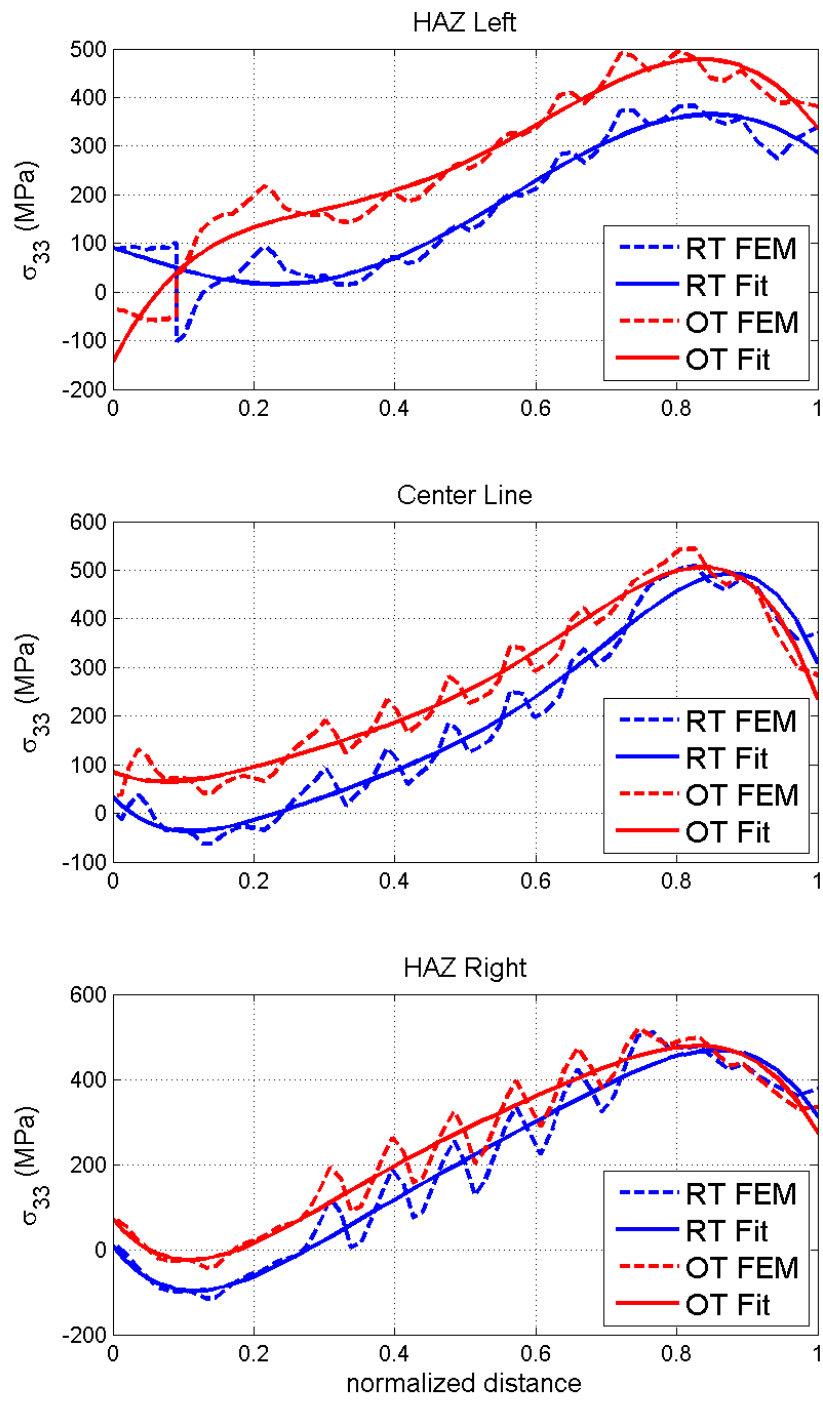


Figure 91 Hoop stress polynomial fit for weld case IV.3.

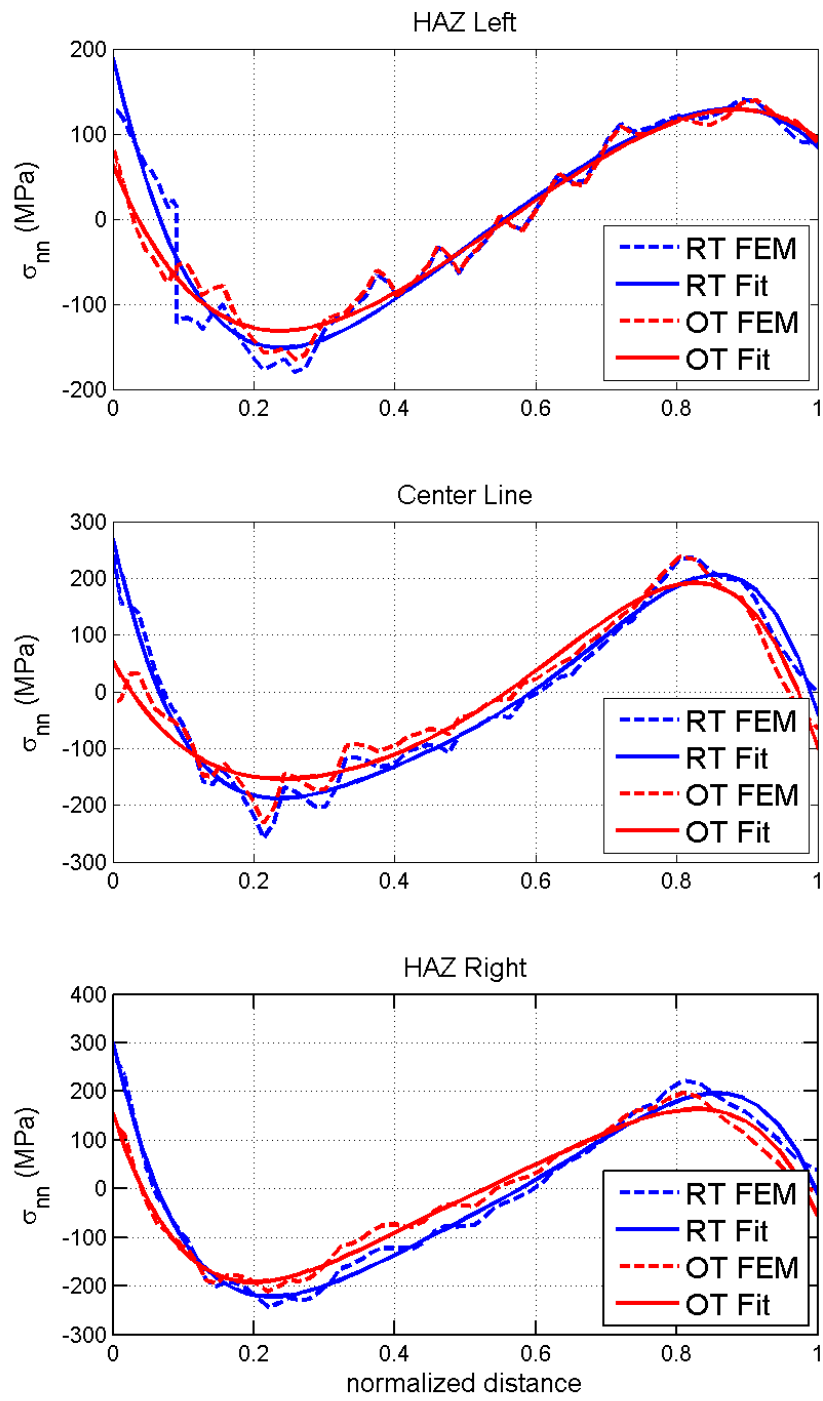


Figure 92 Normal stress polynomial fit for weld case IV.3.

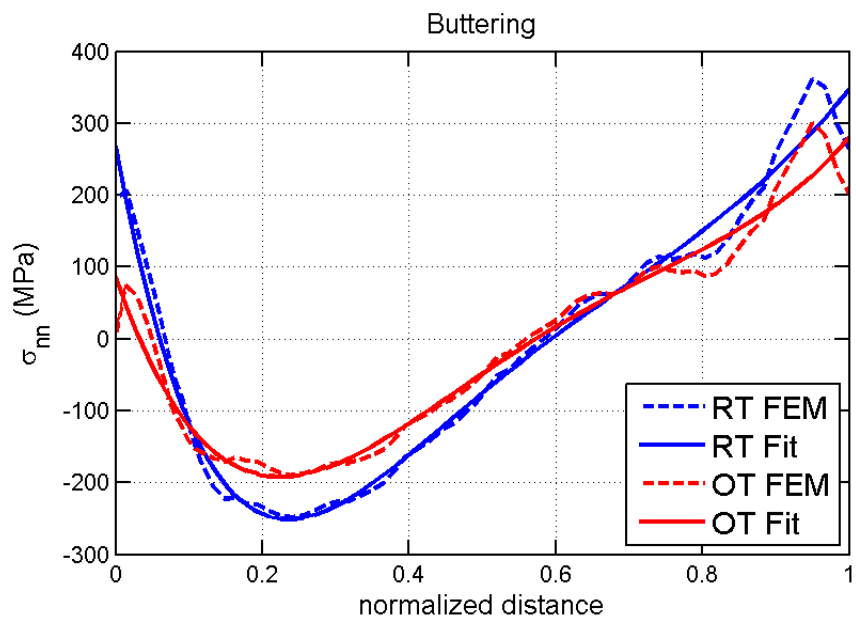
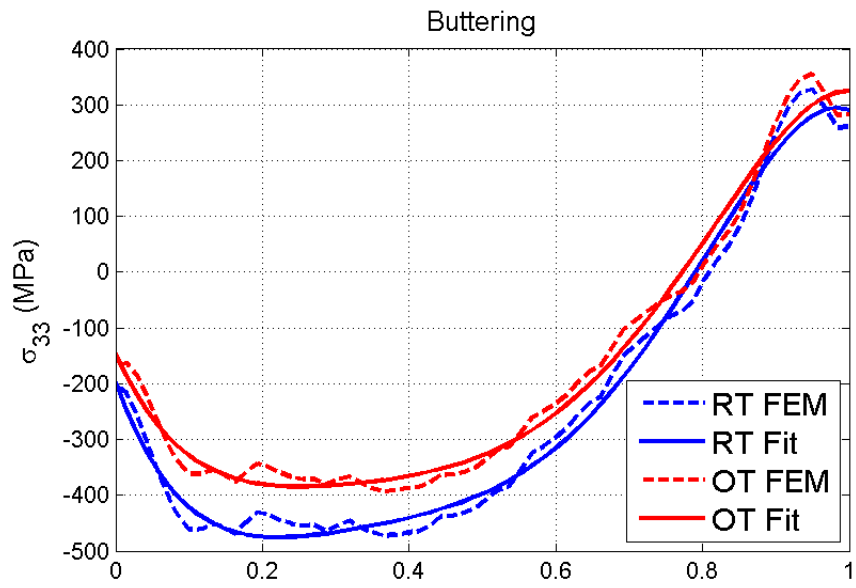


Figure 93 Hoop and normal stress polynomial fit for weld case IV.3.

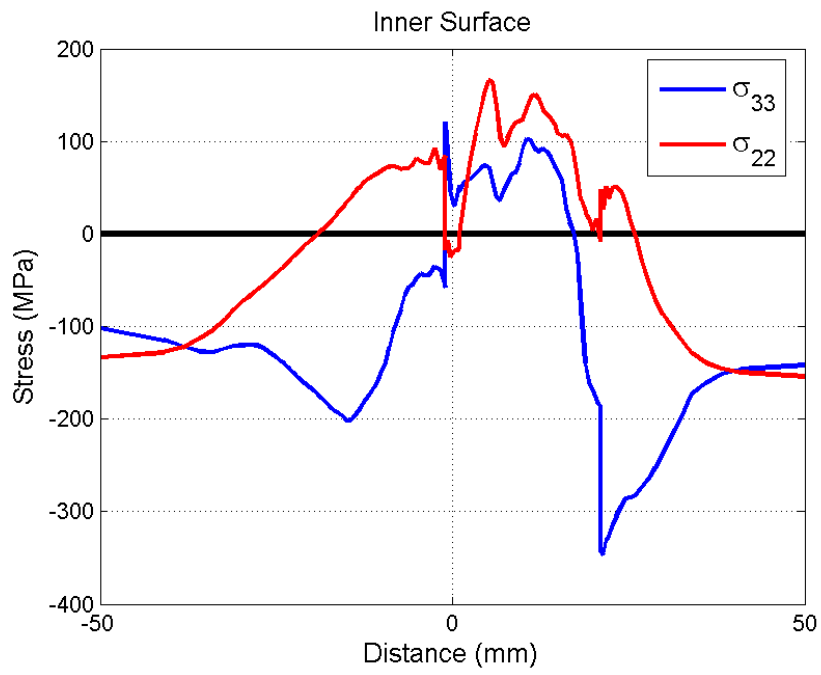


Figure 94 Hoop and axial stresses at the inner surface at Operation Temperature (OT) for weld case IV.3.

Weld case IV.4

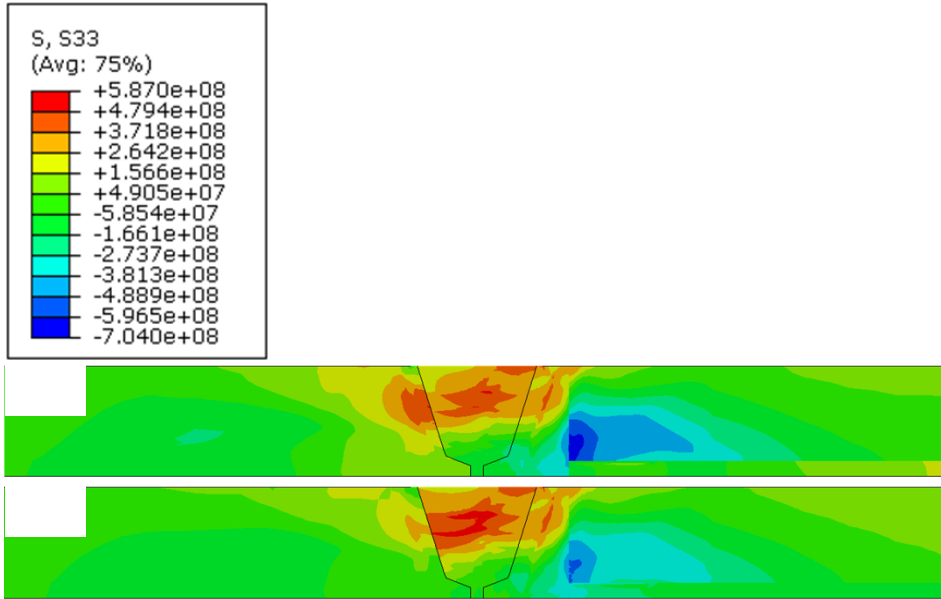


Figure 95 Hoop stress (S33) at: (a) Room Temperature (RT) and (b) Operation Temperature (OT) for weld case IV.4.

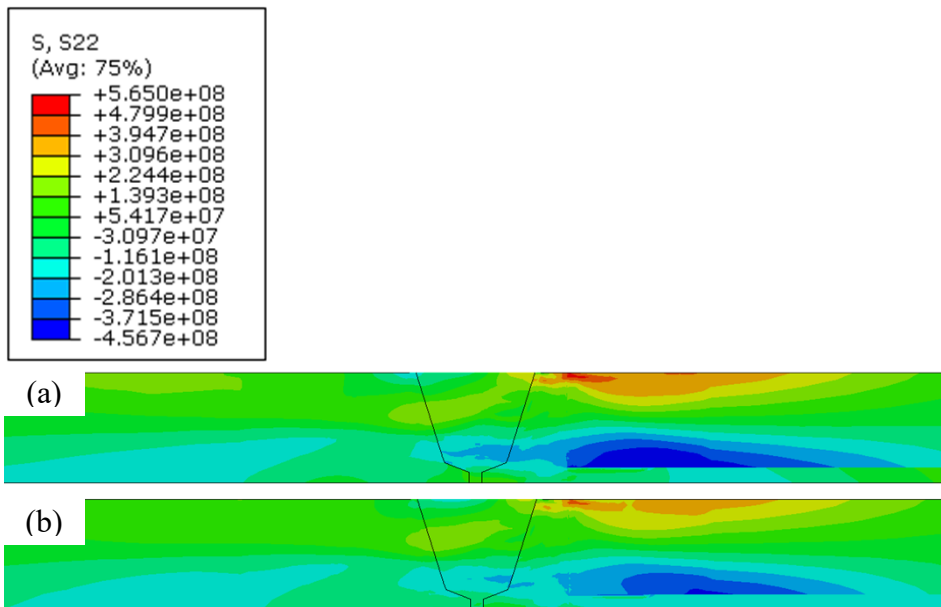


Figure 96 Axial stress S22 at: (a) Room Temperature (RT) and (b) Operation Temperature (OT) for weld case IV.4.

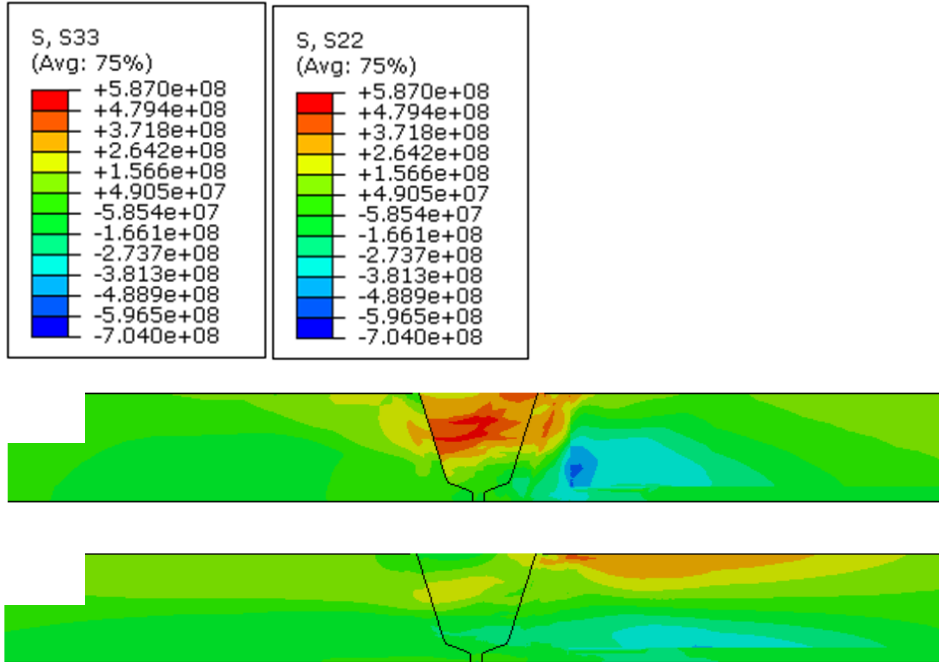


Figure 97 (a) Hoop stress S33 and (b) Axial stress S22 at Operation Temperature (OT) for weld case IV.4.

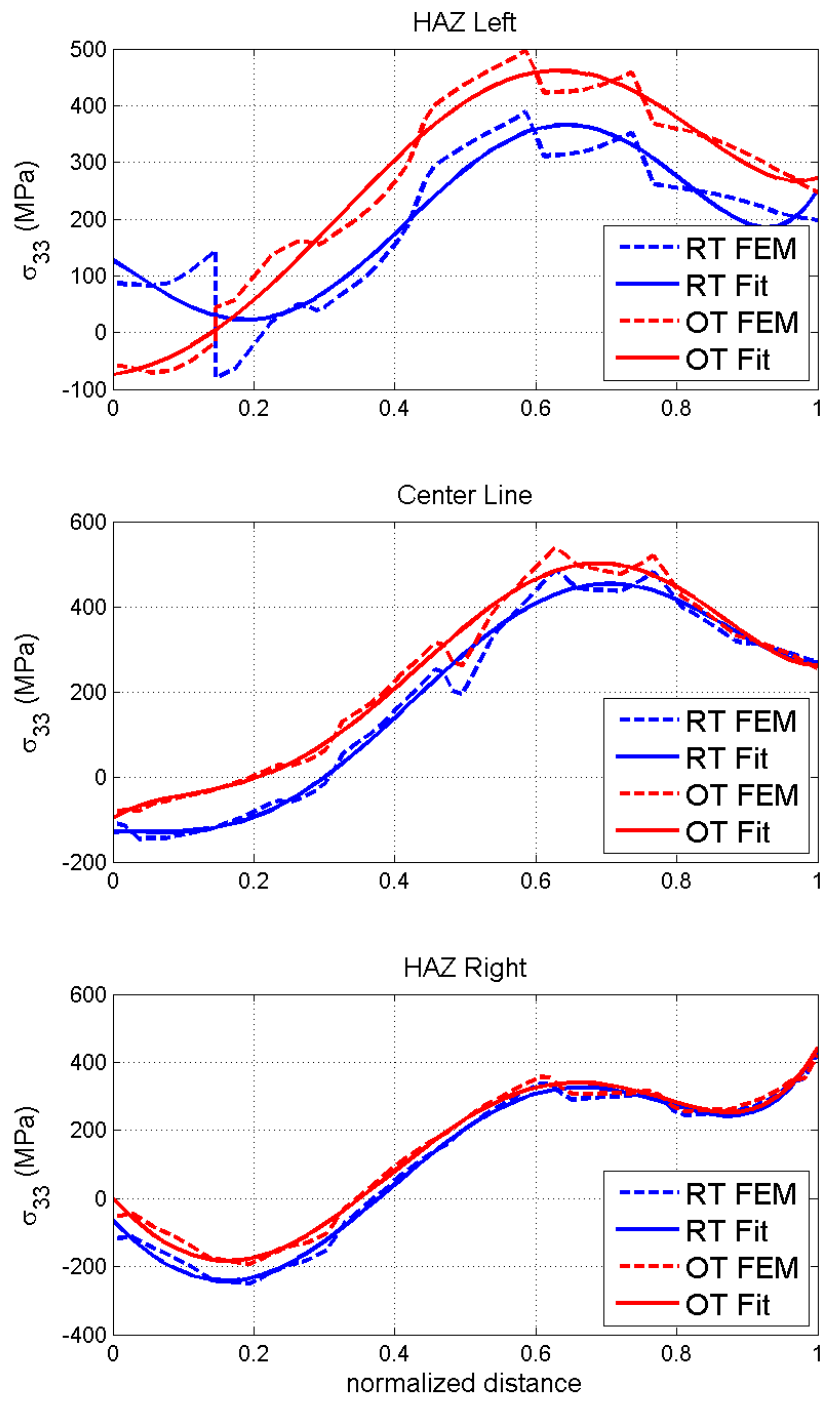


Figure 98 Hoop stress polynomial fit for weld case IV.4.

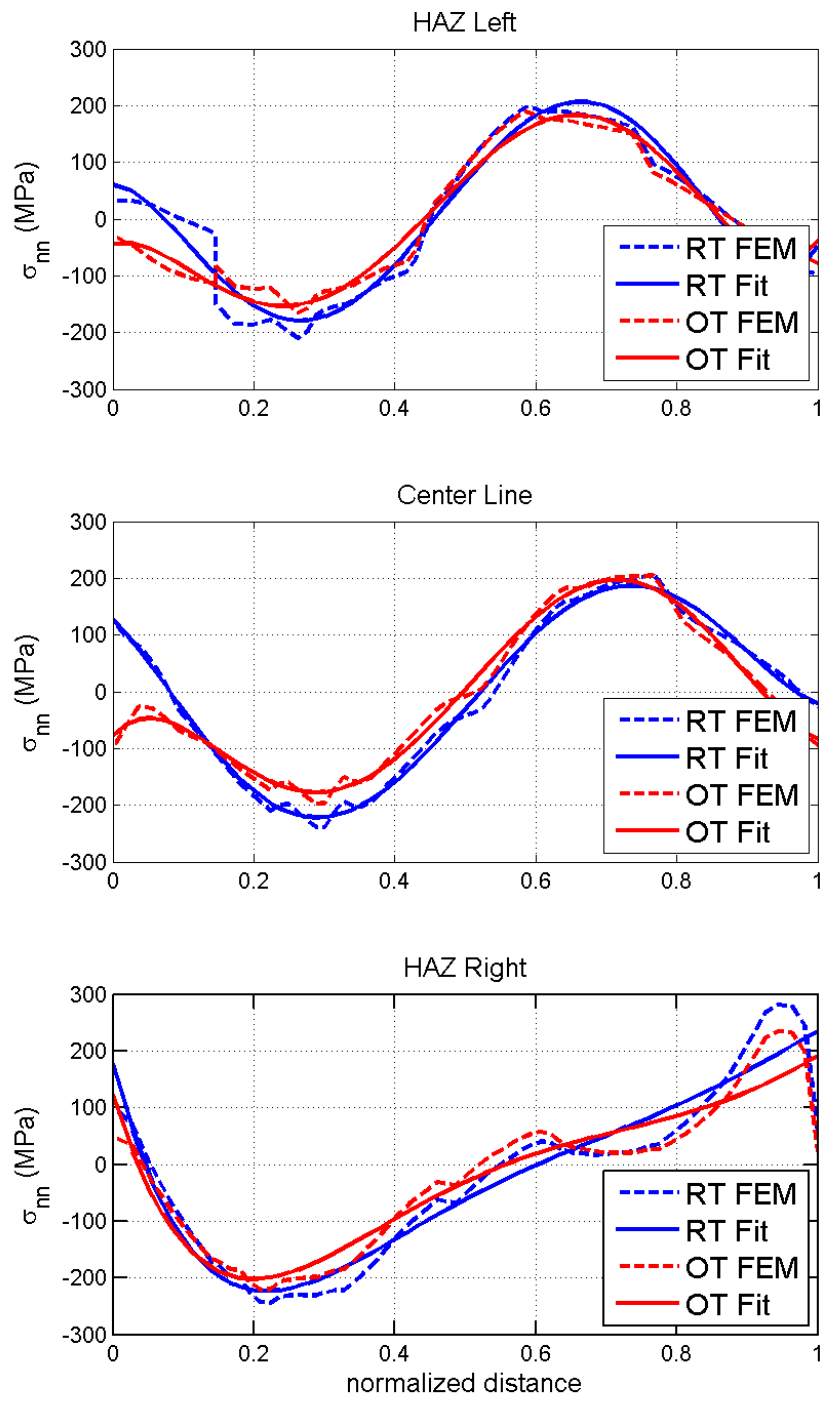


Figure 99 Normal stress polynomial fit for weld case IV.4.

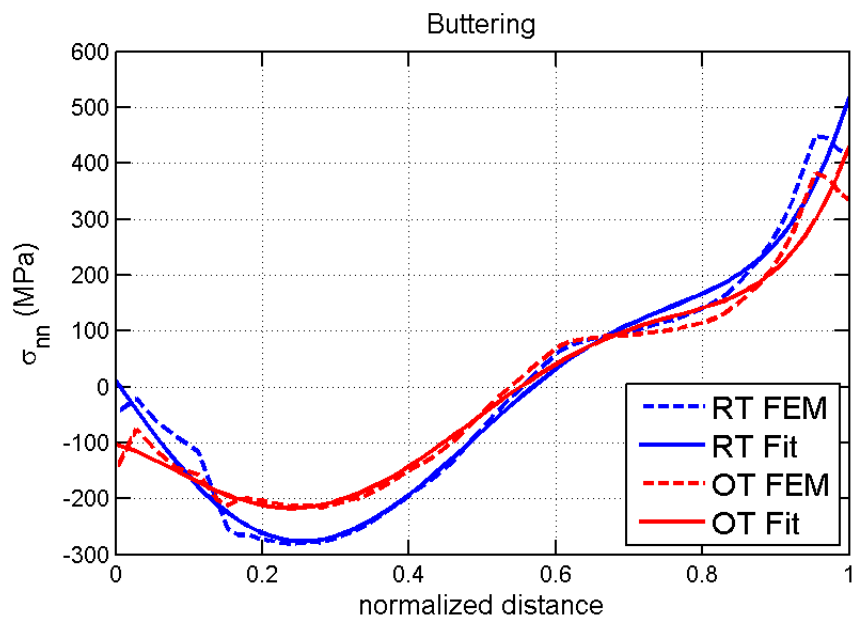
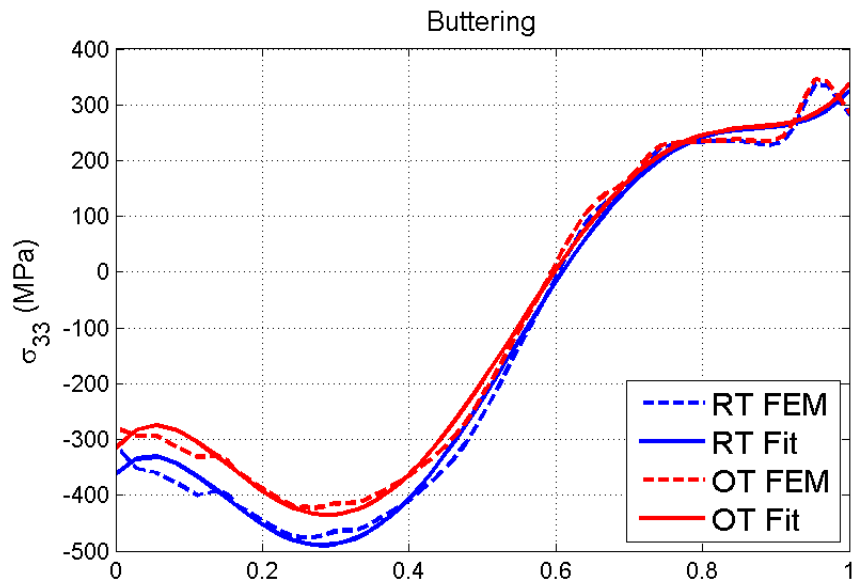


Figure 100 Hoop and normal stress polynomial fit for weld case IV.4.

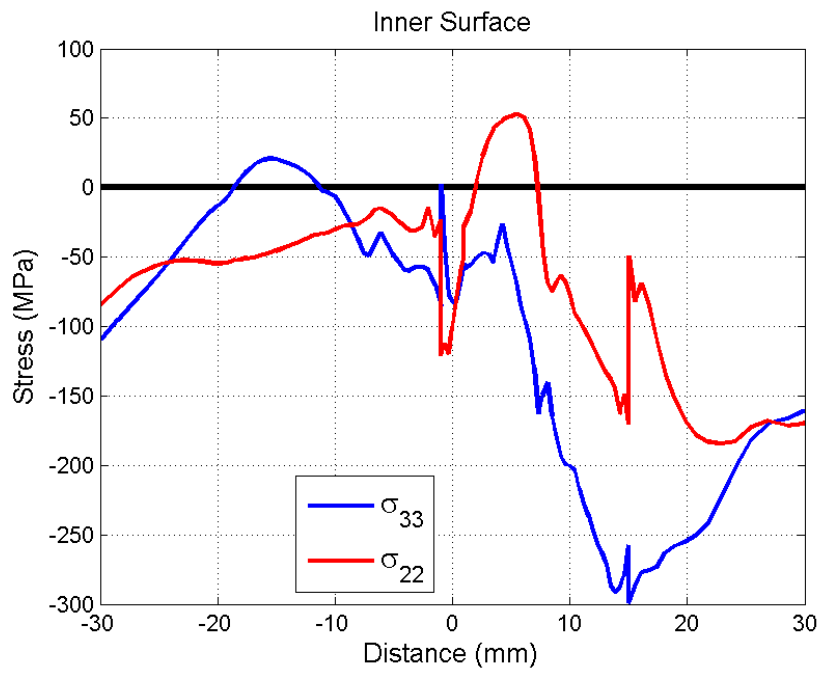


Figure 101 Hoop and axial stresses at the inner surface at Operation Temperature (OT) for weld case IV.4.

Weld case V.1

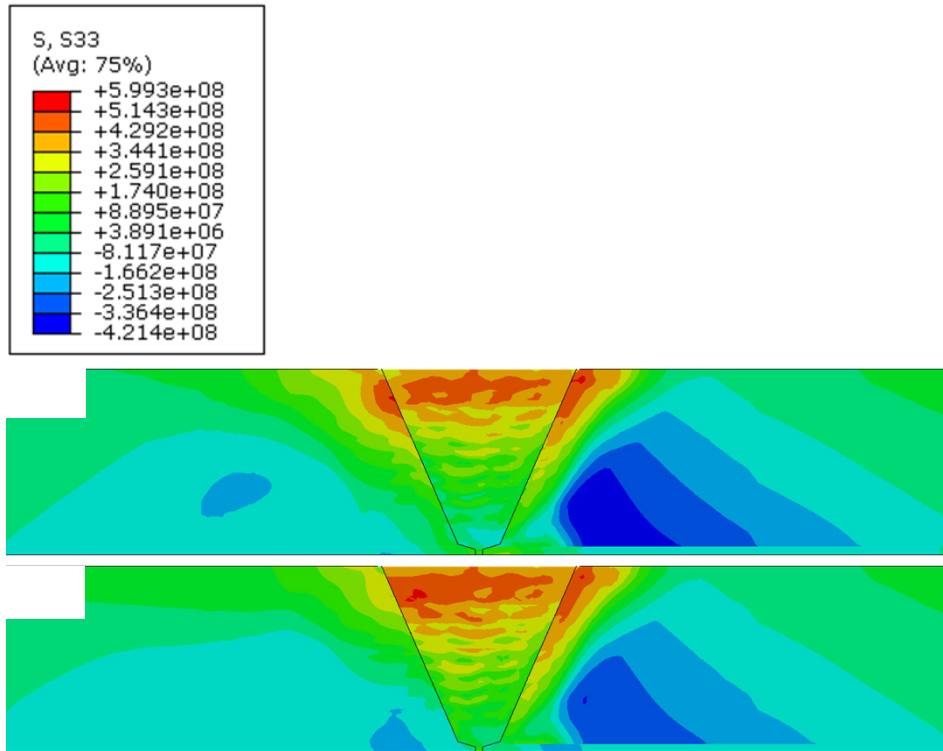


Figure 102 Hoop stress (S33) at: (a) Room Temperature (RT) and (b) Operation Temperature (OT) for weld case V.1.

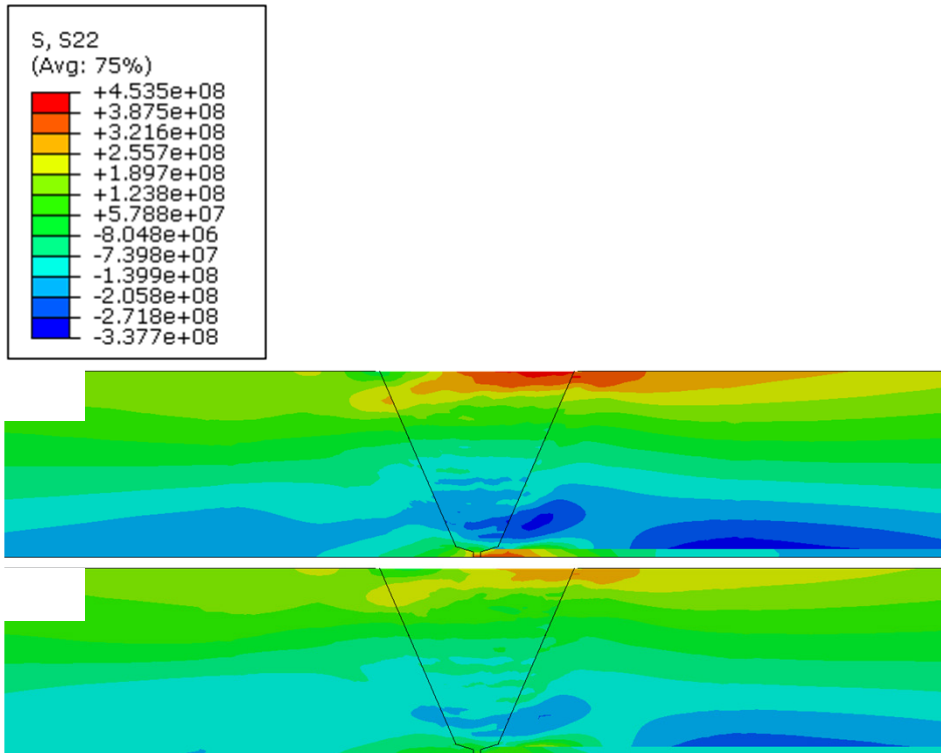


Figure 103 Axial stress S22 at: (a) Room Temperature (RT) and (b) Operation Temperature (OT) for weld case V.1.

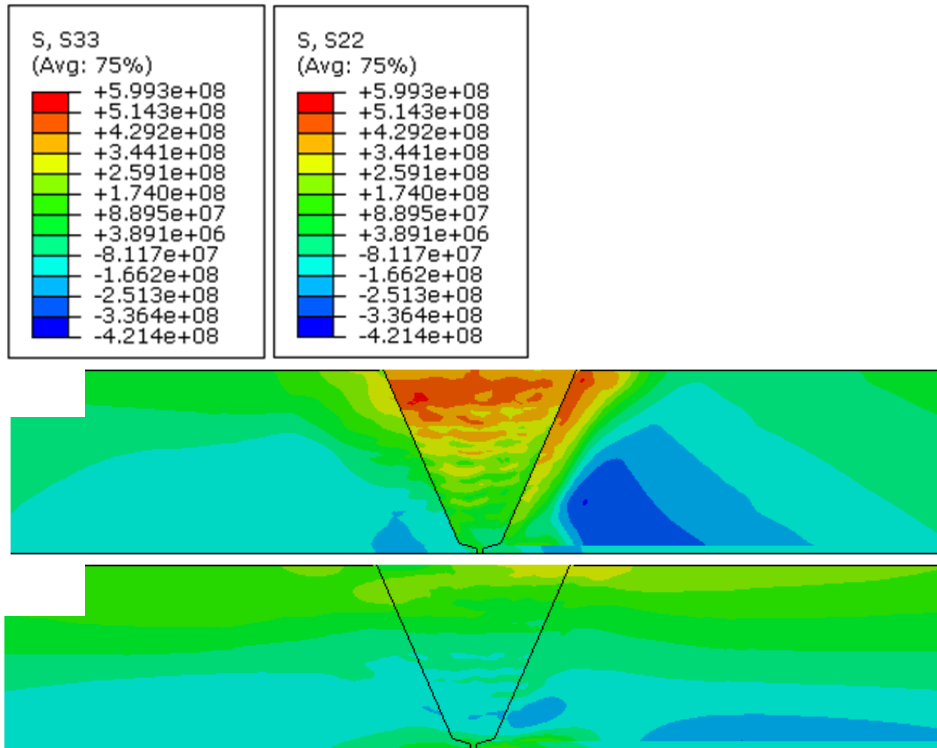


Figure 104 (a) Hoop stress S33 and (b) Axial stress S22 at Operation Temperature (OT) for weld case V.1.

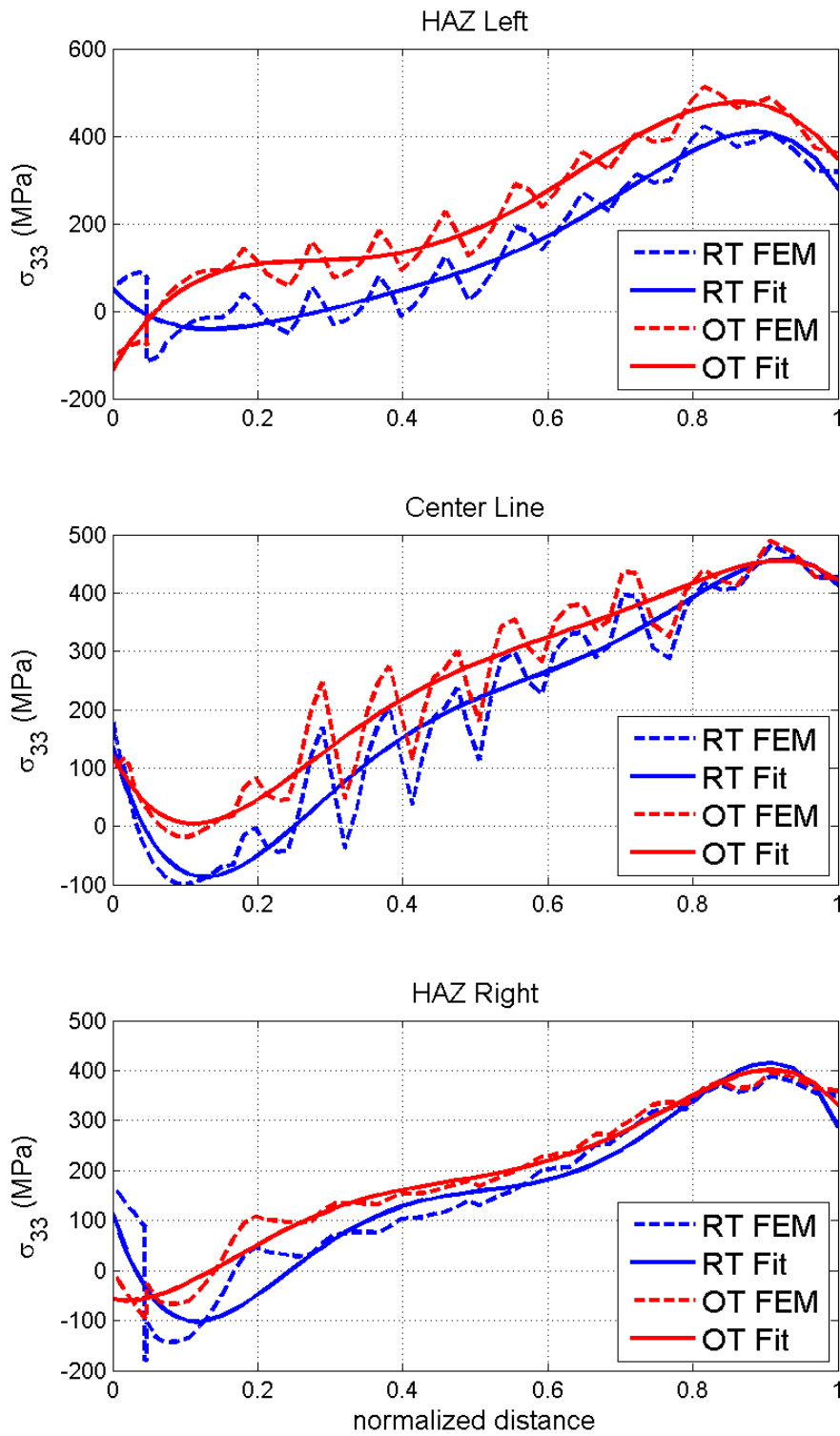


Figure 105 Hoop stress polynomial fit for weld case V.1.

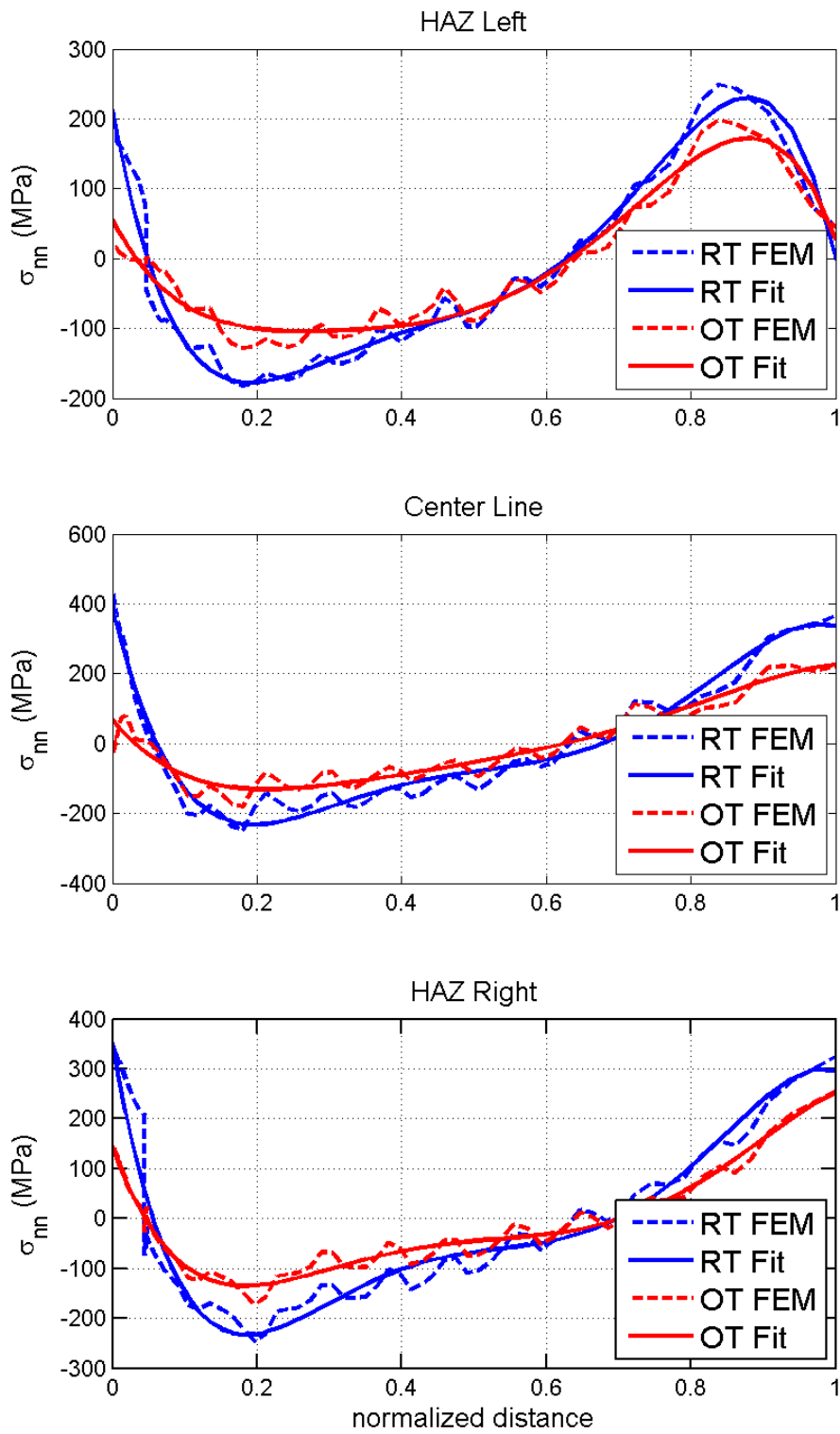


Figure 106 Normal stress polynomial fit for weld case V.1.

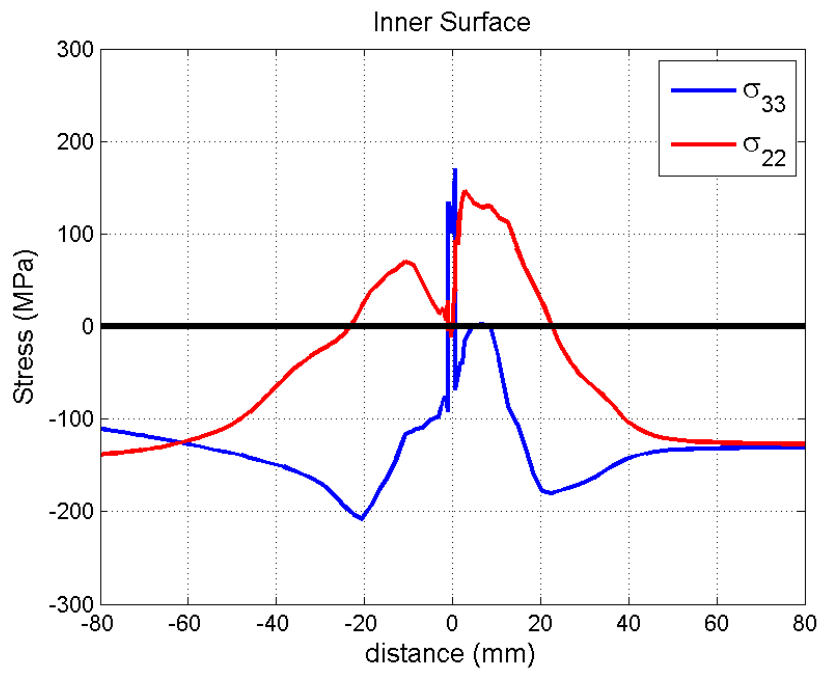


Figure 107 Hoop and axial stresses at the inner surface at Operation Temperature (OT) for weld case V.1.

Weld case VI.1

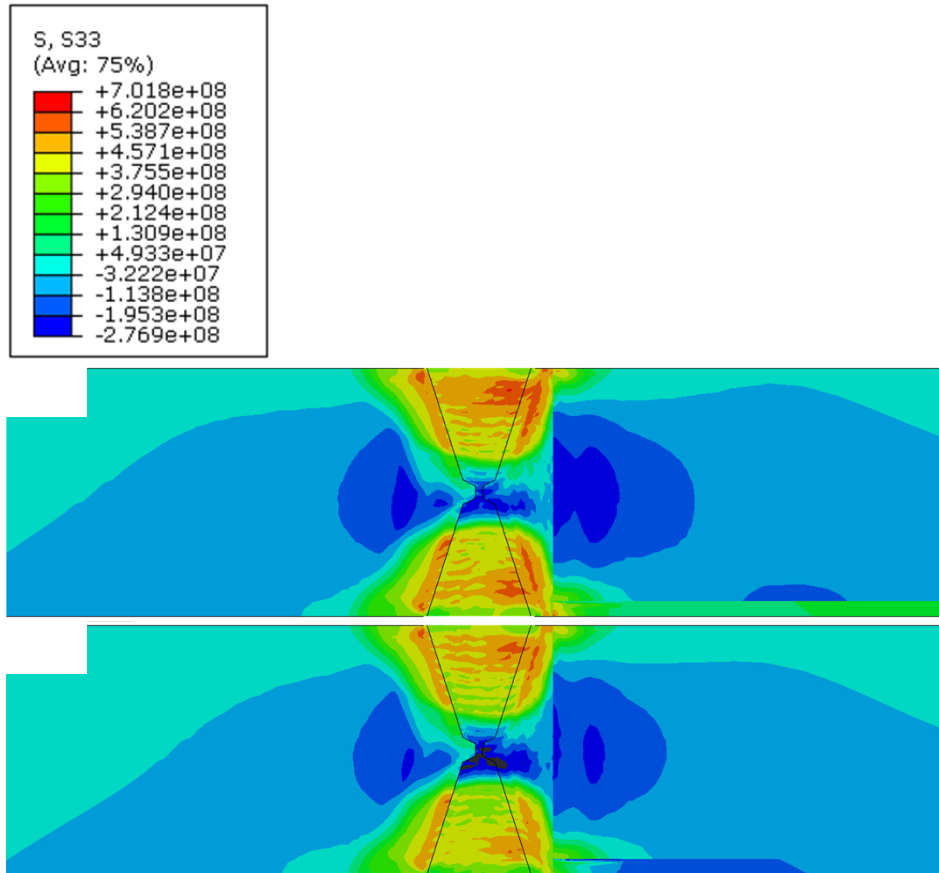


Figure 108 Hoop stress (S33) at: (a) Room Temperature (RT) and (b) Operation Temperature (OT) for weld case VI.1.

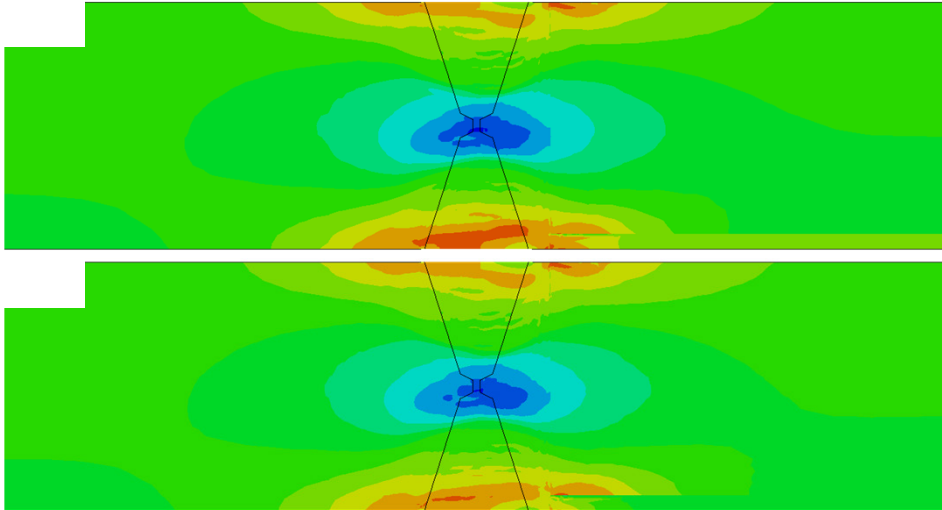
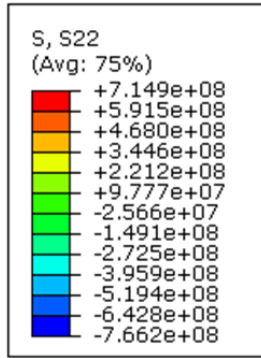


Figure 109 Axial stress S22 at: (a) Room Temperature (RT) and (b) Operation Temperature (OT) for weld case VI.1.

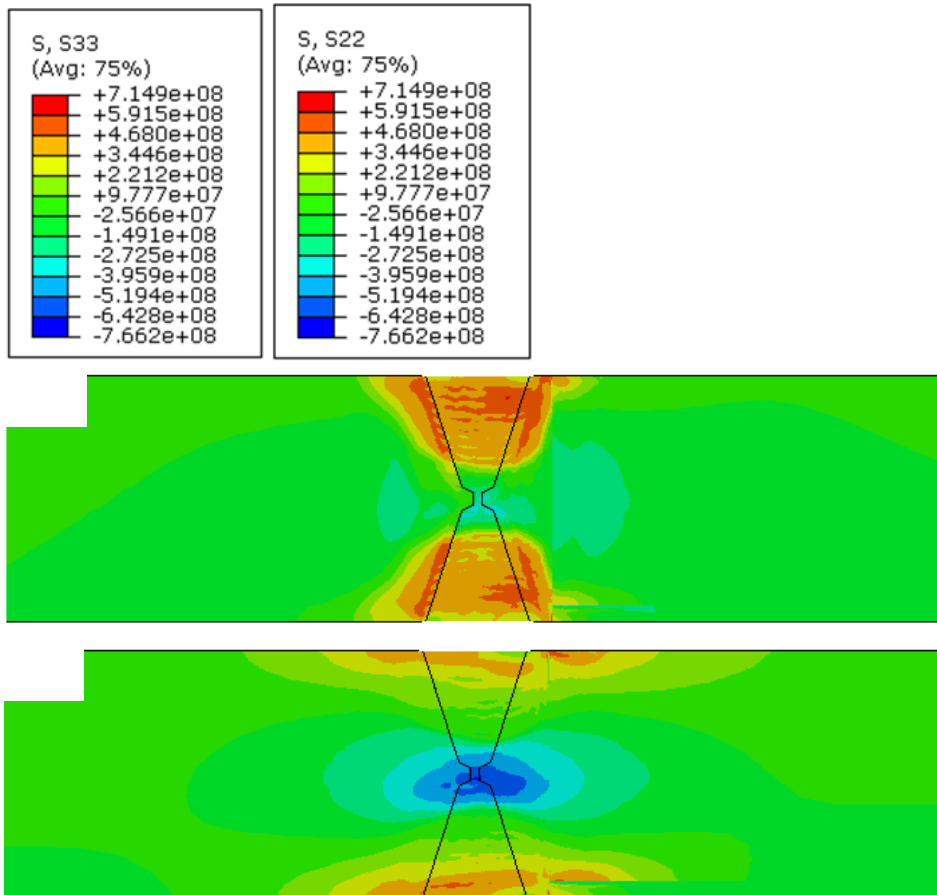


Figure 110 (a) Hoop stress S33 and (b) Axial stress S22 at Operation Temperature (OT) for weld case VI.1.

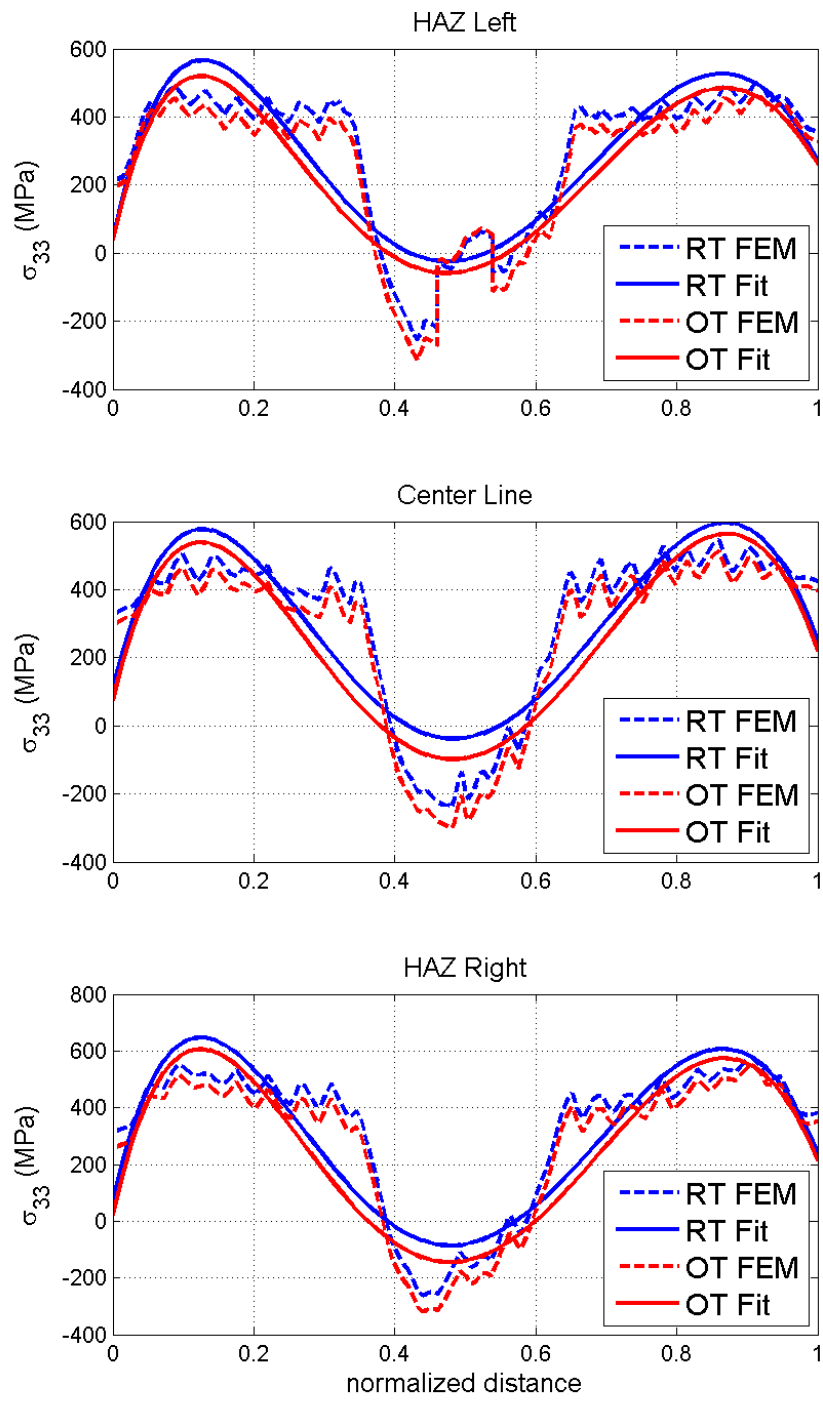


Figure 111 Hoop stress polynomial fit for weld case VI.1.

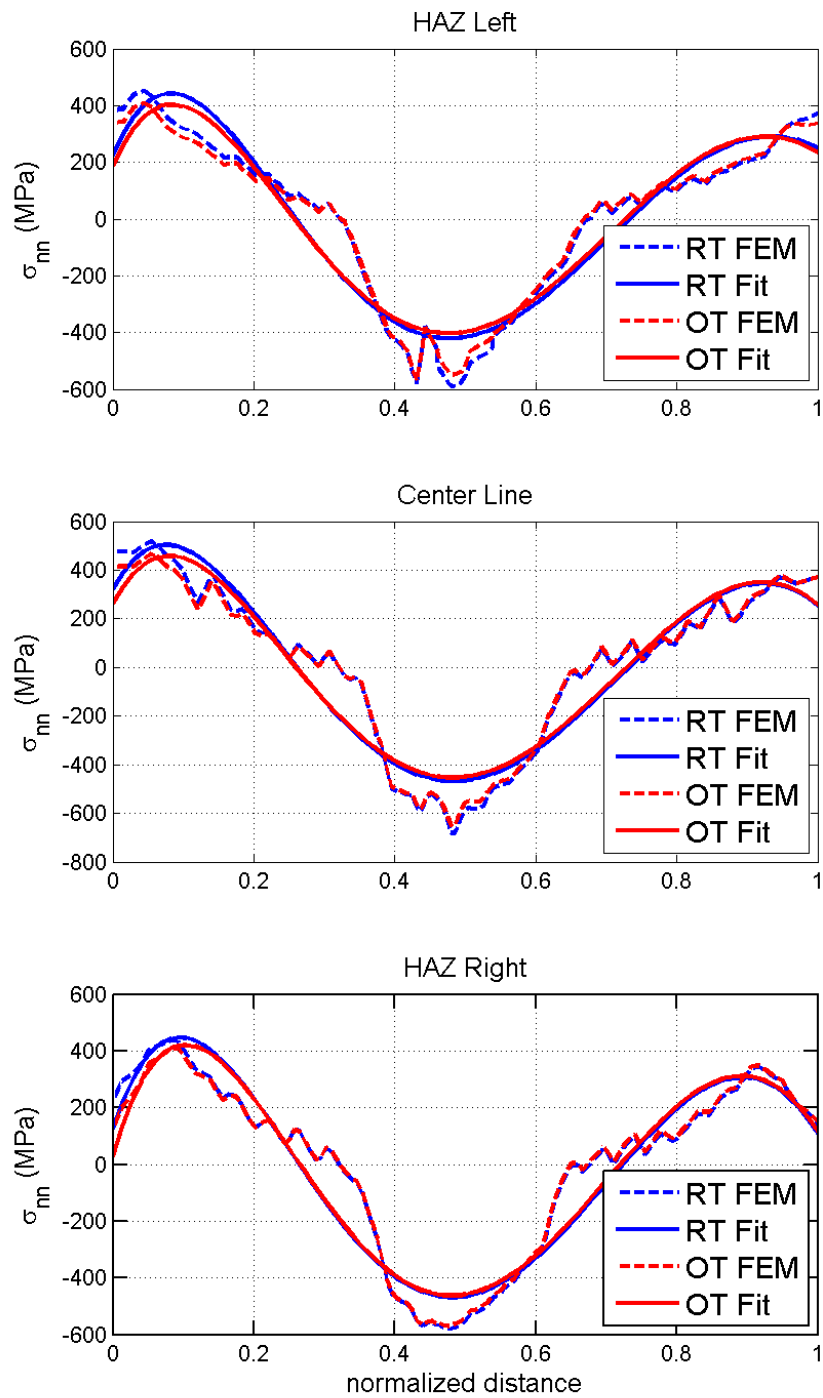


Figure 112 Normal stress polynomial fit for weld case VI.1.

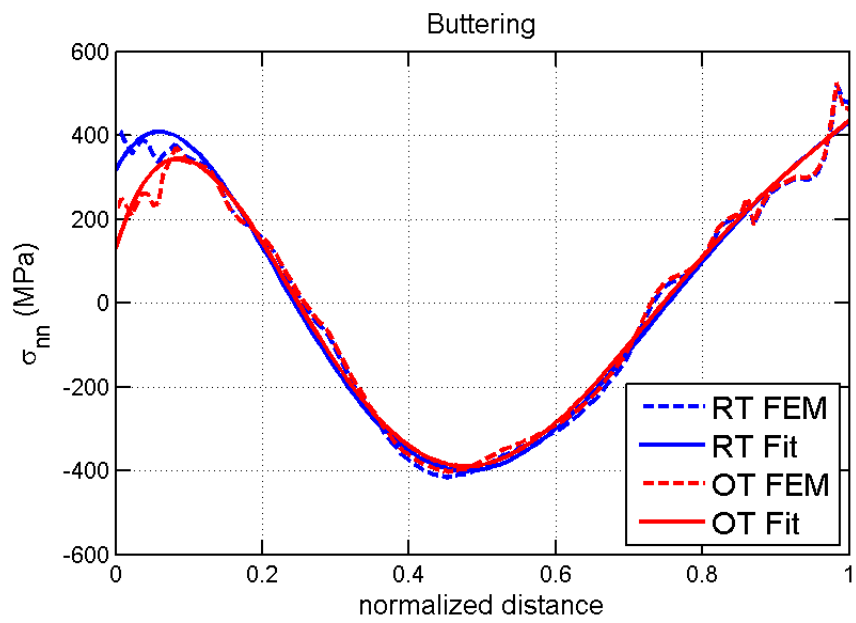
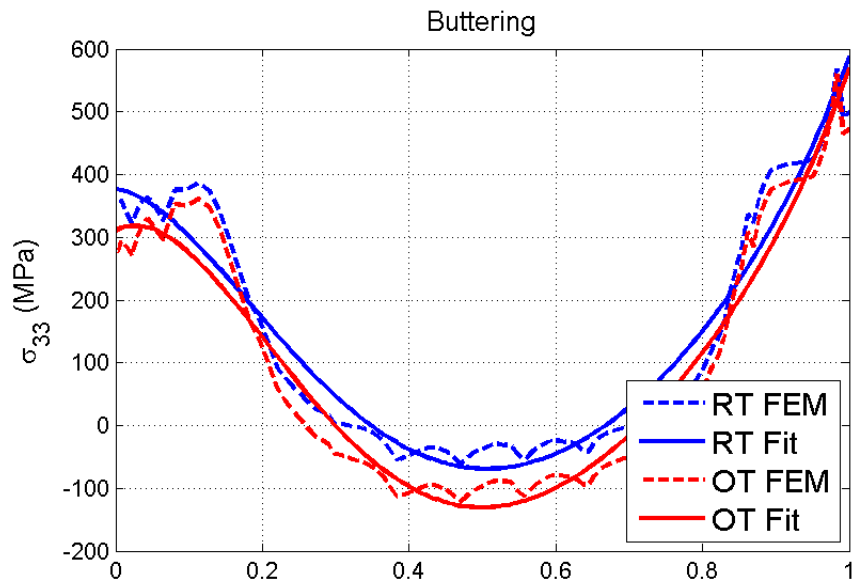


Figure 113 Hoop and normal stress polynomial fit for weld case VI.1

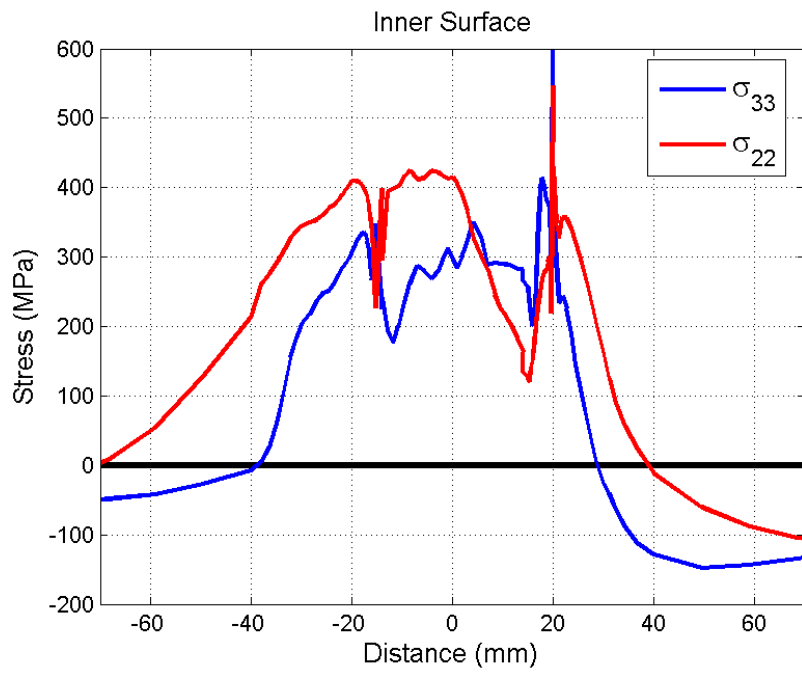


Figure 114 Hoop and axial stresses at the inner surface at Operation Temperature (OT) for weld case VI.1.

Appendix C – Effect from pressure testing

Example for weld case IV.2.

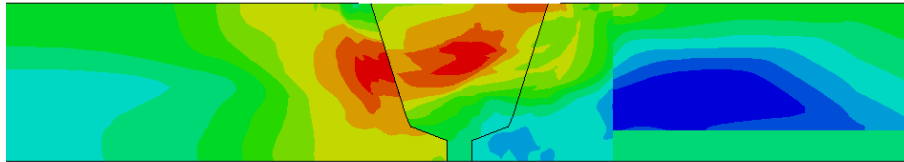
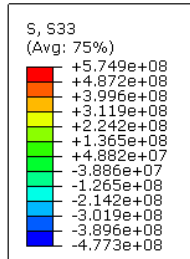


Figure 115 S33; Room temperature; as welded

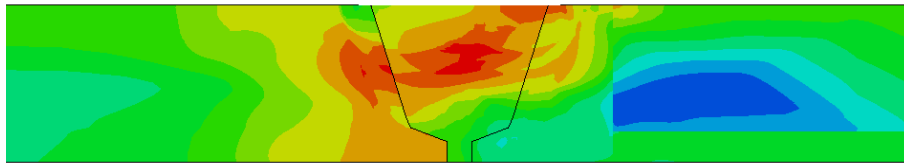


Figure 116 S33; Pressure testing

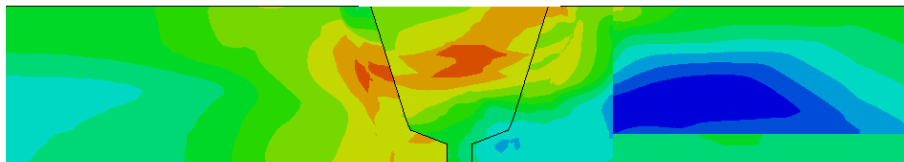


Figure 117 S33; Room temperature; after pressure testing

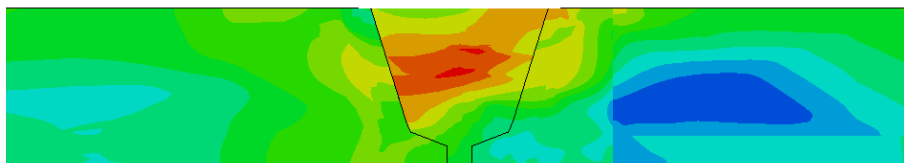


Figure 118 S33; Operation temperature

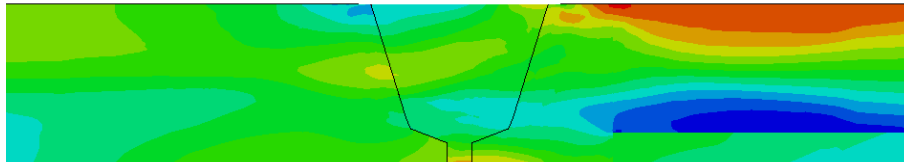
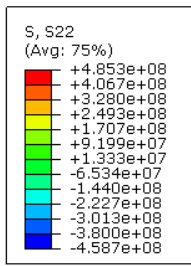


Figure 119 S22; Room temperature; as welded

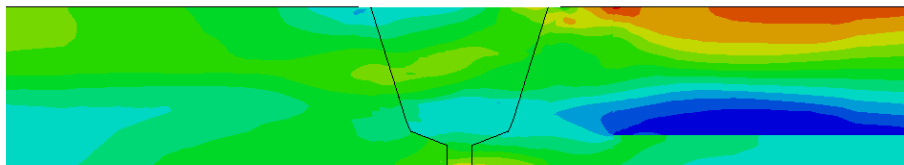


Figure 120 S22; Pressure testing

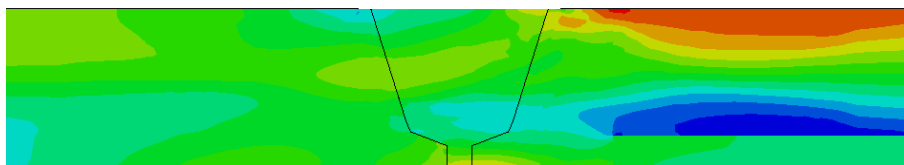


Figure 121 S22; Room temperature; after pressure testing

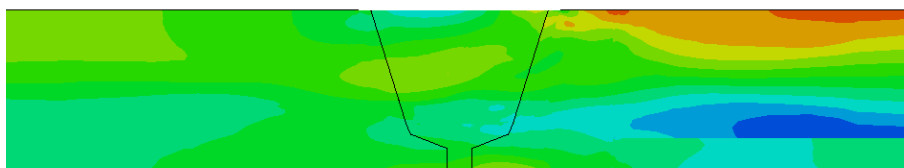


Figure 122 S22; Operation temperature

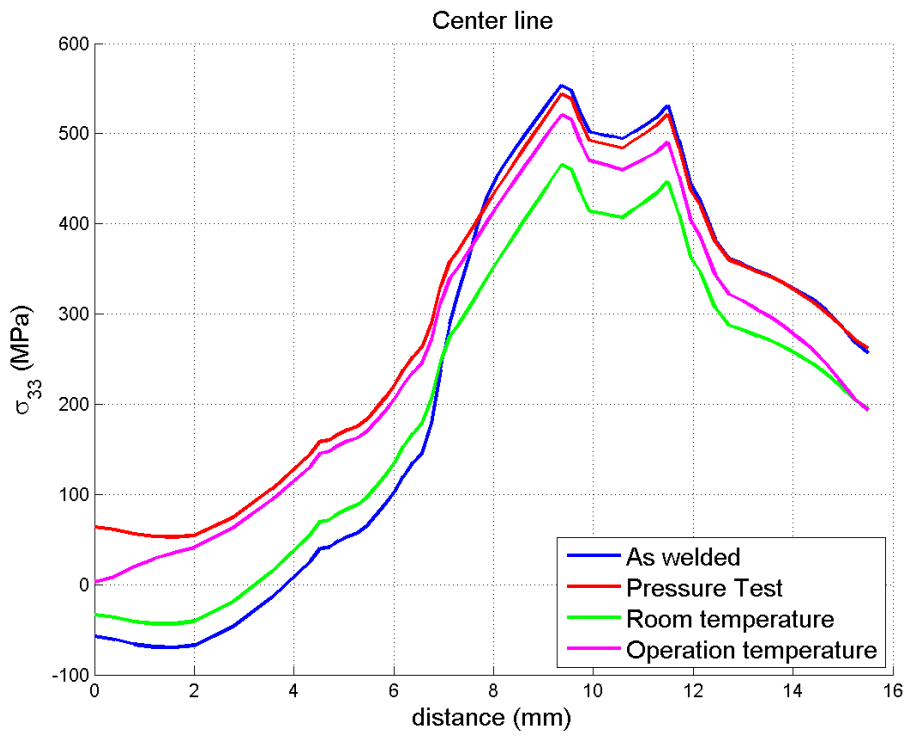


Figure 123 S33; Center Line

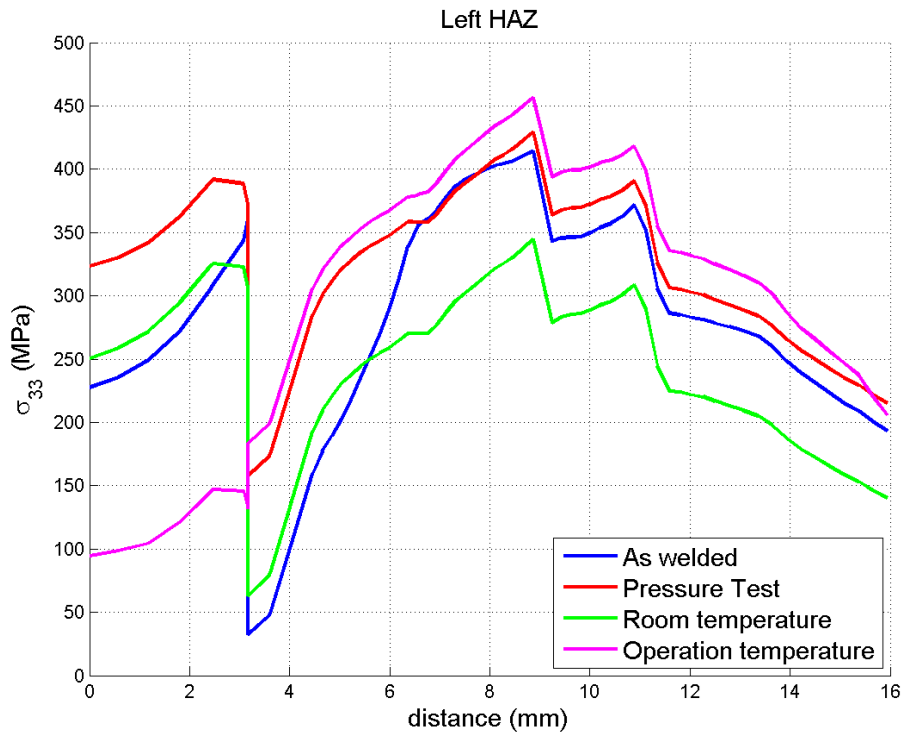


Figure 124 S33; Left HAZ

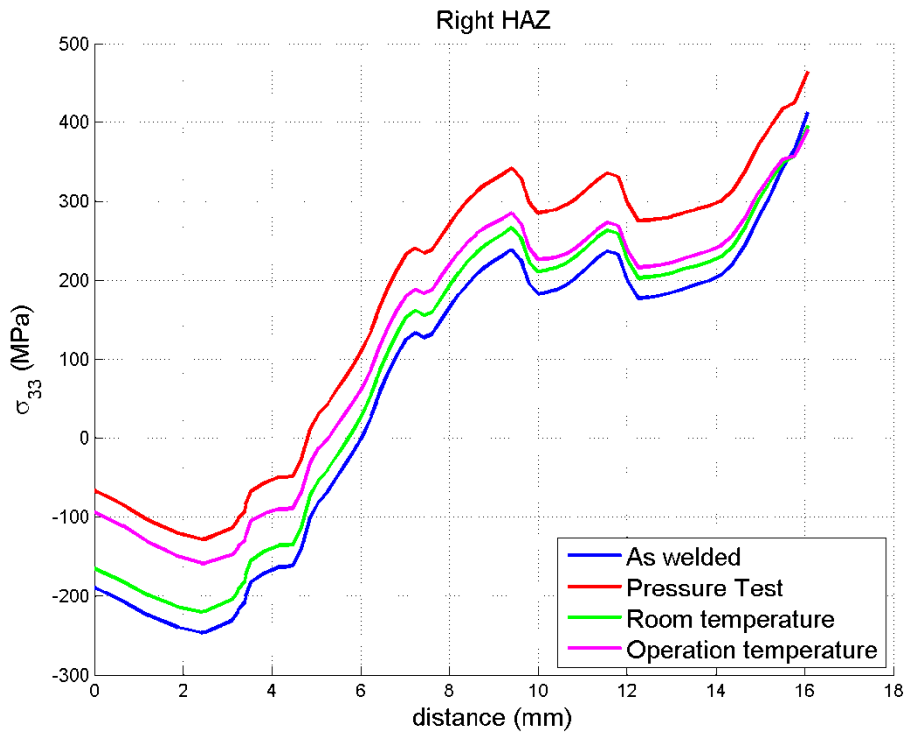


Figure 125 S33; Right HAZ

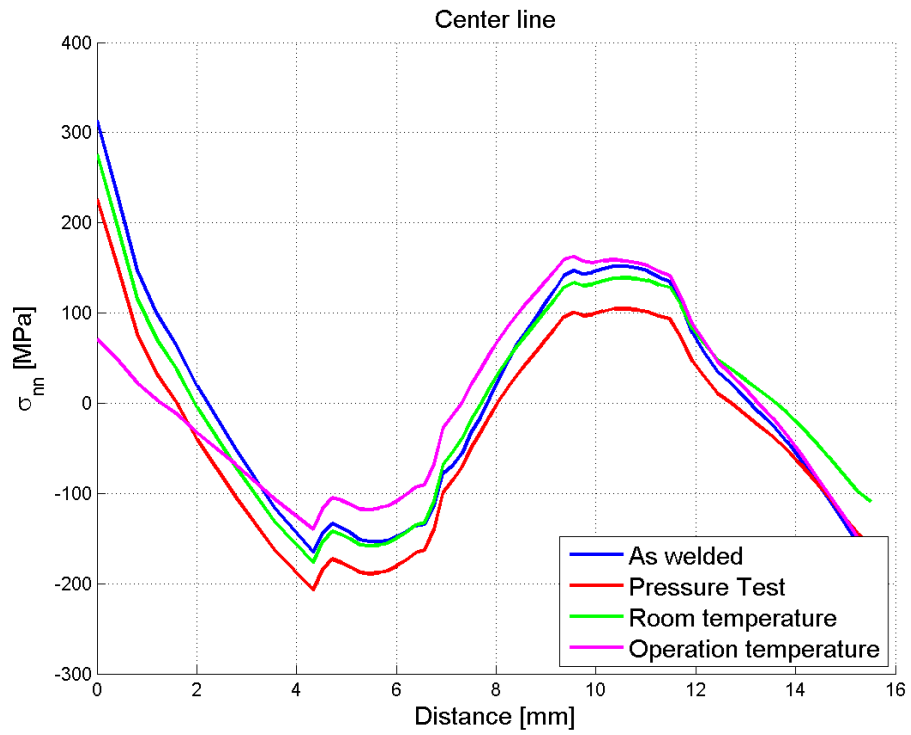


Figure 126 S22; Center Line

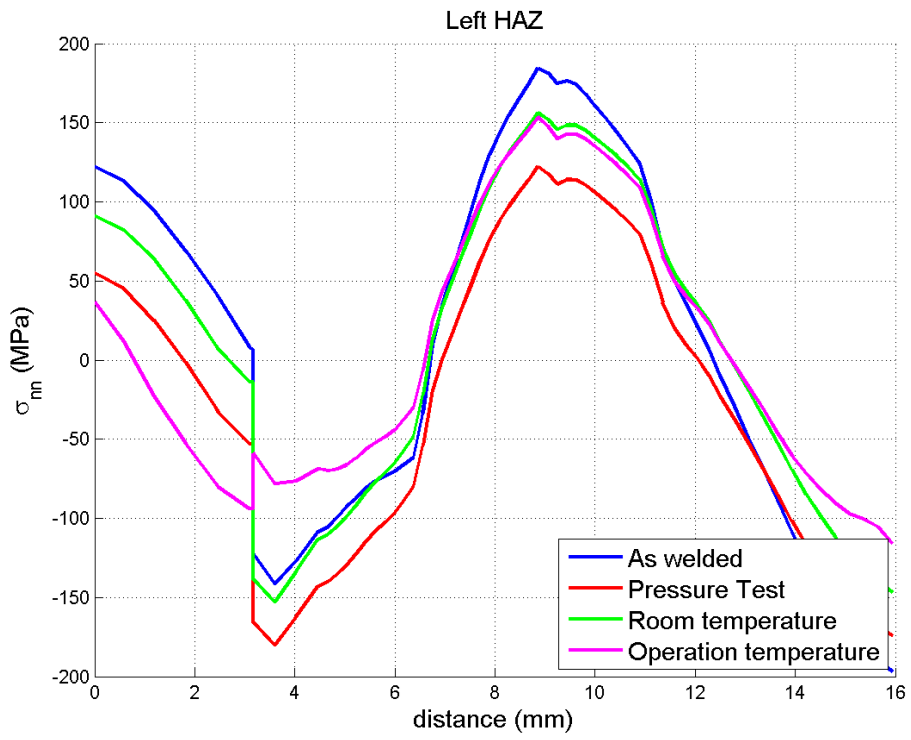


Figure 127 S22; Left HAZ

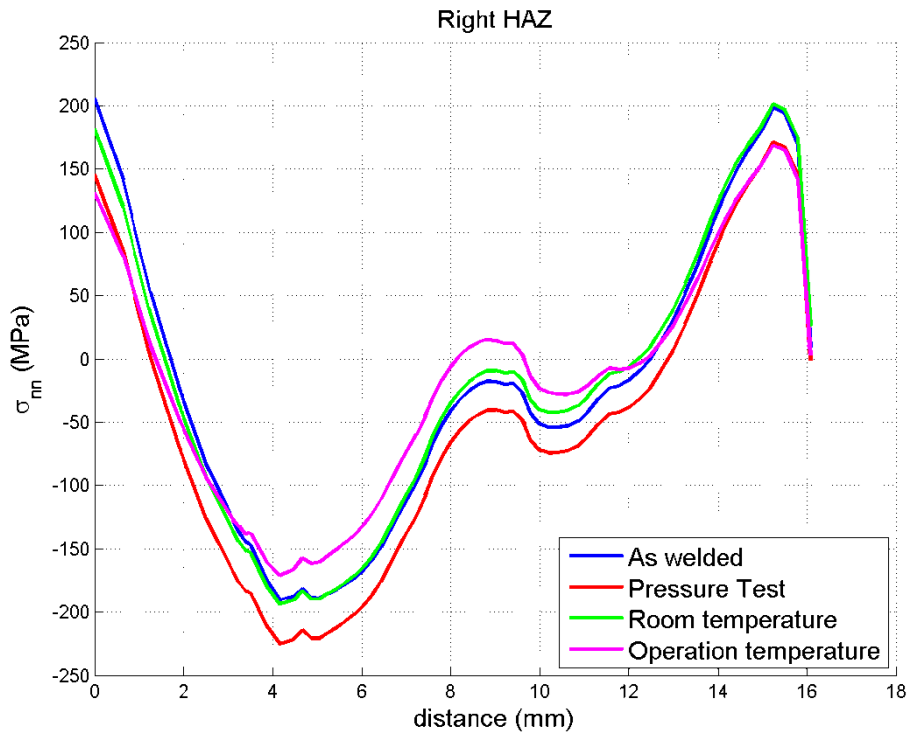


Figure 128 S22; Right HAZ

Appendix D – Sensitivity study of reduction in heat input

Example for weld case IV.3.

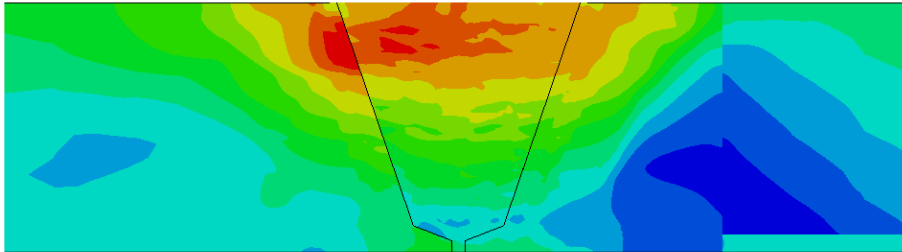
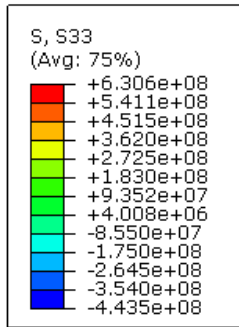


Figure 129 S33, Regular heat input, room temperature, as welded.

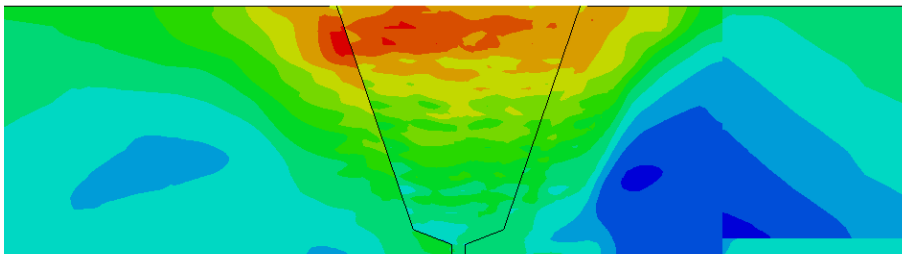


Figure 130 S33, Low heat input, room temperature, as welded.

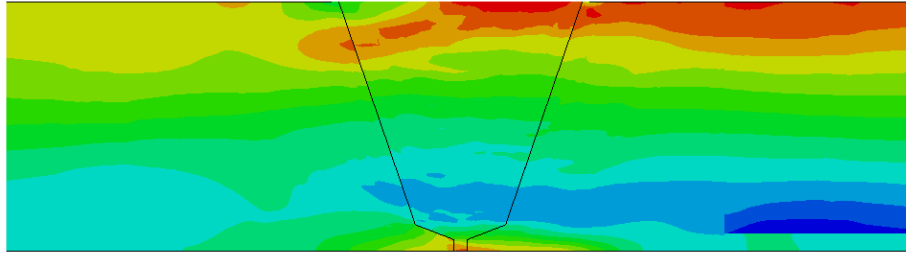
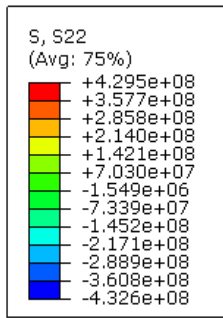


Figure 131 S22, Regular heat input, room temperature, as welded.

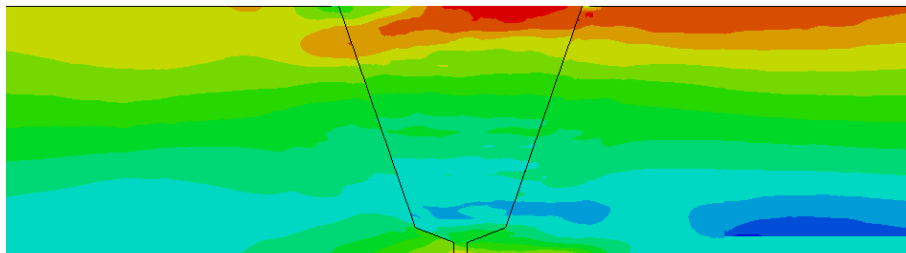


Figure 132 S22, Low heat input, room temperature, as welded.

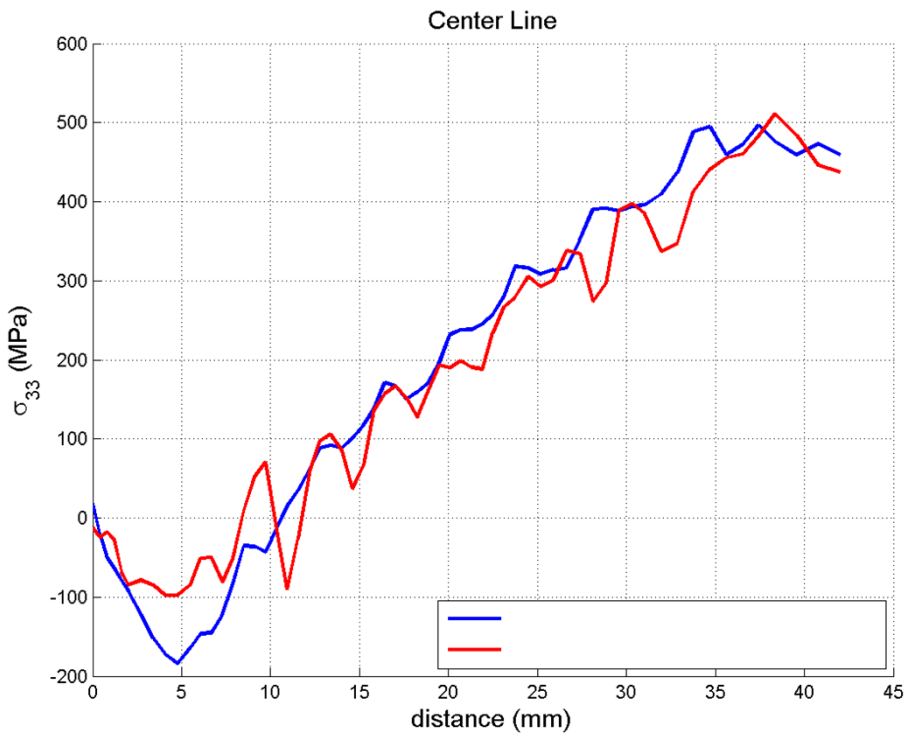


Figure 133 S33, Center Line

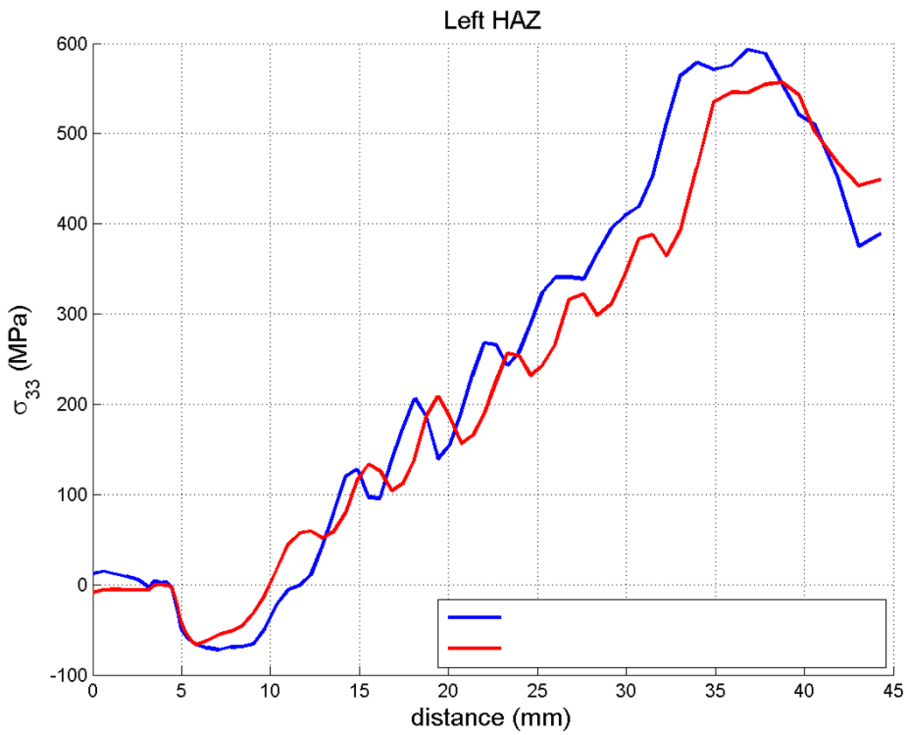


Figure 134 S33, Left HAZ

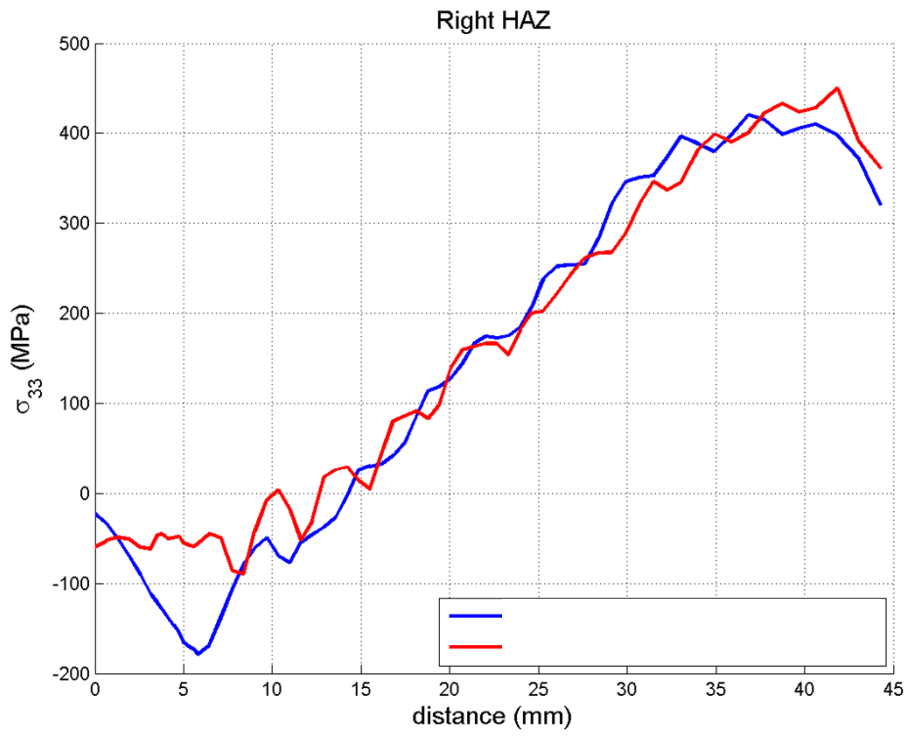


Figure 135 S33, Right HAZ

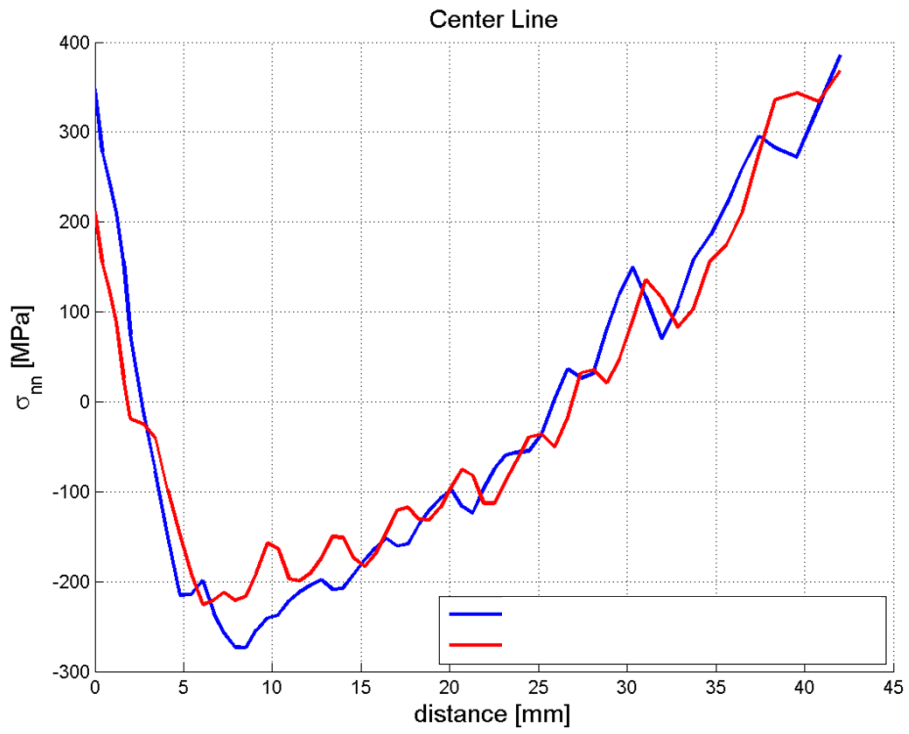


Figure 136 S22, Center Line

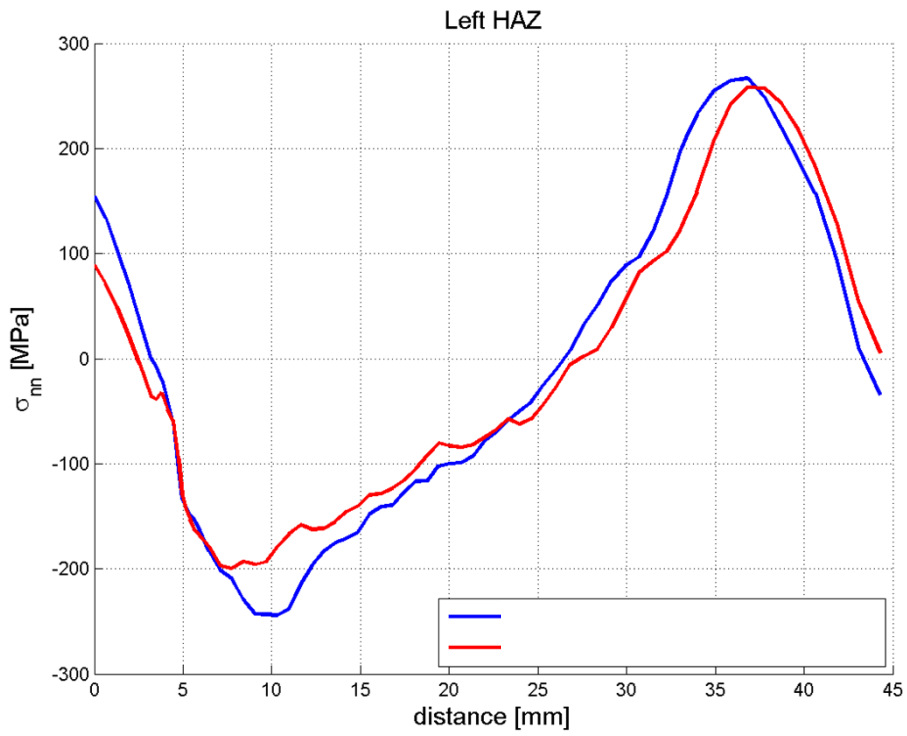


Figure 137 S22, Left HAZ

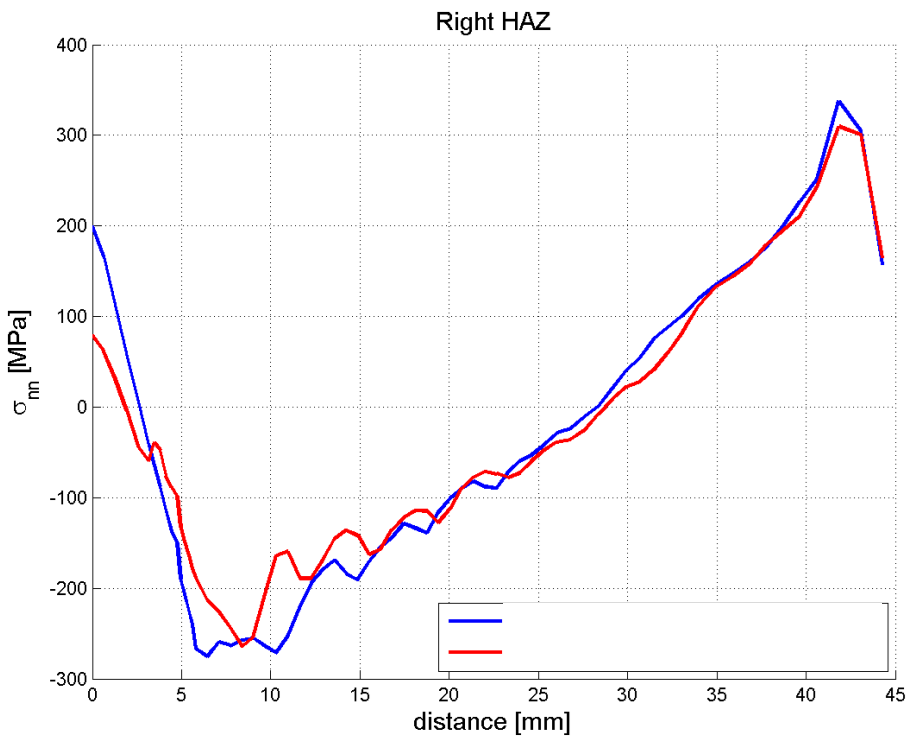


Figure 138 S22, Right HAZ

Appendix E – Effect from extensive machining of welds

Detailed comparison of stress profiles along different lines at the weld, for simulation without considering machining (previous results), and simulation considering extensive machining (new results), for weld case I.1 and weld case I.4.

Weld case I.1

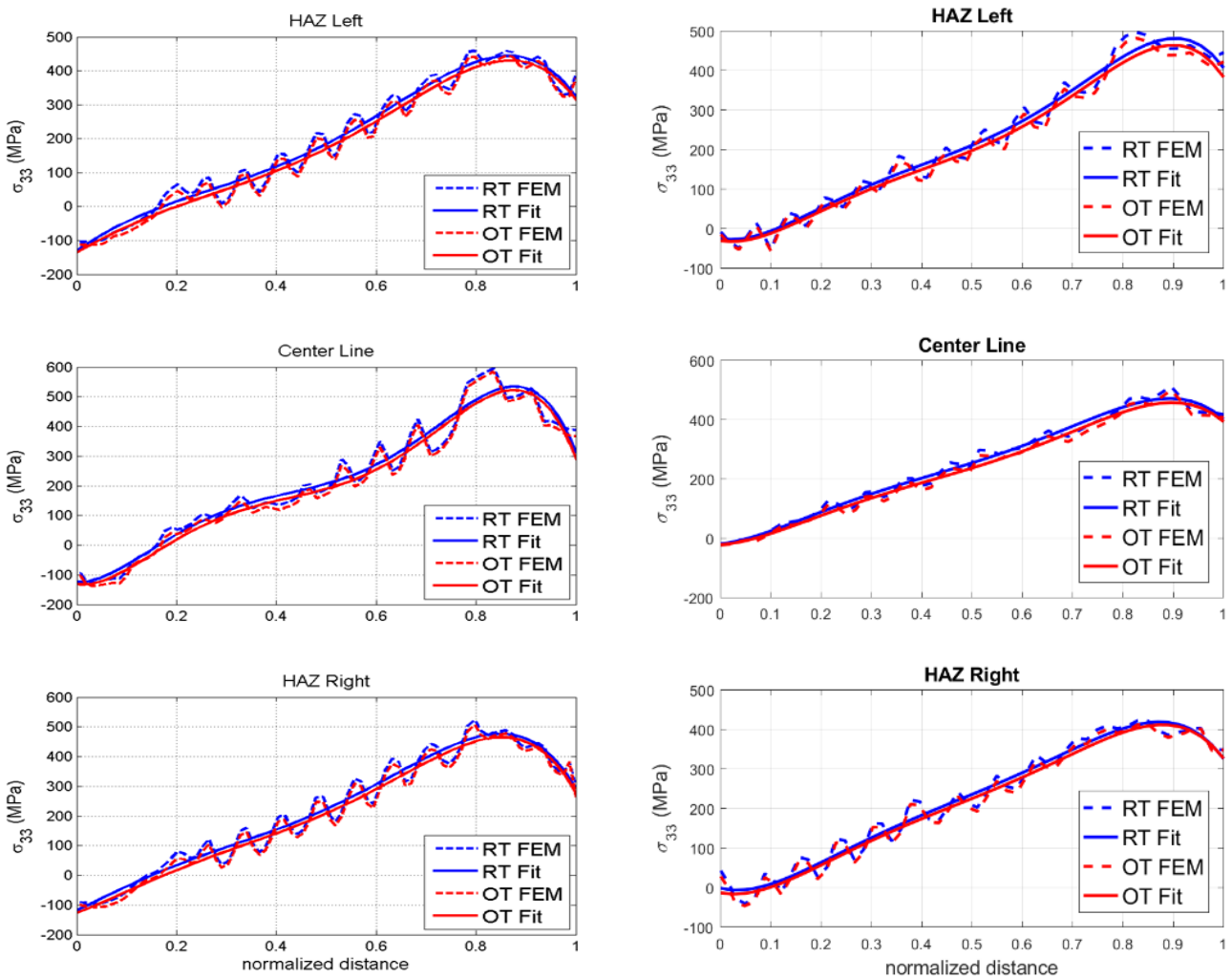


Figure 139 Hoop stress polynomial fit for weld case I.1. Results without and with simulation of the machining is presented on the left and on the right, respectively.

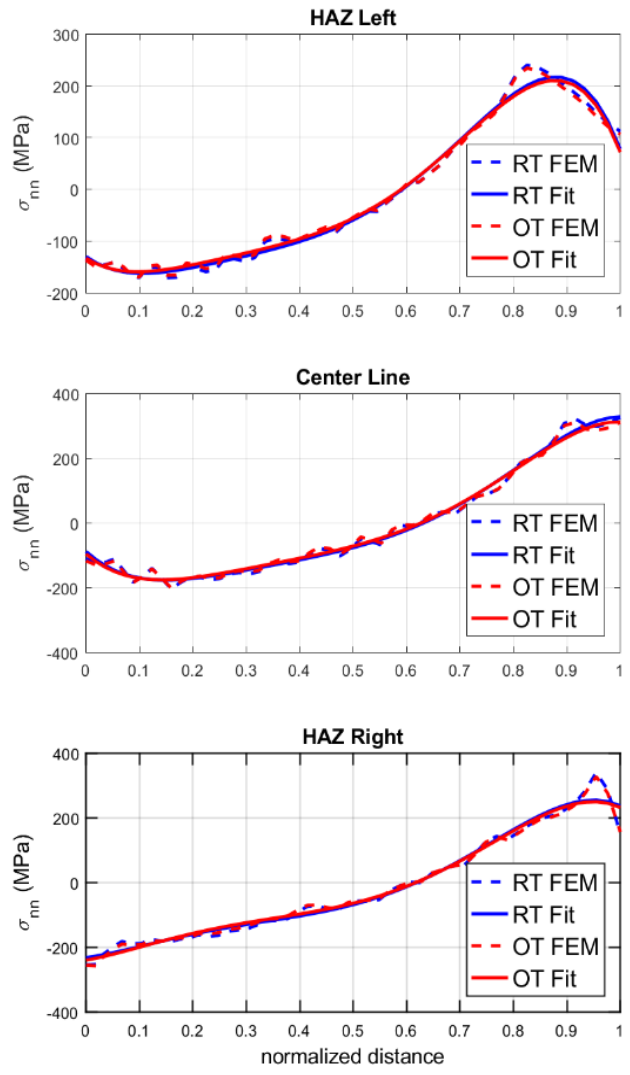
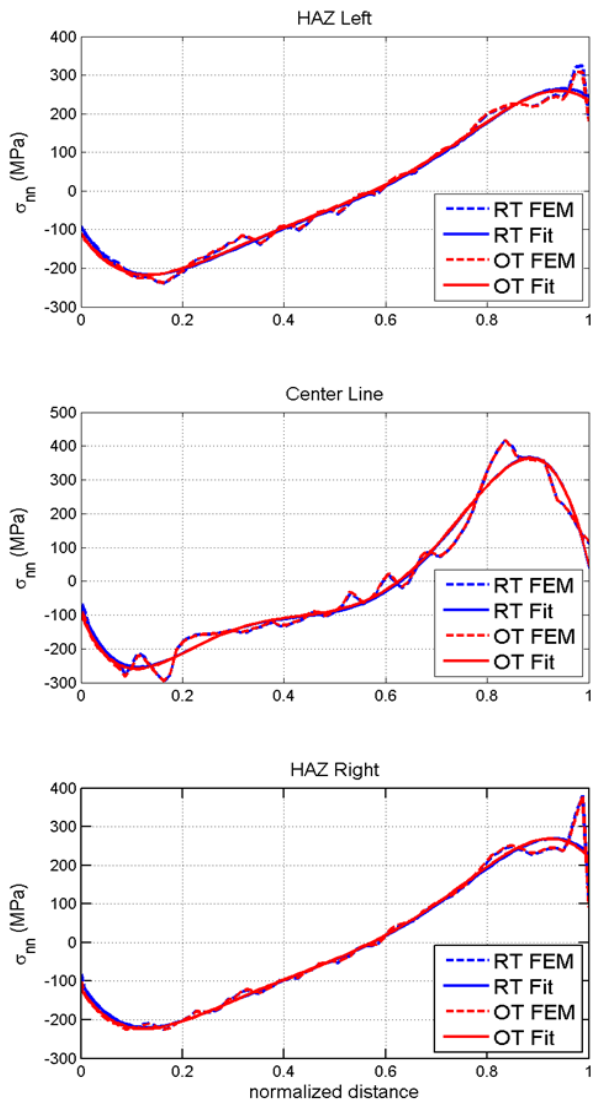


Figure 140 Normal stress polynomial fit for weld case I.1. Results without and with simulation of the machining is presented on the left and on the right, respectively.

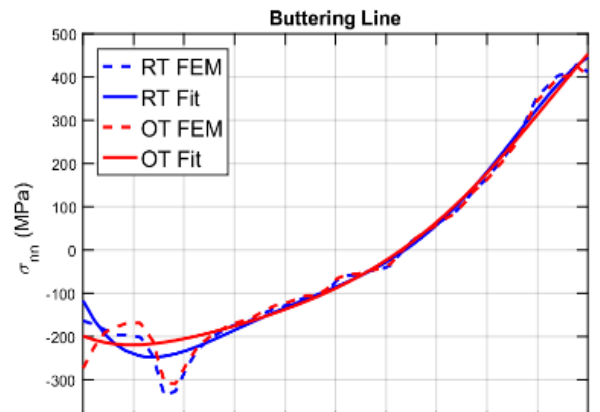
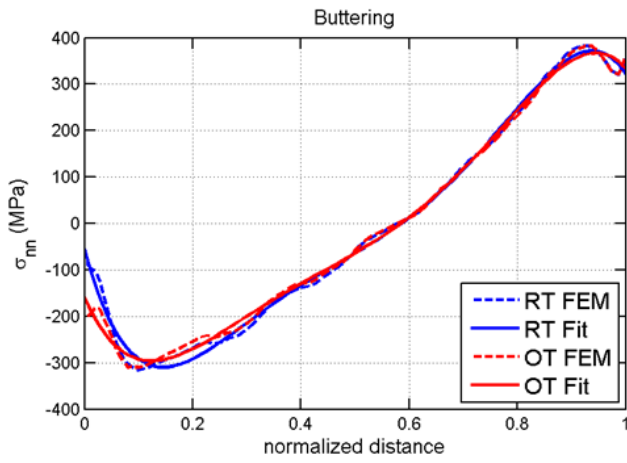
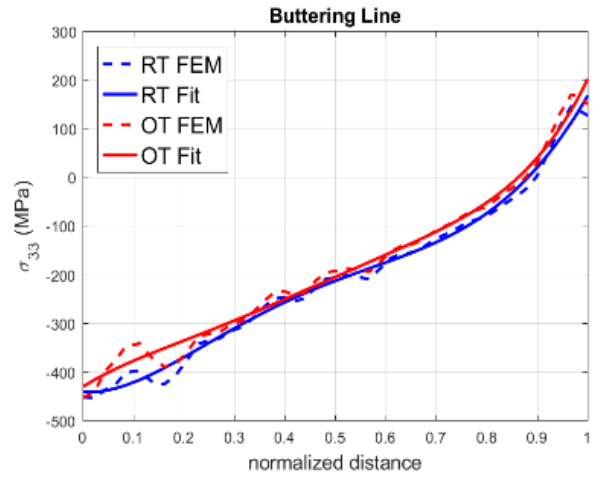
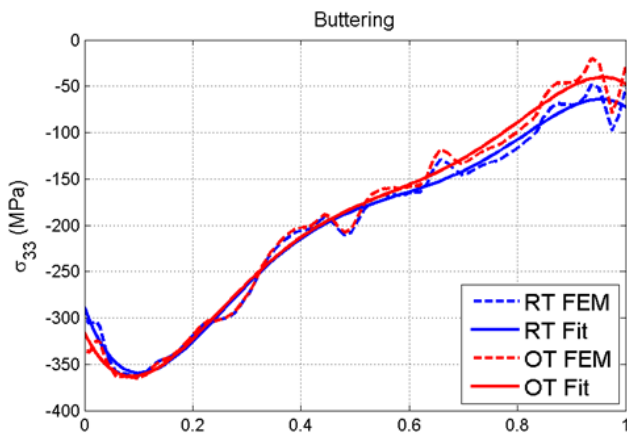


Figure 141 Hoop and normal stress polynomial fit for weld case I.1. Results without and with simulation of the machining is presented on the left and on the right, respectively.

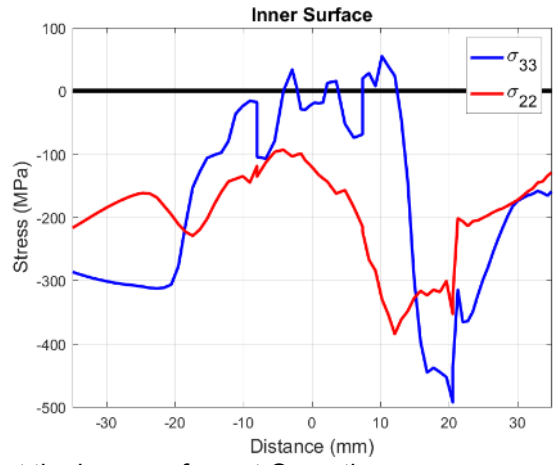
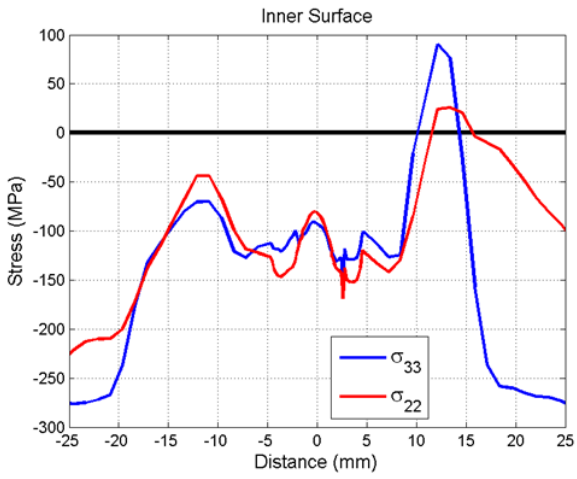


Figure 142 Hoop and axial stresses at the inner surface at Operation Temperature (OT) for weld case I.1. Results without and with simulation of the machining is presented on the left and on the right, respectively.

Weld case I.4

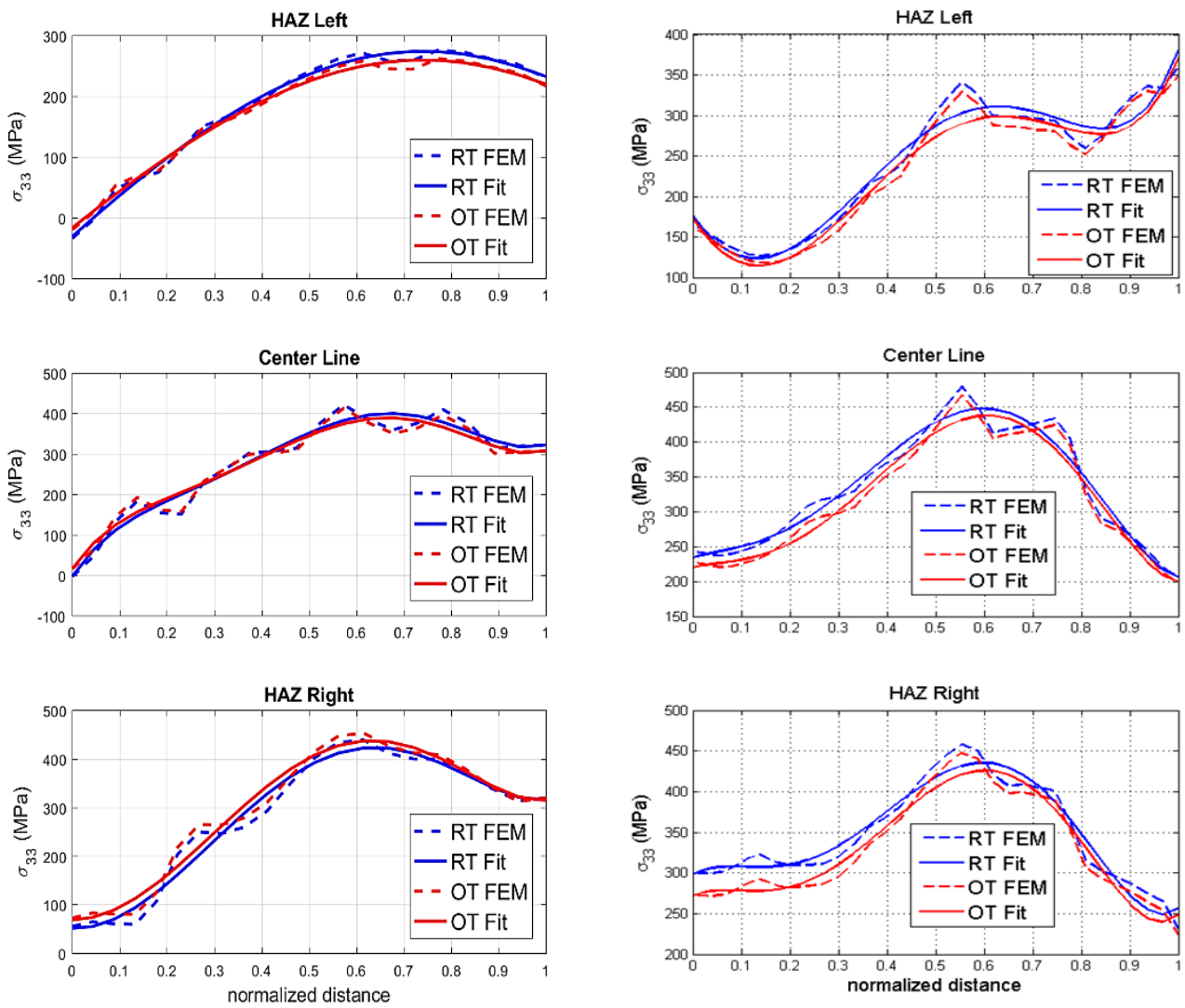


Figure 141 Hoop stress polynomial fit for weld case I.4. Results without and with simulation of the machining is presented on the left and on the right, respectively.

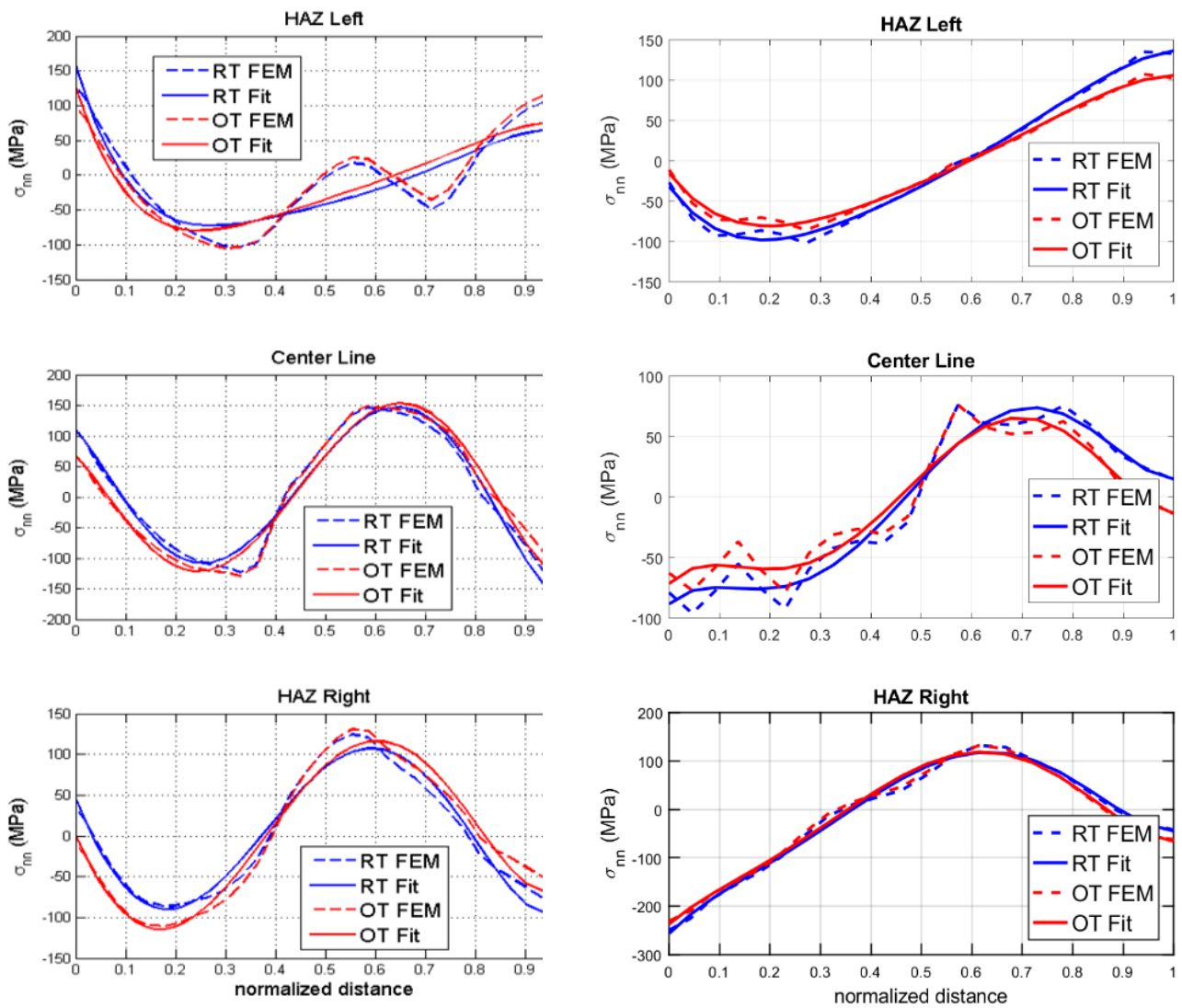


Figure 142 Normal stress polynomial fit for weld case I.4. Results without and with simulation of the machining is presented on the left and on the right, respectively.

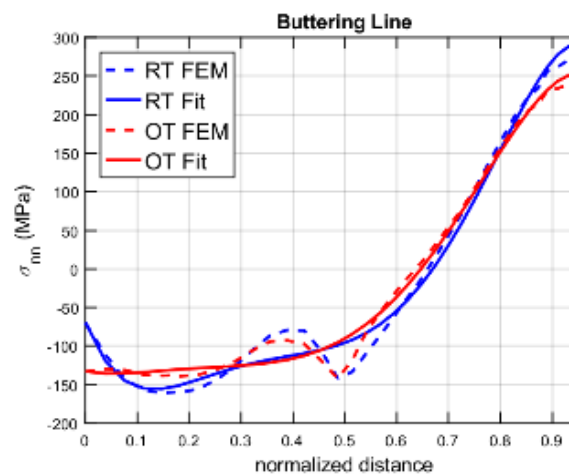
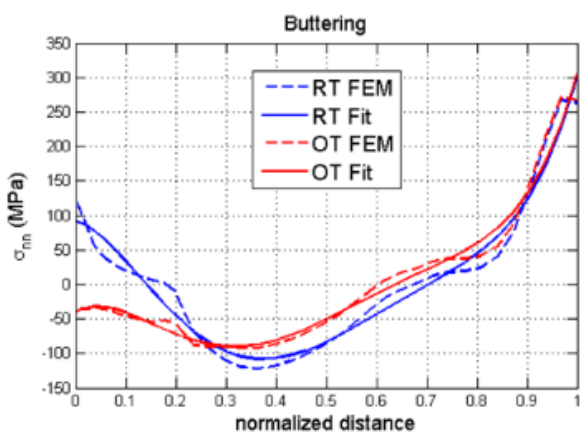
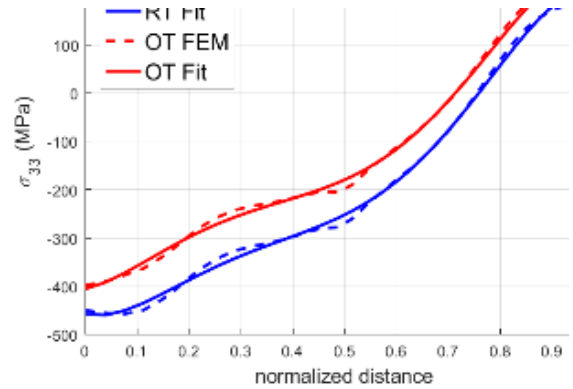
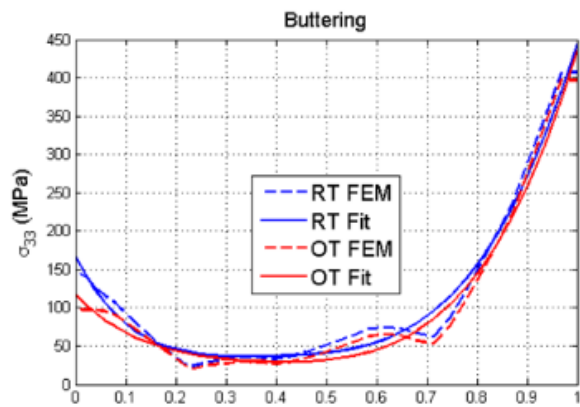


Figure 143 Hoop and normal stress polynomial fit for weld case I.4. Results without and with simulation of the machining is presented on the left and on the right, respectively.

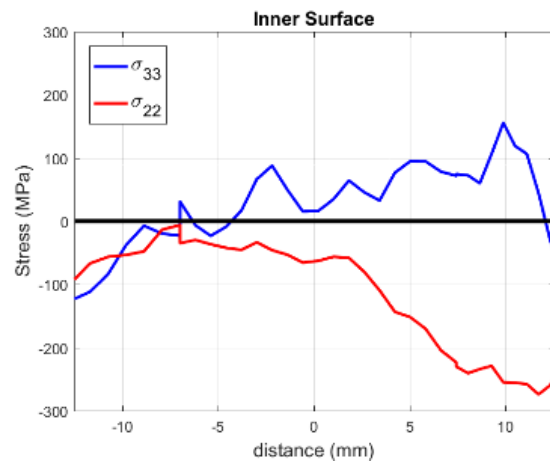
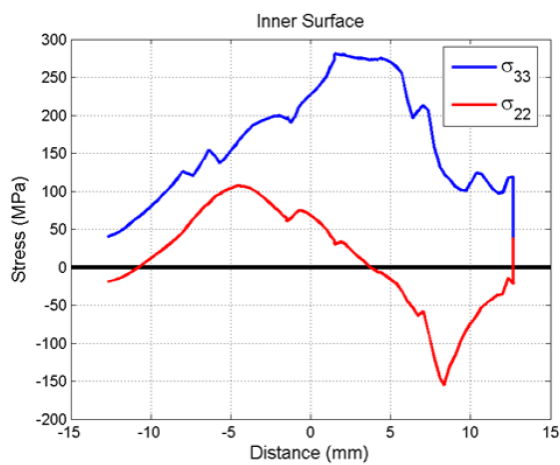


Figure 144 Hoop and axial stresses at the inner surface at Operation Temperature (OT) for weld case I.4. Results without and with simulation of the machining is presented on the left and on the right, respectively.

The Swedish Radiation Safety Authority (SSM) works proactively and preventively with nuclear safety, radiation protection, nuclear security, and nuclear non-proliferation to protect people and the environment from the harmful effects of radiation, now and in the future.

You can download our publications from www.stralsakerhetsmyndigheten.se/en/publications. If you need alternative formats such as easy-to-read, Braille or Daisy, contact us by email at registrator@ssm.se.

Strålsäkerhetsmyndigheten
SE-171 16 Stockholm
+46 (0) 8-799 40 00
www.stralsakerhetsmyndigheten.se
registrator@ssm.se

©Strålsäkerhetsmyndigheten